Assessing the Norwegian Offshore Wind Resources: Climatology, Power Variability and Wind Farm Siting

Ida Marie Solbrekke

Thesis for the degree of Philosophiae Doctor (PhD)
University of Bergen, Norway
2022

UNIVERSITY OF BERGEN

Assessing the Norwegian Offshore Wind Resources: Climatology, Power Variability and Wind Farm Siting

Ida Marie Solbrekke

Thesis for the degree of Philosophiae Doctor (PhD)
at the University of Bergen

Date of defense: 09.09.2022

Year: 2022

Title: Assessing the Norwegian Offshore Wind Resources: Climatology, Power Variability and Wind Farm Siting

Name: Ida Marie Solbrekke

Print: Skipnes Kommunikasjon / University of Bergen

Preface

This synthesis and collection of scientific papers are submitted for the degree of pilosophiae doctor (PhD) in renewable energy at the Geophysical institute and Bergen Offshore Wind Center, University of Bergen. This has been a four-year PhD position, including one year of duty work with contributions to several courses and student supervisions. This PhD has been a part of the Bergen Offshore Wind Center (BOW). BOW is an interdisciplinary research center established in 2018 by the University of Bergen to coordinate and strengthen the research and education in offshore wind energy. The center has three focus areas: Wind resources, site selection and wind farm operations. In addition to BOW, I have also been enrolled in the CHESS Research School.

This thesis consists of an introductory part and four scientific papers. Chapter 1 gives the motivation and scientific background. The first part of the chapter sets this thesis into scientific context, discussing the current offshore wind power situation in Norway, the relevant research front addressing the lack of knowledge, and briefly state how this thesis contributes to these current research gaps. The raised objectives and research questions are listed at the end of chapter 1. Chapter 2 discusses the Norwegian offshore wind resource climatology, variability and the corresponding wind power potential, but also briefly discusses the ongoing activity in the Norwegian offshore area. Chapter 3 gives a brief introduction to the data used in this study. More detailed information on the data can be found in each paper. An introduction to the papers is given in chapter 4: stating the papers objective; a short summary of each study; followed by the main findings in bullet points. Lastely, a closing future outlook is given in Chap. 5. The four papers constituting this thesis are included in chapter 6, and are listed below in progressive order:

1. **Solbrekke, Ida M.**, Kvamstø, Nils G., Sorteberg, Asgeir, (2020) *Mitigation of wind power intermittency through interconnection of production sites*, Wind Energy Science **5/4**

2. **Solbrekke, Ida M.**, Sorteberg, Asgeir, Haakenstad, Hilde, (2021) *The 3 km Norwegian reanalysis (NORA3) a validation of offshore wind resources in the North Sea and the Norwegian Sea*, Wind Energy Science **6/6**

3. **Solbrekke, Ida M.**, Sorteberg, Asgeir, (2022) *NORA3-WP: A high resolution wind power dataset for the Baltic, North, Norwegian, and Barents Seas*, Accepted for publication in Scientific Data - Nature **-/-**

4. **Solbrekke, Ida M.**, Sorteberg, Asgeir, (2022) *Offshore Wind Farm siting - Suitability Scores for the Norwegian Economic Zone Using Multi-Criteria Decision Analysis*, Submitted to Energy Policy **-/-**

Scientific contributions during the PhD period that are not a part of this thesis:

- Ringkjøb, Hans K., Haugan, Peter, **Solbrekke, Ida M.** (2018) *A review of modelling tools for energy and electricity systems with large shares of variable renewables*, Renewable and Sustainable Energy Reviews **96/-**
- Cheynet, Etienne, **Solbrekke, Ida M.**, Diezel, Jan Markus, Reuder, Joachim (2022) *A one-year comparison of new wind atlases over the North Sea* Accepted for publications in Journal of Physics - Conference Series (IOP science)

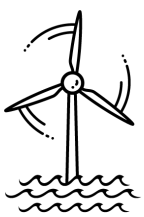

Abstract

The Norwegian offshore wind resources are outstanding. Yet, no wind farms are commissioned in the Norwegian waters. Considering emission reduction targets and predicted increase in electricity demand, the Norwegian government has in the recent years started to look towards the marine environment for energy extraction. Exploiting the offshore area for wind power deployment requires large-scale mapping and improved understanding of the Norwegian offshore wind resource characteristics. This thesis deals with wind resource assessment and related wind power estimates, mitigation of unwanted wind power production events, and wind farm siting considering the Norwegian offshore area. Observations and data from "the 3 km Norwegian Reanalysis (NORA3)" form the basis for the results in this thesis.

The results from this thesis are divided into four research papers. The first paper deals with mitigation of wind power intermittency through interconnection of allocated wind farms in the North and Norwegian Seas using observations. By interconnecting production sites unwanted power events, like variability and zero-production events, were drastically reduced. In this paper we also investigate the main atmospheric circulation associated with long-lasting zero-events. The average atmospheric pattern resulting in too low winds for power production is a associated with a high-pressure system located over the connected sites. Whereas, the average atmospheric situation associated with too strong winds is a low-pressure systems located to the north of the connected sites.

The second paper investigates whether NORA3 can serve as a wind resource dataset in the planning phase of new wind farm projects. We carry out an in-depth near-hub-height validation of the wind resources in NORA3 towards offshore wind power using different statistical measures. We conclude that NORA3 is well suited for wind power estimates, but gives slightly conservative estimates on the offshore wind metrics. For example, the model output is biased towards lower wind power estimates due to an overestimation of the wind speed events below typical rated wind speed limits (u <11-13 ms^{-1}) and an underestimation of high wind speed events (u >11-13 ms^{-1}).

In the third paper we present a new high resolution wind power related dataset named 'NORA3-WP: A high-resolution offshore wind power dataset for the Baltic, North, Norwegian, and Barents Seas". The dataset is based on NORA3 and covers the North Sea, the Baltic Sea and parts of the Norwegian and Barents Seas. NORA3-WP is an open access dataset intended for use in research, governmental management and for stakeholders to attain relevant wind resource and wind power information in the planning phase of a new wind farm project. NORA3-WP is the first wind power related dataset covering the entire Norwegian economic zone (NEZ).

In the fourth paper we assembly multidisciplinary datasets (NORA3-WP, among others) presenting the first mapping of wind power suitability scores (WPSS) for the entire Norwegian offshore area. The method used to generate the WPSS is a Multi-criteria decision analysis (MCDA) framework including

an analytical hierarchical process (AHP) approach considering wind resources, techno-economic aspects, social acceptance, environmental considerations, and met-ocean constraints. Results are obtained through a baseline scenario representing a decision-maker that does not prioritize one set of criteria strongly, but realizes the importance of selecting areas that are economically sound as well as having a low potential for social conflicts. We test the robustness of the results obtained in the baseline scenario by including three different actors with distinct preferences for siting of a wind farm: "the investor", "the environmentalist", and "the fisherman". The results show that the southern part of NEZ is the region that is most suitable and robust for offshore wind power deployment. Offshore areas in the Norwegian part of the Barents Sea and the near-coastal areas outside mid-Norway are also suited, but these regions are rather sensitive to tuning of the criteria importance.

Abstrakt

De norske havvindressursene er fantastiske. Likevel er det ingen operative vindparker i de norske havvområdene. Tatt i betraktning både utslippsmål og forventet økning i elektrisitetsforbruk har regjerningen nå begynt å vise interesse for kraftproduksjon til havs. Å utnyttelse de norske havvområdene til vindkraftproduksjon krever en storskala kartlegging og økt kunnskap om vindressursene. Denne doktorgradsavhandlingen tar for seg kartlegging av vindressursene, tilhørende vindkraftestimat, reduksjon av uønskede hendelser i vindkraftproduksjonen, og optimal plassering av fremtidige havvindparker. Observasjoner og data fra "the 3 km Norwegian Reanalysis (NORA3)" danner datagrunnlaget for resultatene i avhandlingen.

Resultatene er fordelt på fire forskningsartikler. Den første artikkelen ser på hvordan vi kan utnytte den naturlige variasjonen i værsystemene til fordel for vindkraftproduksjonen. Artikkelen svarer på mye vi kan forvente å redusere vindkraftvariabilitet ved å koble sammen vindparker i Nordsjøen og Norskehavet. Ved å koble sammen produksjonssteder vil uønskede vindkrafthendelser, som variabilitet og null-hendelser, reduseres drastisk. I tillegg har vi sett på hvilke værsystemer som er forbundet med langvarige null-hendelser. Typisk vil langvarige null-hendelser, hvor vinden er for svak til å generere vindkraft, sammenfalle med et høytrykk lokalisert over de sammenkoblede vindparkene. På den andre siden, langvarige null-hendelser forårsaket av veldig høy vind vil typisk være forbundet med et lavtrykk nord for de sammenkoblede vindparkene.

Den andre artikkelen tar for seg hvorvidt NORA3 kan egne seg som et vindressursgrunnlag i planleggingsfasen av nye havvindprosjekter. Ved hjelp av statistiske metoder gjennomfører vi en grundig validering av vinddataene fra NORA3 i typiske vindturbinhøyder. Konklusjonen er at NORA3 er godt egnet for vindkraftestimering, men at datasettet tenderer mot å gi konservative estimat. For eksempel, modellen underestimerer den observerte vindkraftproduksjonen fordi modellen overestimerer antall hendelser med vind under en typisk nominell vindhastighet (u <11-13 ms^{-1}), og underestimerer antall hendelser med høy vindhastighet (u >11-13 ms^{-1}).

I artikkel tre presenterer vi et nytt vindkraftrelatert datasett: "NORA3-WP: A high-resolution offshore wind power dataset for the Baltic, North, Norwegian, and Barents Seas". Datasettet er basert på NORA3, og dekker områdene Nordsjøen, Østersjøen og deler av Norskehavet og Barentshavet. NORA3-WP er åpent tilgjengelig for nedlastning, og er generert for å tilrettelegge for at forskere, politikere og besluttningstakere enkelt skal ha tilgang til vindressurser og vindkraftrelatert data i planleggingsfasen av nye havvindprosjekter. NORA3-WP er det første vindkraftrelaterte datasettet som dekker hele den norske økonomiske sonen (NØS).

I den siste artikkelen tar vi i bruk relevante datasett (bl.a NORA3-WP) for å presentere den første kartleggingen av hvor egnet de norske havområdene er for vindkraftutbygging. Vi bruker en metode kalt "multi-criteria decision analysis (MCDA)" i tillegg til "analytical hierarchical process (AHP)" hvor vi inkluderer

kriterier innenfor vindressurser, teknoøkonomiske aspekt, sosial aksept, miljøhensyn og maritime begrensninger knyttet til vind- og bølgeforhold. Resultatet genereres gjennom en baseaktør. Denne aktøren har ikke sterke preferanser for ett sett av kriterier, men ser derimot viktigheten av en et prosjekt med økonomisk lønnsomhet, samt lav forutsetning for potensielle arealkonflikter. Hvor robuste resultatene er blir testet ved å opprette andre aktører med mer distinkte kriteriepreferanser for en fremtidig havvindpark: "investoren", "miljøaktivisten" og "fiskeren". Resultatene viser at den sørlige delen av NØS er relativt sett den best egnede og mest motstandsdyktige regionen for havvindutbygging. Den norske delen av Barentshavet og langs kysten av Midt-Norge er også områder som er godt egnet for havvindproduksjon, men her er resultatene mindre motstandsdyktige mot endringer i hvilke kriterier som er viktige.

Acknowledgements

Ida Marie Solbrekke
Bergen, April 2022

Finishing this PhD had not been possible without my main supervisor, Asgeir Sorteberg. He had faith in me when my self-belief was lost. I will forever be grateful. Thank you for our scientific discussions, all the laughter and talks about everyday life. Thank you for helping me, for your advice and understanding along the way. Thank you for finding time for me in your busy schedule, for giving me scientific freedom, and for being the reasonable one when my ideas got a bit far-fetched. I would also like to thank my co-supervisor, Nils Gunnar Kvamstø, for all the guidance through the first paper. Thank you for our interesting discussions and for your supervision.

A huge thank you to Øyvind Breivik, my phd-mentor, for having faith in me when I lost mine. Thank you for all your advice and motivation, and help with data retrieval. Thank you for all our mountain runs answering all my "during a PhD, is it normal to"-questions. Also, a thank you to Finn Gunnar Nielsen for all the scientific discussions and advice along the way, it has been a pleasure. To Ragnhild Nyheim and Torill A. Eidsvaag for cheering on me at a daily basis. A thank you to Kristin G. Frøysa for always reminding me of the relevance of my research towards the industry and the society. A huge thank you to Ole Johan Aarnes, Hilde Haakenstad and Magnar Reistad at the Meteorological intitute for providing data, answering questions, and for solving programming issues. Thank you to Lea Svendsen and Algot Peterson for proof-readings. To Ignacio Herrera Anchustegui for stepping up and helping me with legal issues related to offshore wind. Furthermore, a huge thank you to friends and colleagues at BOW and GFI for making the PhD-time both fun, pleasant and memorable.

Last but not least I would like to thank my dear family. Algot Peterson for cheering me up when I had troublesome days, and for celebrating with me during happy times. As he has gone through a phd-period himself his help and advice along the way have been priceless. Also, a huge thank you to my lovely boys, Jørgen and Magnus, for always putting a smile on my face as they light up and run towards me after a long day at work.

"Any fool can know. The point is to understand."

Albert Einstein

Contents

Preface i

Abstract iii

Abstrakt v

Acknowledgements vii

1 Motivation and background 1
1.1 Objectives and research questions 5

2 The Norwegian offshore wind resources and wind power 7
2.1 The wind resources 7
2.1.1 The fluctuating nature of the wind 8
2.2 Current and future power situation 12
2.2.1 Hydropower 12
2.2.2 The Norwegian offshore wind power potential 13
2.3 Wind power in numbers 14
2.4 The Norwegian offshore area 18

3 Data 21
3.1 Data from numerical weather prediction models 21
3.2 NORA3 22
3.3 NORA3-WP 23

4 Introduction to the papers 25

5 Future perspectives 29

6 Papers 31
Paper I 33
Paper II 51
Paper III 72
Paper IV 89

Bibliography 135

1 Motivation and background

The largest global emission driver is the energy sector (*IEA*, 2021a). The three main categories for global power production are fossil fuels (coal, natural gas, petroleum, etc,.), nuclear power, and renewable energy sources (RES), where the fossil part generates 63% of the global electricity production and 84% of the whole power sector (electricity, transport, and heat). See Fig. 1.1. The power sector needs to undergo massive changes in order for Norway and the rest of the World to fulfill their international obligations towards emission reduction targets.

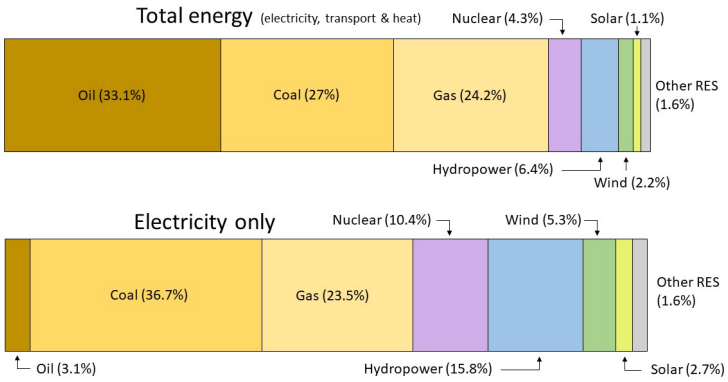

Figure 1.1: Primary energy and electricity mix. The figure is generated based on the numbers in the report by the British Petroleum (BP) from 2020 (British Petroleum (BP), 2020).

A factor threatening the emission reduction targets is the predicted increase in global energy demand. The U.S Energy Information Administration (EIA) projects an increase in the global energy demand of almost 50 % between 2018 and 2050, with the electricity consumption increasing even more (79%) (*Energy Information Administration (EIA)*, 2021). In the near future, the electricity demand will grow faster than the share of RES, making climate mitigation difficult (*IEA*, 2021b).

As a result of increased power demand and climate mitigation, RES have experienced an explosive growth over the recent years. In 2000 the total electricity generation from RES was slightly more than 2500 TWh. By contrast, in 2020 the total generated electricity from RES was 7500 TWh (*IEA*, 2021c); an increase of 300% in 20 years.

The amount of new global renewable capacity is also expected to increase. A report by *IEA* (2021a) predicts that during 2021-2026 the installed capacity of RES will increase by 50% compared to the installed capacity between 2015 and 2020. Wind energy, both onshore and offshore, will take a large portion of this growth in new installation and electricity generation in the years to come. Today,

the global electricity production from wind is around 1800 TWh. By 2026 this amount is predicted to be nearly doubled (3200 TWh) (*IEA*, 2021c).

Besides a general growth in installed wind capacity, IEA foresees a shift in wind energy technology use. After 2025, the share of electricity from onshore wind power will level out and the offshore share will increase rapidly. By 2040 the share of electricity from onshore wind power will intersect with the share from offshore wind power. This curve-crossing implies that by 2040 offshore wind power will constitute the largest portion of the electricity mix in the EU (*IEA*, 2019).

Floating offshore wind is an immature technology with a huge potential. *Bosch et al.* (2018) found that the majority (two third) of the global offshore wind energy potential is located at deep waters (> 60 m). For Norway, approximately 96 % of the offshore area has an ocean depth exceeding 60 m (see Fig. 1.2). Beyond 60 m the only economical feasible wind power option is floating technology (*Bosch et al.*, 2018). With a technology shift towards offshore and floating wind farms, the Norwegian offshore areas become attractive for wind power production.

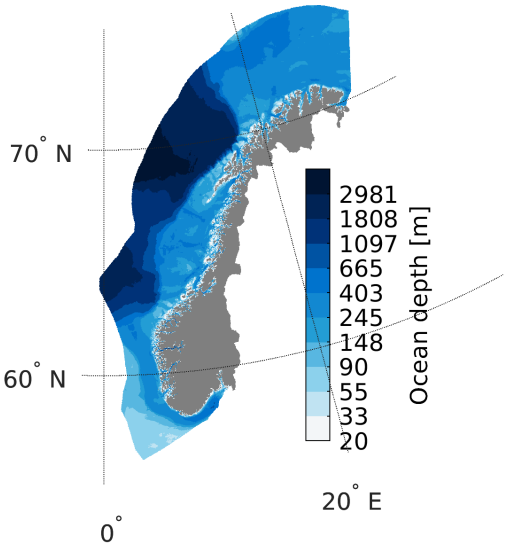

Figure 1.2: Ocean depth [m] at the Norwegian economic zone.

The wind power potential at the Norwegian offshore area is excellent. *Zheng et al.* (2016) mapped the global offshore wind power potential and ranked the areas outside Norway in the highest category, corresponding to a wind power potential of more than 400 Wm^{-2}. An offshore wind resource study by *Soares et al.* (2020) found the Norwegian offshore wind power potential to be between 800-1200 Wm^{-2}. *Bosch et al.* (2018) also state that Norway has one of the world's best offshore wind resources, with a potential of producing almost 16,000 TWh/year.

Despite the excellent offshore wind conditions no offshore wind farms are commissioned in the Norwegian waters. Yet, in June 2020 the Norwegian government

decided to open the first two offshore areas for concession of large-scale wind power production (*The Norwegian government*, 2020): Sørlige Nordsjøen II (SN2) and Utsira Nord (UN). SN2 is located on the border of the Danish Economical zone. SN2 covers 2591 km^2 and is planned to host 3 GW of bottom fixed wind turbines. UN is located west of Haugalandet on the Norwegian western coast. UN is smaller than SN, covering 1010 km^2. UN is located at deep waters (200-300 m), over the Norwegian trench, acquiring the licensed 1.5 GW to be floating wind power technology.

Opening of SN2 and UN marks the beginning of Norway's offshore wind power development. In February 2022, the Norwegian government assigned the Norwegian Energy and Water Directorate (NVE) to carry out an impact assessment in the context of opening more offshore areas for wind power application (*The Norwegian government*, 2022). Ensuring a sustainable large-scale exploitation of the Norwegian marine area requires among others an extensive and in-depth understanding of the wind resource.

An improved understanding of the wind resource is pointed out to be one of the grand challenges in wind energy research (*Veers et al.*, 2019; *Wood*, 2020). The wind resource spans multiple dimensions, where the energy originates from large-scale uneven heating of the Earth's surface and dissipates as heat in the surface layer. The first grand challenge is tied to dimensions; energy dissipates from large-scale through meso-scale to micro-scale, and the fact that processes in each dimension are modeled in fundamentally different ways. In this context, a large-scale mapping and improved understanding of the Norwegian offshore wind resource characteristics is important.

Mapping the wind resource requires good quality data. Since observations over open ocean are sparse, a comprehensive resource assessment requires among others high resolution wind resource and wind power related data covering the entire Norwegian offshore area. Until now, such data ensemble does not exist. However, a couple of high-resolution wind resource data sets do exist, like the New European Wind Atlas (NEWA) (*Dörenkämper et al.*, 2020) and the Global Wind Atlas (GWA) (*Badger and Jørgensen*, 2011). Both NEWA and GWA are downscalings of the new reanalysis product from the European Centre of Medium-Range Weather Forecasts (ECMWF); ERA5 (*Hersbach et al.*, 2020), using the Weather Research and Forecasting model (WRF). NEWA covers the European countries and parts of the surrounding offshore areas, while GWA has global onshore and near-coastal coverage. A high-resolution dataset covering the entire Norwegian offshore area is fundamental for a complete wind resource assessment. However, neither of these wind atlases (NEWA, GWA) cover the entire Norwegian offshore area.

Over the recent years the Norwegian Meteorological institute has generated a new, freely available, high-resolution dataset, called NORA3 (*Haakenstad et al.*, 2021). NORA3 is also a dynamical downscaling of ERA5, but is generated using a different numerical weather prediction model than NEWA and GWA; the HARMONIE-AROME model (*Seity et al.*, 2011; *Bengtsson et al.*, 2017). NORA3 provides hourly data in a 3×3 km horizontal grid for the Northern Europe, the Baltic Sea, North Sea, Norwegian Sea and parts of the Barents Sea, and thereby fully covers the Norwegian offshore area.

Utilizing this newly developed, freely available, high-resolution dataset (NORA3), covering the entire Norwegian marine environment, one of the aims in this thesis deals with an in-detail validation of NORA3 towards offshore wind resources and wind power estimates (paper II). The NORA3 dataset was not created specifically for wind power purpose. The near surface wind estimates (10 m.a.s.l.) are extensively validated against observations and compared against NORA10 and ERA5 reanalysis in *Haakenstad et al.* (2021). Nevertheless, a detailed near-hub-height validation towards wind power related variables is lacking. Therefore, using advanced statistical measures we perform a near-hub-height validation of NORA3 wind estimates and the related wind power production, demonstrating how NORA3 can serve as a wind resource data set in the planning-phase of future Norwegian offshore wind power installations.

Even though NORA3 provides wind data, an open access wind power related dataset for the entire Norwegian marine area does not exist. Upon analysis researchers, analysts, stakeholders, and decision makers have to generate their own wind power estimates from datasets like NORA3, NEWA, or GWA. This is computationally expensive and time consuming. In this context, a part of my thesis is tied to generate a freely, open-access wind power dataset based on NORA3. Paper III is a data descriptor enclosing the generation process of a wind power dataset covering the entire Norwegian marine area called; "NORA3-WP: A high resolution wind power data set for the Baltic, North, Norwegian, and Barents Sea". The purpose of NORA3-WP is to generate an easy access wind power dataset intended for use in research, governmental management and for stakeholders to attain relevant wind resource and wind power information in the planning phase of a new Norwegian offshore wind farm project.

Large-scale exploitation of the Norwegian offshore area for power production introduces a number of challenges, one of which is the variable nature of the energy source (*Veers et al.*, 2019; *Wood*, 2020). As the wind resource spans multiple spatial and temporal scales, this multi-scale characteristic together with technical turbine limitations result in a highly fluctuating power production and even power-discontinuities of various duration. However, fluctuating wind power production is shown to be dampened by connecting dispersed wind power farms (*Archer and Jacobson* (2007); *Dvorak et al.* (2012); *Grams et al.* (2017); *Kempton et al.* (2010); *Reichenberg et al.* (2014, 2017); *St. Martin et al.* (2015)). The idea behind connecting wind farms is that the linked sites experience different weather at a certain time. Thus, combining these wind farms creates one, area-aggregated, power production with reduced wind power fluctuations. No previous research have investigated this smoothing effect in European offshore areas, or more specifically in the Norwegian waters. Therefore, the first part of my thesis (paper I) investigates the wind power smoothing effect, through interconnection of wind farms in the Norwegian offshore area.

In addition to an in-depth understanding of the wind resource and its variability, a large-scale exploitation of the Norwegian offshore area requires a multi-disciplinary research focus to reduce or even avoid potential conflict of interests. The Norwegian marine environment is already used for multiple purposes (fishing, shipping, military activity, oil- and gas activity etc,.). In addition, ecologically valuable areas such as spawning grounds, bird nesting, and protected areas pose

limitations on areas available for offshore wind power deployment. Therefore, a sustainable use of the marine environment involves consideration of wind resources and techno-economic aspects, as well as social acceptance, environmental considerations, and met-ocean constraints. Through a unique ensemble of dataset (NORA3-WP, among others) the last part of my thesis facilitates for a sustainable development and usage of the Norwegian offshore area for energy extraction. Paper IV deals with addressing wind power suitability scores for the entire Norwegian marine environment in the context of pinpointing optimal sites for new offshore wind farms.

1.1 Objectives and research questions

Offshore wind power in the Norwegian marine environment is at an initial stage. This thesis evaluates and assesses the Norwegian offshore wind resources and addressing some of the challenges and opportunities therein. The following two main goals and underlying research questions were raised:

1. Assessing the Norwegian offshore wind power potential through observations and numerical data.
    (a) To what degree can unwanted wind power events, like variability and zero-production events, be reduced through wind farm interconnection in the Norwegian marine area?
    (b) Is it possible to link large-scale atmospheric situations to long-lasting wind power zero-production events?
    (c) To what degree can the 3-km Norwegian reanalysis (NORA3) serve as a wind resource data set for planning of offshore wind power application?
        i. Using offshore wind observations and data from the host reanalysis (ERA5) to perform an in-depth near-hub-height validation and comparison of NORA3.
    (d) Can we create a high quality, peer-reviewed, open access, wind power related dataset based on NORA3 covering the entire Norwegian offshore area to facilitate for stakeholders and decision-makers in the early planning-phase of new offshore wind projects?
2. Determine the offshore wind power suitability for the entire Norwegian marine area considering relevant parameters and potential conflicting interests.
    (a) Using Multi-criteria Decision Analysis (MCDA) and Analytical Hierarchical process (AHP); is it achievable to attain relative wind power suitability scores for the entire Norwegian economic zone considering wind resources, techno-economic aspects, social conflicts, environmental considerations, and met-ocean constraints?
    (b) Include different actors with distinct preferences for siting of a wind farm; how robust are these wind power suitability scores with respect to tuning of criteria-importance?

(c) Is it possible to pinpoint the most suitable Norwegian offshore area for wind power application?

2 The Norwegian offshore wind resources and wind power

This chapter gives an insight into the Norwegian climatological wind speed characteristics and why Norway has such favorable wind conditions. In addition, corresponding wind speed variability, the Norwegian offshore wind power potential, and a brief discussion of the Norwegian offshore area are also included.

2.1 The wind resources

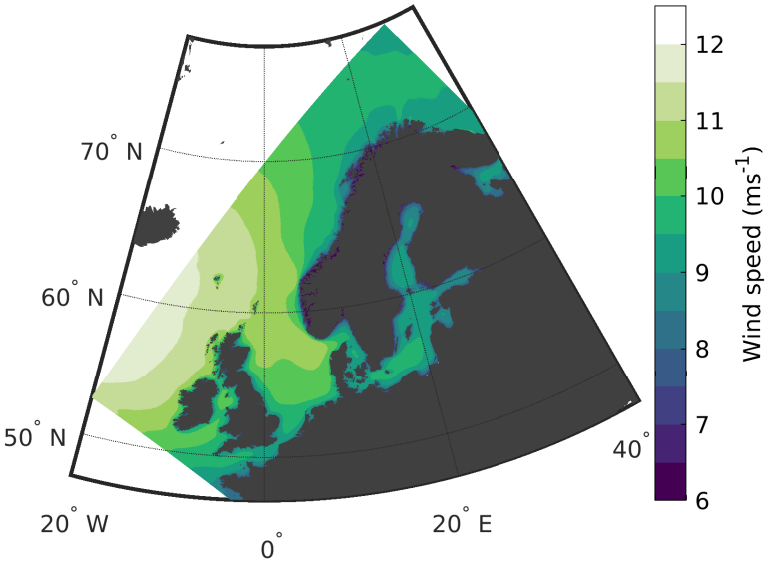

Figure 2.1: Average offshore wind speed (ms^{-1}) *from 1996-2019 at 150 m.a.s.l.. Data from NORA3-WP (Solbrekke and Sorteberg, 2022).*

The number of extra-tropical cyclones in the North Atlantic is high (*Hoskins and Hodges*, 2019). On average, these extra-tropical cyclones move from west to east, where the jet-stream[1] and these cyclones constantly influence each other. Traveling along the jet-stream, many of these low-pressure systems affect the weather in Norway and northern Europe.

The extra-tropical low-pressure systems are formed as cold air from the north meets the warm tropical air from south, creating a region with steep horizontal temperature and humidity gradients. A small disturbance along this sharp gradients create a chain reaction of events, where the upper and lower part of the atmosphere affect and reinforce each other. Ascend of warm and humid air

[1] A region of very strong winds caused by density reduction with altitude

and descend of cold and dry air convert potential energy into kinetic energy feeding this disturbance. As this disturbance grows alongside a flow-divergence the pressure drops creating a local low pressure. This local low pressure results in a spatial pressure gradient pointing towards the center of low pressure. To obtain equilibrium, air flows towards the center to eradicate the low air pressure. But, since the Earth rotates, the flow gets deflected towards the right (on the northern hemisphere) resulting in a low-pressure system rotating anti-clockwise. These rotating weather systems move warm and humid air northwards and cold and dry air southwards resulting in local, reduced, horizontal humidity and temperature gradients. This air-in-motion is what you and I refer to as *wind*.

Norway is located in the latitudinal belt where the meridional temperature gradient on average is sharp (around 60°N), resulting in frequent passage of extra-tropical cyclones. Due to the numerous passing of spatio-temporal weather systems at these latitudes the average Norwegian offshore wind speed is high. Figure 2.1 show the climatological offshore wind resource for the period 1996-2019 (data from NORA3-WP). The average wind speed range from 9-11 ms^{-1}. The highest wind speeds are found west of Scotland, with a general decrease towards east. Following this, Southern Norway experiences on average higher wind speeds than the Northern part of Norway. This climatological wind speed difference between the Southern and Northern Norway is tied to the fact that the low pressure systems more often is at an earlier stage in the life cycle, associated with more intense wind, when they struck Southern Norway.

Besides the general tendency of a reduced climatological wind speed from west to east, there are some geographical differences. Instead of an uniform decrease of wind speeds from west to east, relative high wind speeds extend all the way into the western and southern coast of Norway (see the light green patch extending all the way into the Norwegian coast in Fig. 2.1). This climatological wind speed pattern is a result of wind interaction with "Langfjella" mountain range . Langfjella extends 1000-2500 m into the atmosphere and splits eastern and western Norway trough this elongated mountain range. A flow interacting with Langfjella can generate flow acceleration or deceleration depending on the wind speed, wind direction, atmospheric stability, etc. (*Barstad and Grønås*, 2005).

Figure 2.1 also illustrates that the mean wind speed is higher along some of the fjord-axis. This increased mean wind speed in some of the fjords is tied to acceleration of air as the flow passes through a relative narrow fjord; if the available volume of air decreases the flow can accelerate to conserve mass.

Flow-topography interaction affects the local wind pattern, but also the climatological wind resources throughout the entire Norwegian offshore area, giving a wind speed climatology characterized by high and variable wind speeds.

2.1.1 The fluctuating nature of the wind

Areas with frequent passage of extra-tropical cyclones have favorable conditions for wind power production due to the high wind speed accompanying these systems. Furthermore, these systems also cause wind variability, both in space and time.

The wind encloses a wide range of spatial and temporal scales involving small

systems existing for a blink of an eye to annual, global patterns lasting for several years. These wind characteristics lead to a highly fluctuating wind resource and an even more intermittent wind power production.

The wind power production is not linearly following the wind speed, as illustrated by the straight, dashed line in Fig. 2.2. The wind power production is rather a function of the wind speed cubed (solid line). However, due to the turbine specifications and for sheltering purposes the actual wind power production ("WP production" in Fig. 2.2) is not following this cubed relation for all wind speeds. The turbine is not producing wind power when the wind speed is below the cut-in wind speed limit of the turbine. When the wind exceeds this limit the wind power production follows the cubed wind speed relation until the wind reaches the rated wind speed limit. When the wind speed is at and above the rated wind speed limit the turbine blades are pitched; some of the air passes the turbine blades without energy extraction. This is done to obtain maximum energy extraction and ensuring that the turbine does not exceed its maximum rotational speed. When the wind speed gets too strong (above the cut-out limit of the turbine) the wind power production is terminated. This is done to shelter the wind turbine and the equipment from the harsh drag forces from the wind. This non-linear relation between the produced wind power and the wind speed causes a highly fluctuating wind power production (see Fig. 2.3).

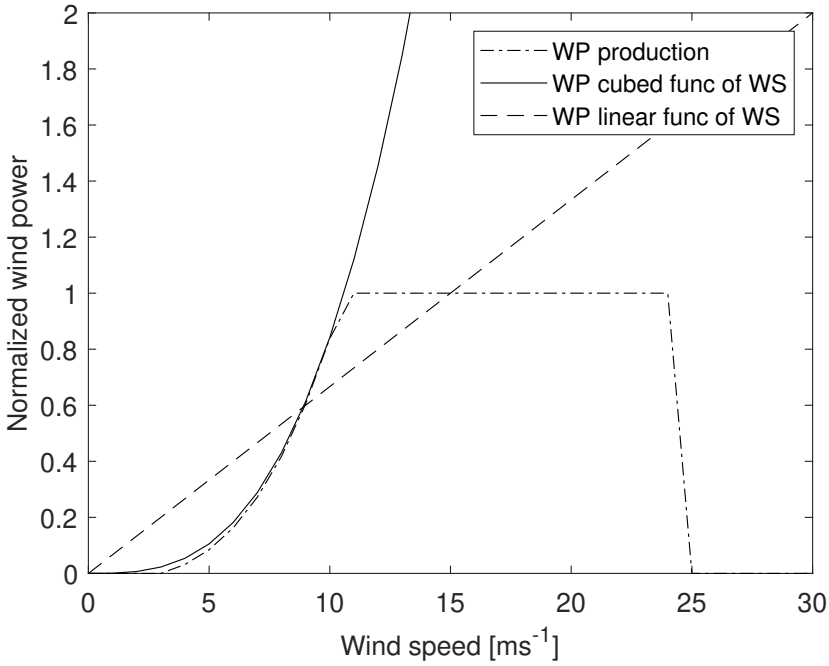

Figure 2.2: Different wind power production curves (normalized according to the "WP production curve") in relation to the wind speed [ms^{-1}]. WP: wind power; WS: wind speed; func: function. The cut-in, rated, and cut-out wind speed limits in the "WP production" curve are taken from the IEA 15 MW reference turbine (Gaertner et al., 2020).

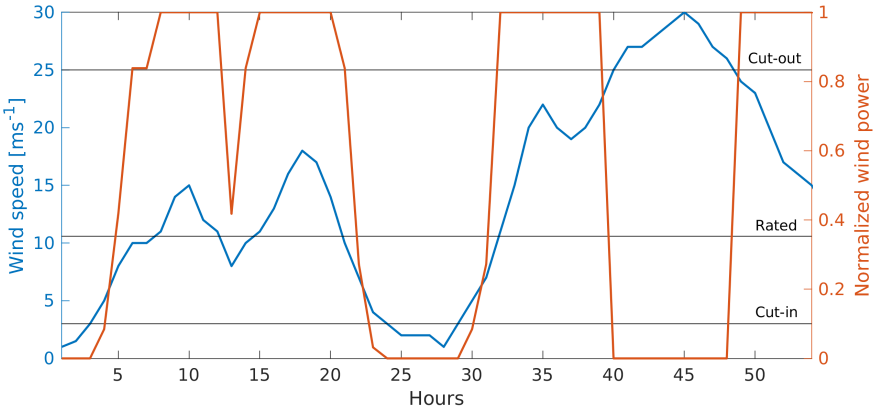

Figure 2.3: Wind speed time series (blue) and the corresponding wind power production (orange) calculated using the "WP production" curve from Fig. 2.2.

The wind power variability is an issue with several potential solutions, partially or fully solving the problem. One solution is to convert the wind energy into an energy carrier, like hydrogen (*Apostolou and Enevoldsen* (2019) and the references therein). Whenever the produced wind power exceeds the power demand, the surplus power is used to generate hydrogen. Later, when the power demand exceeds the generated wind power the stored power in the energy carrier is released. Another solution to mitigate wind power variability is to use pumped hydro storage (*Benitez et al.*, 2008). When the wind power exceeds the power demand, the surplus wind energy is used to pump water up to a reservoir increasing the potential energy of the water. Whenever there is a power demand exceeding the wind power production, the water is released, converting the potential energy into kinetic energy, generating electricity to cover the power deficit.

Interconnection of wind farms is another solution to the wind power variability issue. The wind power smoothing effect by coupling production sites was first studied by Kahn in 1979 (*Kahn*, 1979). Kahn evaluated the reliability of geographically distributed wind generators in a California case-study. As weather patterns are heterogeneous their spatial irregularity can be used for the sake of reducing wind power intermittency. The idea behind coupling allocated wind farms is that the interconnected sites will experience different weather at a certain time. Then, there will be a potential to reduce wind power variability as the wind farms are area-aggregated.

Interconnecting two wind farms with wind power correlation coefficient r = -1 would be ideal in terms of reducing wind power variability. Then, the combined power production would be completely out of phase and the sum of the individual power productions would be constant in time[2]. Figure 2.4 shows correlation coefficient (linear relation) between a hypothetical wind turbine at a point inside the area of Sørlige Nordsjø II (SN2), and all other grid-points in the NORA3-WP domain for the year 2004. Following from the figure is that no sites are completely

[2]given equally installed capacity at each wind farm

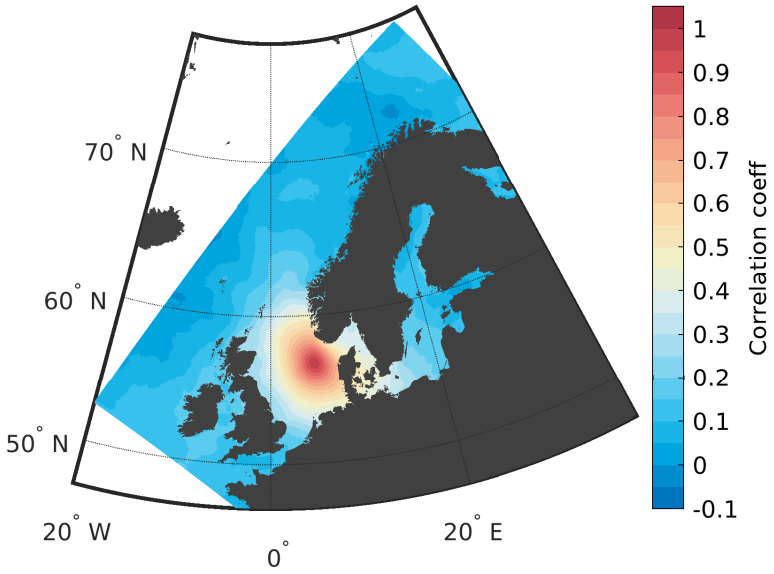

Figure 2.4: The correlation coefficient of hourly wind power production (2004) between a site inside the area Sørlig Nordsjøen II (lat: 56.81, lon: 05.30) and all other grid points covered by NORA3-WP. The power production is calculated using the DTU 10 MW reference turbine (Wang et al., 2020) using hourly wind power production data from NORA3-WP at 119 m.a.s.l. (Solbrekke and Sorteberg, 2022)

anti-correlated (r = -1) with SN2. However, some sites have r ≈ 0, meaning that the hourly wind power production at these sites are completely uncorrelated. The grid points close to SN2 have high correlation coefficient (r > 0.7), meaning that their hourly wind power productions are synchronized; when SN2 produces at rated power it is highly likely that the grid points in close proximity also produce at rated power. Combining a wind farm at SN2 with a wind farm at Utsira Nord (located off the Norwegian coast of Haugalandet, south of Bergen) would result in a r ≈ 0.6. This means that there is a co-variability between the sites, and that an interconnection would, to some extend, reduce some of the wind power fluctuations.

2.2 Current and future power situation

2.2.1 Hydropower

As mentioned in Sect. 2.1 the low pressure activity in Norway is high. In addition to ensuring good wind conditions these weather systems also transport atmospheric moisture. Precipitation forms and falls out as air rises and the moisture in the air condenses. The amount of precipitation that falls out depends on the moisture content in the atmosphere, the atmospheric stability, background flow, and the geographic location and topography. Bergen is a Norwegian city located on the west-coast, surrounded by steep mountains and located at the foot of the large Norwegian mountain range *Langfjella*. Since the prevailing wind direction in southern Norway is between south and west (*Barstad and Grønås*, 2005) the moist offshore air is pushed up the mountains, cools adiabatically, and precipitation forms and falls out. The annual precipitation is on average 2,500 mm/m^2, with maximum precipitation during autumn. The combination of moist air transportation by low-pressure systems and the Norwegian topography have contributed to hydropower being the backbone of Norwegian electricity generation for more than a century. In addition, this combination of flow direction and moist air is the reason why the main energy source for electricity generation in Norway is hydropower, constituting more than 90% of the Norwegian electricity generation. 1739 hydropower facilities, with an installed effect of 33 GW are producing on average 140 TWh/year (*The Norwegian Water Resource and Energy Directorate*, 2022).

Despite the large fraction of hydropower in the Norwegian electricity mix, the electricity demand increases alongside electrification of the society, and today's hydropower facilities are not producing enough to cover the predicted increase in Norwegian electricity demand of 30-50 TWh/year (*Statnett*, 2019). Therefore, alongside an increase in efficiency and installation of new hydropower facilities (total potential of 23 TWh/year (*The Norwegian Water Resource and Energy Directorate*, 2020)) to meet the predicted rise in energy demand, other renewable energy sources (RES) have to be exploited - one of which is offshore wind power.

2.2.2 The Norwegian offshore wind power potential

As discussed in Sect. 2.1, and illustrated by previous research (*Bosch et al.*, 2018; *Zheng et al.*, 2016) the Norwegian offshore wind resources are outstanding. Using data from the wind power dataset NORA3-WP (*Solbrekke and Sorteberg*, 2022) I have calculated the total wind energy potential for the entire Norwegian economic zone; approximately 14,000 TWh/year[3] (see Sect. 2.3 for more details). Comparing the total Norwegian offshore yearly wind power production to the yearly electricity generation from the hydropower, the offshore wind potential is 100 times larger than the current hydropower.

Some of the Norwegian offshore areas have wind conditions better suited for wind power exploitation than other areas. The capacity factor (CF) is a common performance measure of a wind turbine or a wind farm. For a given time period, CF is the fraction between the produced wind power and the maximum wind power production. CF values (onshore and offshore) typically range between 20-50 % (*Boccard*, 2009; *Bhandari et al.*, 2020), but higher vales are recorded. In March 2021, Hywind Scotland[4] hits a new 12-month record (March 2020-March 2021) with a CF-value exceeding 57%. With that, Hywind Scotland is the UK wind farm with the highest capacity credit (*Equinor*, 2021; *Energy Numbers*, 2021).

Figure 2.5 illustrates the average monthly CF (1996-2019) calculated using the IEA 15 MW reference turbine (*Gaertner et al.*, 2020) with data from NORA3-WP. Excluding the area northwest of UK, the highest CF values are found in the North Sea, exceeding 60%. In this region the turbines on average produce 60% of installed capacity. Further north the CF values are slightly lower, but still exceeding 50%.

An area south of southern Norway has CF values exceeding 65%. These high CF values occur due to the favorable wind characteristics for wind power production. This high CF region has the largest portion of wind speed events between rated and cut-out wind speed limits of the IEA 15 MW turbine (cut-in[5]: 3 m/s, rated[6]: 10.59 m/s, cut-out[7]: 25 m/s). This large portion of wind events between rated and cut-out wind speed limits is a result of an interaction between the air flow and the Norwegian topography. When the wind has a northerly component the flow is accelerated around the tip of Southern Norway. If the undisturbed wind speed is not too high the down-wind accelerated air stream would still be in the range of productive wind speeds; between the cut-in and cut-out wind speed limits. Or even better, the flow would transition from a wind speed between cut-in and rated to an accelerated flow that generates rated wind power production (between rated and cut-out wind speed limits). The flow-topography interaction in this region ensures a wind speed climatology highly favorable for wind power production.

Norway is fortunate; parts of this high-power-potential area, with CF-values

[3] excluding wake effects
[4] The World's first floating offshore wind farm
[5] The wind speed limit where the turbine starts to produce wind power
[6] The wind speed limit where the turbine transitions to produce maximum turbine capacity
[7] The wind speed limit where the wind power production is terminated

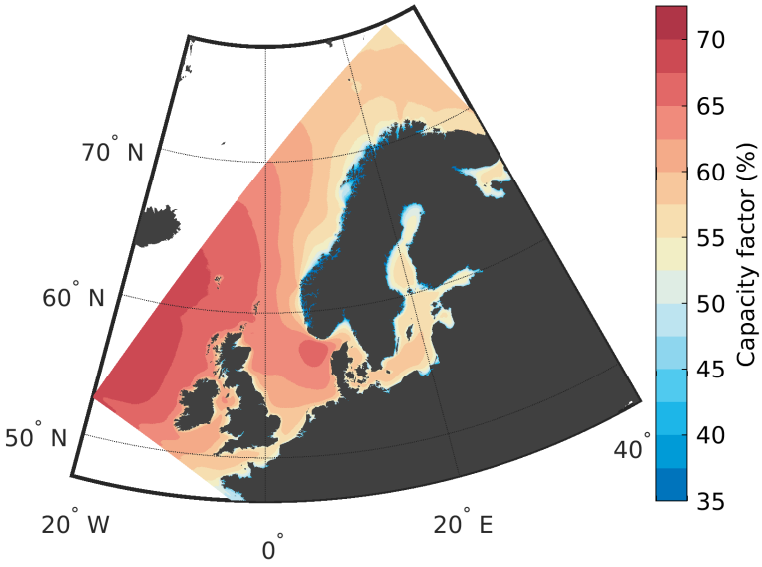

Figure 2.5: Average offshore monthly capacity factors (CF) for the period 1996-2019. The CF values are calculated using the IEA 15 MW reference turbine (Gaertner et al., 2020) and data from NORA3-WP (Solbrekke and Sorteberg, 2022).

exceeding 65%, are located in the Norwegian economic zone (NEZ). The Norwegian fraction of this area has the potential of producing on average 392 TWh/year (using IEA 15 MW reference turbines with 2 km spacing, and excluding wake effects). This would have covered all of Norway's final energy consumption in 2020 (211 TWh) almost two times (*Energy facts Norway*, 2022).

2.3 Wind power in numbers

Power is usually measured in *watt* [W]: *megawatt* (MW = 10^6 W), *gigawatt* (GW = 10^9 W), *terrawatt* (TW = 10^{12} W), etc,. *Watt* quantifies the amount of work carried out over a given time. Besides the "*40W*" printed on a light bulb or the amount of monthly energy consume (KWh) written on the electricity bill, most people are rather unfamiliar with *watt*, especially in large quantum. Therefore, using the NORA3-WP wind power dataset (*Solbrekke and Sorteberg*, 2022) I have put *watt* in a relevant context and made some comparisons for comprehensive purposes.

The new reference wind turbine developed by the International Energy Agency (IEA) is a 15 MW wind turbine with a rotor diameter of 240 m (*Gaertner et al.*, 2020). For comparison, the World's largest passenger airplane is an Airbus A380, with a wingspan of 80 m. Lining up three of these airplanes would fit inside the rotor disk of this turbine. Illustrated in Fig. 2.6.

If the IEA turbine produces rated power in 1 hour the generated power is 15

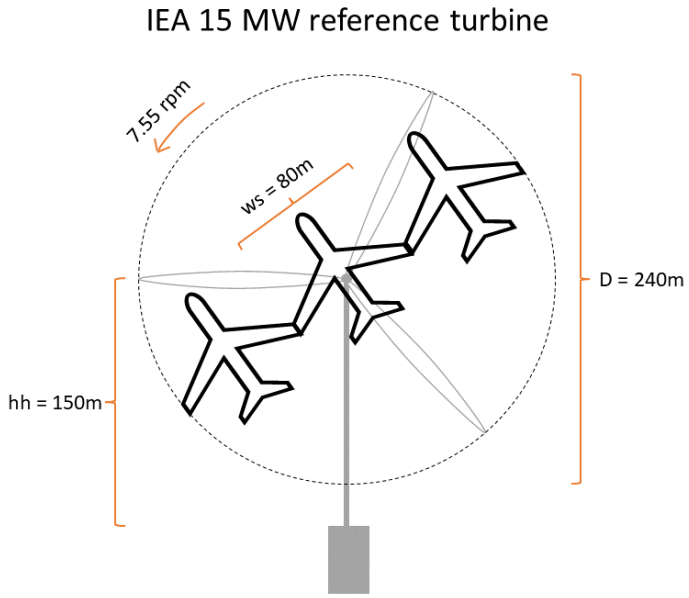

Figure 2.6: Illustrating the size of the IEA 15 MW reference turbine (Gaertner et al., 2020) by fitting three Airbus A380 (80 m wing span (ws)) inside the rotor disk. The turbine hub height (hh), rotor diameter (D), and rotational speed in rounds per minute (rpm) at and above rated wind speed (10.59 ms^{-1}) are also given.

MW $\times$ 1h = 15 MWh. Putting this number into context; how much electricity is 15 MWh? To fully charge the battery of a Tesla model X 75D, how many rounds does the IEA 15 MW turbine have to rotate? The IEA turbine rotates 7.55 rounds per minute (rpm) at and above the rated wind speed (10.59 ms^{-1}) (*Gaertner et al.*, 2020). That corresponds to 0.126 rounds per second (rps). The electrical range of a Tesla model X 75D is 75 KWh. The energy generated by the IEA 15 MW turbine in 1 sec is:

$$\frac{15MW}{3600s} = 0.0042\frac{MW}{s}. \tag{2.1}$$

The number of seconds the turbine have to generate at rated power to produce enough electricity to charge the Tesla model X:

$$\frac{0.075MW}{0.00412\frac{MW}{s}} = 17.98s \tag{2.2}$$

Lastly, the number of rounds the turbine rotates during that time is:

$$0.126rps \times 17.98s = \mathbf{2.26\ rotations}. \tag{2.3}$$

So, the IEA turbine have to rotate 2.26 rounds to generate enough electricity to charge the battery of a Tesla model X 75D from 0% to 100%.

The total yearly wind power production for the entire Norwegian economic zone (NEZ)[8] can be calculated to demonstrate the huge potential of the Norwegian offshore wind resource. Assuming a turbine spacing of 2 km, corresponding to ≈ 8 turbine diameters of the IEA 15 MW turbine. To obtain data every 2 km I perform a nearest-neighbor interpolation of the 3 km NORA3-WP wind power data. Subsequently, the total sum of yearly wind power at NEZ (excluding wake losses) is obtained by summing the generated wind power for all the grid points:

$$\sum_{x=1}^{X} \overline{P_h^w} \times 8760h = \mathbf{14{,}000\ TWh}, \tag{2.4}$$

where X is the number of grid points in the downscaled NORA3-WP grid, one for every 2 km. $\overline{P_h^w}$ is the monthly average of hourly wind power production for each grid point, and 8760 is the numbers of hours in a year. So, the total yearly wind power production at NEZ is 14,000 TWh. If an offshore area with wind turbines were to produce the same amount of yearly electricity production as the hydro power (140 TWh), the average area needed would be:

$$\frac{140TWh}{14000TWh} = 0.01. \tag{2.5}$$

Hence, only 1% of the Norwegian offshore area is needed to produce on average 140 TWh/year using wind turbines.

How large area corresponds to 1 % of NEZ? Total area on NEZ is obtained by multiplying the number of grid point inside NEZ with the grid-point area of 3×3 km. Recalling that NORA3-WP has 652 grid point in X-direction and 1149 grid points in Y-direction, in total 749148 grid points. However, only 104620 of the grid points are a part of NEZ. Thus, the area of NEZ is

$$A_{NEZ} = 104620 \times 3000m \times 3000m = 9.416 \times 10^5 km^2. \tag{2.6}$$

So, 1% of NEZ = $\mathbf{9416\ km^2}$, corresponding to a square with sides = 97 km (see pink square in Fig. 2.7). In other words, the same amount of yearly electricity as provided by the Norwegian hydropower (140TWh/year) can be produced by installing 1850 of IEA's 15 MW turbine in the square with area of 9416 km^2. In terms of energy density, the wind power will provide $\frac{140TWh}{9416km^2} = 0.015\frac{TWh}{km^2}$. Considering the area of the reservoirs, the hydropower provides $\frac{140TWh}{5930km^2} = 0.024\frac{TWh}{km^2}$ (*The Norwegian society for the Conservation of Nature*, 2021). Thus, the hydropower is more area efficient, providing more electricity per area, than offshore wind power.

The electricity demand for Norwegian households is on a good trend. The electricity consumption for an average household has decreased since 1993. In 2016, the yearly electricity demand for an average Norwegian household was 16,000 KWh (*Statistics Norway*, 2018). Installing wind turbines in the entire NEZ, with 2 km spacing, will on average provide $\frac{14{,}000TWh/year}{16{,}000KWh/year}$ = 875,000,000 Norwegian households with electricity. This is 328 times as many households that actually

[8]The Norwegian economic zone (NEZ) usually refers to the offshore area from 12-200 nm from the Norwegian baseline. Here, NEZ also includes the territorial waters (0-12 nm).

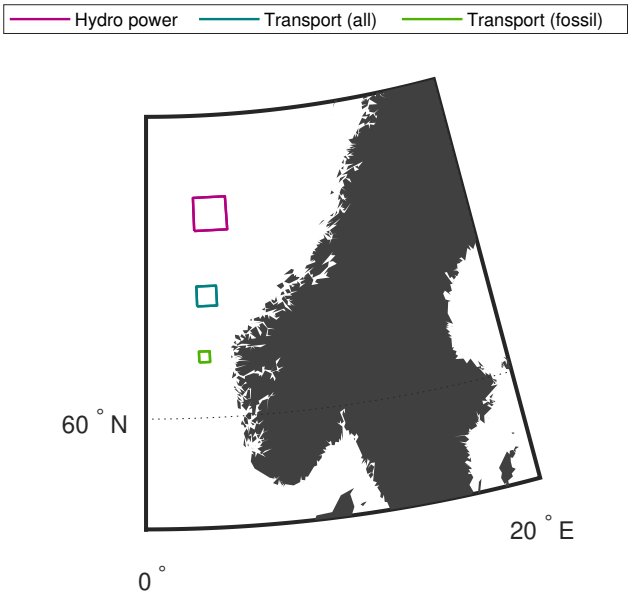

Figure 2.7: Required offshore areas with wind turbines to produce the same amount of yearly electricity provided by the hydro power (140 TWh/year, pink square) and final energy consumption for transport (52 TWh/year in 2020, petrol square). The green square corresponds to an area producing enough wind power to cover the fossil part of the transportation (44.7 TWh) taking into consideration the engine efficiency (90% efficiency of electric transportation compared to 30% for the fossil transportation) (Energy facts Norway, 2022).

exist in Norway (Norwegian households in 2022: 2,666,507 (*Statistics Norway*, 2022)).

Besides electricity for households, the area required for offshore wind power can also be compared to other sectors and consumers. The final energy consumption in Norway in 2020 was 211 TWh, where the transport sector used 52 TWh (*Energy facts Norway*, 2022). 86% of the energy used for transportation came from fossil energy sources. If 100 % of the energy needed for transportation were to be replaced by offshore wind energy, the required area would be a square box of 59 km×59 km. See the turquoise square in Fig. 2.7. However, replacing the fossil part of the transportation (86% = 44.72 TWh) with electricity form wind turbines, and taking into account the that a fossil-fueled engine has an efficiency of ≈ 30% compared to an efficiency of ≈ 90% of an electric car, this results in;

$$P = \frac{44.72 \times 0.3}{0.9} = 14.9TWh, \tag{2.7}$$

where P is the actual energy needed to be produced by the wind turbines in order to replace the fossil fuel part of the transport sector. Producing 14.9 TWh/year requires only a square with sides of 32 km, hosting 256 of IEA's 15 MW turbine. See the smallest square in Fig. 2.7.

2.4 The Norwegian offshore area

Norway has the longest coastline in Europe. The majority of Norway's mainland boarder is not connected to another country but rather to the open ocean. In 1976, decided by law and in accordance with the United Nations Convention on Law of the Sea (UNCLOS), an area extending 200 nautical miles offshore from the Norwegian baseline was created and named *The Norwegian Economic Zone* (NEZ). Creating this zone ensures Norway's right to the resources and to regulate the traffic and economic activities in the offshore area in the close proximity to the Norwegian mainland.

The total Norwegian offshore area is approximately 941600 km^2, where only 1% of the area installed with wind turbines would on average generate the same amount of yearly electricity as the hydropower (140TWh/year). Despite the small area required, decisions regarding new areas for wind power deployment are not only a function of the wind resources, but rather a multidisciplinary issue affecting many parties and interests.

The Norwegian offshore area is used for various purposes and activities, like; shipping, fishing, oil and gas production, and military practice. For instance, the fishing industry contributes to 4% of the Norwegian GDP (*SINTEF*, 2018). Using the data in NORA3-WP 104620 grid points are located in the Norwegian economic zone (NEZ)[9], where 589 of these are occupied with oil and gas activities, corresponding to only 0.6% of the area of NEZ. Despite the small occupied area, the oil and gas sector is Norway's largest in terms of value creation, revenues for the governments, investment and export value (*Norsk Petroleum*, 2022a). In the North Sea there are 71 oil and gas fields in production, 21 in the Norwegian Sea and 2 in the Barents Sea (*Norsk Petroleum*, 2022b).

In addition to fishing, shipping, and oil and gas production there are ecologically valuable areas critical for the sub-sea biodiversity, and areas important for fish growth and spawning. Also, coastal areas for bird-nesting also need to be treated carefully. In addition, there are protected areas gathered in a marine protected plan posing limitations for new offshore activities. All of these fields need careful consideration in the process of future wind farm siting to reduce or even avoid conflicts.

In 2010 the Norwegian Government decided to generate a national strategy for extraction of energy from wind and other renewable resources at NEZ. The Norwegian Government assign the The Norwegian Water Resource and Energy Directorate (NVE) the task to carry out a strategic impact assessment for the Norwegian marine area regarding wind offshore wind power production. The report was finished in 2012 enclosing offshore wind resources and the potential wind power production for 15 pre-selected offshore areas at NEZ (*The Norwegian Water Resource and Energy Directorate*, 2012).

Based upon the report from NVE the Norwegian government, through the ministry of petroleum and energy, decided in June 2020 to open two of these 15 pre-selected areas for large-scale offshore wind deployment; Utsira Nord (UN) and Sørlige Nordsjøen II (SN2) (*The Norwegian government*, 2020). UN is an area

[9]The Norwegian economic zone (NEZ) usually refers to the offshore area from 12-200 nm from the Norwegian baseline. Here, NEZ also includes the territorial waters (0-12 nm).

covering ≈ 1000 km^2 and is located off the coast of Haugalandet, south of Bergen. This area is decided to host 1.5 GW of wind turbines distributed on three to four wind farms. SN2 is a larger area covering ≈ 2600 km^2 and is located on the border to the Danish economic zone. At SN2 the 3 GW of prescribed installed wind power capacity will be distributed into three wind farms.

Besides the opening of UN and SN2 the Norwegian government will in the years to come open several Norwegian offshore areas for wind power application, both in the context of national emission reduction targets, to ensure energy security, and to meet the increasing electricity demand. Deciding to open new areas is an extensive and thorough process, and a lot has happened during the last 10 years since the release of the report from NVE, especially regarding high resolution wind resource datasets. Following this, in February this year the Norwegian government, for the second time, assigned NVE to the task of carrying out a new strategic impact assessment in the context of opening even more Norwegian offshore areas for wind power deployment (*The Norwegian government*, 2022).

3 Data

The scientific results in this thesis are mainly based on numerical data from *The 3 km Norwegian reanalysis (NORA3)* (*Haakenstad et al.*, 2021). Observational data have been used to quantify the effect of interconnecting wind farms for the purpose of reducing unwanted wind power events in the North and Norwegian Seas (Paper I). Observational data are also used in the near-hub-height validation of the NORA3 (Paper II).

The observed data used in paper I and II are recorded at six oil and gas platforms and one met-mast, see Table 3.1. More information on the sites and the observational data, in addition to a detailed description of the post-processing routine of the observation are found in Paper I and Paper II.

Table 3.1: Name, site positions (lat, lon), wind sensor height (m.a.s.l.), and the water depth [m] in the area are listed. The sensor at Ekofisk is listed with two heights, since the sensor was moved from 69 m.a.s.l. to 103 m.a.s.l. in 2004.

Platform	Lat	Lon	Sensor height [m]	Water depth [m]
Fino1	54.02	06.59	102	28
Ekofisk	56.55	03.21	69/103	75
Sleipner	58.36	01.91	136	110
Gullfaks C	61.22	02.27	141	216
Draugen	64.35	07.78	78	250
Heidrun	65.33	07.78	131	350
Norne	68.01	08.07	45	380

3.1 Data from numerical weather prediction models

A large part of this thesis concerns processing and usage of data from a numerical weather prediction (NWP) model. Data from NWP models are generated by solving primitive prognostic equations describing time evolution of physical variables. Since these equations are nonlinear partial differential equations, impossible to solve exactly through analytical methods, the evolution of these prognostic variables are discretized. This means that the derivatives of the equations are approximated by finite differences, breaking the problem into a finite number of steps allowing for an approximated solution to each variable in any of these finite steps. The NWP models produce a forecast or a hindcast/reanalysis by using the solution to the equations at time step t to calculate an approximated solution at time step $t+1$, and so on.

Data from NWP models can either be model output created as iterations going from the present (t) and into the future ($t+1$) creating a "forecast". Or, the model can solve the equations starting sometime in the past ($t-1$), integrating forward in time and reconstructing the past, ending at the present date (t), called a "hindcast" or "reanalysis". Unlike a weather forecast, where the model uses an analysis as the starting point, a reanalysis uses a mix of observational data

with a short-range forecast as the starting-point for the iterations. The main difference between a reanalysis and a hindcast is tied to whether the NWP model assimilates observations and/or satellite data or not; A reanalysis is generated using data assimilation, hindcast is not.

The NWP model provides one output for each grid cell in the model domain, in this case one value for every 3 km. This grid-value will be representative for the whole grid cell (3×3 km) and can therefore be viewed as a spatial averaged grid-cell value.

3.2 NORA3

Forming the basis for paper II, III, and IV is the "*The 3 km Norwegian reanalysis (NORA3)*" created by the Norwegian Meteorological institute (*Haakenstad et al.*, 2021). NORA3 is the first high-resolution climatological description produced with non-hydrostatic model physics covering the Baltic Sea, North Sea, Norwegian Sea, and the Barents Sea. NORA3 has a horizontal resolution of 3 km, producing mainly hourly data for 65 vertical layers. Upon finalizing, NORA3 will cover the time-period from 1979 to present, and will continuously be updated in the years to come.

NORA3 is a result of a dynamical downscale of the recent ERA5 reanalysis from the European Centre of Medium-Range Weather Forecast (ECMWF) (*Hersbach et al.*, 2020). The fields from ERA5 reanalysis provide the initial and boundary conditions, and the downscaling process is carried out using the non-hydrostatic convection-permitting NWP model HARMONIE-AROME, Cy 40h1.2 (*Seity et al.*, 2011; *Bengtsson et al.*, 2017). For the 65 vertical levels HARMONIE-AROME uses a terrain-following pressure-based vertical σ-coordinate (*Simmons and Burridge*, 1981; *Laprise*, 1992). The lowest model level is found at 12 m and the uppermost at 10 hPa, and iterates at a the time step of 60 s, storing hourly model outputs.

A hindcast is generated without using any observations. Since NORA3 is generated based on its own initial conditions, assimilating surface temperature and humidity, NORA3 is actually a reanalysis. Besides assimilating surface temperature and humidity, the rest of the initial surface fields are taken from the previous NORA3 forecast, where the former forecast is adjusted through a combination of surface analysis and the surface-flux method SURFEX[1]. The generation of NORA3 is based on a series of short model runs. Each model run proceeds for nine hours, where the first three hours (from 0 to +2h) of the model run are spin-up, and are not stored. Hence, the data stored in a model run correspond to forecast time +3 to +9. Then, the procedure is repeated until the data for whole time period are downscaled.

Haakenstad et al. (2021) generates NORA3 and documents the generation process. Creating a new dataset from a NWP model requires validation of the model output. *Haakenstad et al.* (2021) perform a near-surface validation of the dataset at 10 m.a.s.l.. They find the near-surface wind field to be greatly improved over its

[1]SURFEX is a land and ocean surface platform describing surface fluxes for four types of surfaces: nature, town, inland water and ocean. (*Masson et al.*, 2013)

host analysis (ERA5), particularly in areas with complex terrain, and along the improved grid-resolving coastlines. NORA3 also outperforms the earlier hydrostatic 10-km Norwegian Hindcast Archive (NORA10) (*Furevik and Haakenstad*, 2012), especially over land. Compared to NORA10 and ERA5, NORA3 is also better at capturing detailed structures of polar lows, and has a lower model bias of maximum wind speeds observed in extratropical cyclones.

More details on the model setup of HARMONIE-AROME upon generating NORA3, physical parameterizations, implementation of surface analysis, land and ocean surface processes, forcing data and model runs, and the near-surface validation results of NORA3 can be found in *Haakenstad et al.* (2021).

3.3 NORA3-WP

"NORA3-WP: A high-resolution wind power data set for the Baltic, North, Norwegian, and Barents Seas" is the wind resource and wind power related data repository generated as a part of this thesis. Nine of the variables stored in NORA3-WP are demonstrated in Fig. 3.1.

Detailed information on the NORA3-WP, the generation process, and example of usage can be found in Paper III.

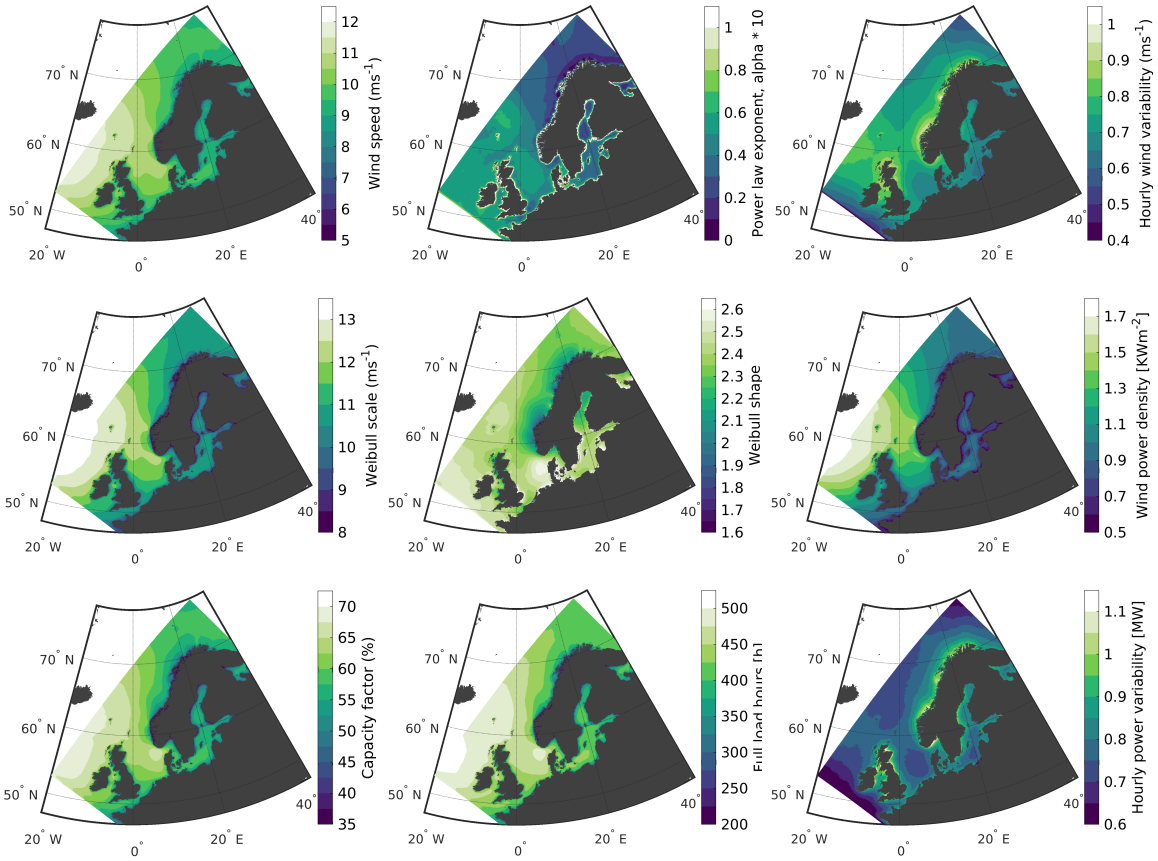

Figure 3.1: Climatological data fields (average between 1996-2019) for nine of the variables in the NORA3-WP dataset. The wind speed related data are valid at 150 m.a.s.l. and the wind power related data are calculated using the IEA 15 MW reference turbine (Gaertner et al., 2020).

4 Introduction to the papers

Paper I: **Mitigation of wind power intermittency through interconnection of production sites**

Solbrekke, Ida M., Kvamstø, Nils G., Sorteberg, Asgeir. (2020), Wind Energy Science, 5(4)

Objectives: Assessing the wind power potential using observations from five offshore sites in the North Sea and Norwegian Sea. Moreover, determine to what degree unwanted wind power events, like variability and zero-production events, can be reduced through interconnection of the five sites in various configurations.

Summary: In paper I we use a unique set of hourly wind speed data observed over a period of 16 years to assess the wind resource and quantify the potential of interconnected offshore wind power production. The study addresses the well-known wind power intermittency problem for five locations along the Norwegian continental shelf. Mitigation of wind power intermittency is investigated using a hypothetical electricity grid. The degree of mitigation is examined by connecting different configurations of sites. Along with the wind power smoothing effect, we explore the risk probability of the occurrence and duration of wind power zero-events due to too low/high winds. Lastly, typical large-scale atmospheric situations resulting in long term shut-down periods are identified.

Main findings:

- For the five sites, the mean wind speeds at 100 *m.a.s.l.* are high, ranging from 9.97 ms^{-1} to 11.25 ms^{-1}.
- Sleipner is the site that most frequently operates at rated power, 31 % of the time. Out of the five sites, Sleipner has the most suitable wind speed characteristics for wind power applications, with the largest portion of the wind speed distribution falling between rated and cut-out wind speed limits.
- Both the wind power variability and the risk of not producing any wind power decrease significantly with an increasing array of connected sites. The risk of no wind power production for a given hour is reduced from 8.0-11.2 % for a single site to less than 4 % for two sites. Increasing the array-size further reduces the risk, but to a lesser extend.
- The pairwise correlation between sites drops off quickly as the distance between the sites increases. However, after $\approx$ 800 km the correlation is reduced to 0.1 and continues to decrease more slowly with increasing distance.
- The average atmospheric weather pattern resulting in wind speed that is too low (too high) to produce wind power is associated with a high- (low-) pressure system near the production sites.

Paper II: **The 3-km Norwegian reanalysis (NORA3) - a validation of offshore wind resources in the North Sea and the Norwegian Sea**

Solbrekke, Ida M., Sorteberg, Asgeir, Haakenstad, Hilde. (2021), Wind Energy Science, 6(6)

Objectives: Determine if the 3-km Norwegian reanalysis (NORA3) can serve as a wind resource dataset for planning of offshore wind power applications. For that, an in-depth near-hub-height validation was carried out using observations, in addition to a comparison with the host reanalysis (ERA5).

Summary: In paper II we carry out an extensive near-hub-height validation of the new high-resolution reanalysis (NORA3) for offshore wind power purposes. The 3-km Norwegian reanalysis (NORA3) is a dynamically downscaled dataset, forced with state-of-the-art atmospheric reanalysis as boundary conditions (ERA5). We conduct an in-depth validation of the near-hub-height simulated wind climatology towards observations to determine whether NORA3 can serve as a wind resource dataset in the planning phase of future offshore wind power installations. We put special emphasis on wind power related matrices and on evaluating the impact of simulated wind speed deviations on the wind power production and the related variability.

Main findings: The NORA3 dataset is well suited for wind power estimates, but gives slightly conservative estimates on the offshore wind metrics:

- Wind speeds in NORA3 are typically 5 % (0.5 ms^{-1}) lower than observed wind speeds.
- For a selected turbine, the simulated wind speed bias results in an underestimation of offshore wind power of 10-20 %.
- NORA3 is biased towards lower wind power estimates due to an underestimation (overestimates) of wind speed events exceeding (below) typical rated wind speed limits (u >(<) 11-13 ms^{-1}).
- The hourly wind speed and wind power variability are slightly underestimated in NORA3. However, the number of hours with zero power production caused by the too high/low winds is well captured.
- The model performs well in capturing spatial co-variability, with only small deviations in the spatial correlation coefficients among the sites.

Paper III: **NORA3-WP: A high-resolution offshore wind power dataset for the Baltic, North, Norwegian, and Barents Seas**

Solbrekke, Ida M., Sorteberg, Asgeir. (2022), in review at Scientific data - Nature

Objectives: Create an open access, high resolution, wind power related dataset, based on NORA3, covering the entire Norwegian offshore area, to facilitate for stakeholders and decision-makers in the early planning-phase of new Norwegian offshore wind projects.

Summary This paper is a data repository describing the content and the generation process of a new wind resource and wind power dataset called "NORA3-WP: A high-resolution wind power dataset for the Baltic, North, Norwegian, and Barents Seas" . NORA3-WP is an open access data set covering the entire Norwegian offshore area. The dataset is intended for use in research, governmental management and for stakeholders to attain relevant wind resource and wind power information in the planning phase of new wind farm project. The variables are available as monthly data, and provides climatological data of 25 wind resource and wind power related variables for the ocean areas surrounding Norway for three selected turbines. In addition, the underlying hourly wind speeds and hourly wind power generation for the three selected turbines are also available for higher frequency analysis and case-studies.

Paper IV: **Offshore Wind Farm Siting - Suitability Scores for the Norwegian Economic Zone Using Multi-Criteria Decision Analysis**

Solbrekke, Ida M., Sorteberg, Asgeir. (2022), submitted to Energy Policy

Objectives: Determine the offshore wind power suitability for the Norwegian economic zone considering relevant parameters and potential conflicting interests. In addition, investigate the robustness of the wind power suitability scores through tuning of relevant criteria-importance. Lastly, pinpointing the most suitable Norwegian offshore area for wind power application.

Summary: In Paper IV we utilize the framework of multi-criteria decision analysis (MCDA) with an analytical hierarchical process (AHP) approach to derive unique wind power suitability scores (WPSS) for the entire Norwegian marine area considering five main goal-affecting criteria: "Wind resource attractiveness" enclosing data on the nature of the wind; "techno-economic aspects" reflecting the wind farm investment costs; "social acceptance" includes interests of potential area conflicts; "environmental considerations" consisting of areas with valuable marine life; and "met-ocean constraints" encloses the wind farm accessibility and related design requirements adapted to the Norwegian offshore environment. The robustness of the result is tested through three additional scenarios, reflecting characters with distinct priorities and focus areas for a wind farm: "the investor", "the environmentalist", and "the fisherman".

Main results:

- In general, the southern part of the Norwegian economic zone receives the highest WPSS. The Norwegian part of the Barents sea also receive rather high WPSS and along the coast of mid-Norway. These areas have optimal combination of wind resources, techno-economic aspects, social acceptance, environmental considerations, and met-ocean constraints.
- Generating characters with distinct priorities for a wind farm involving tuning of the criteria-importance demonstrate that the main result is vigorous to changes in the criteria priority, but that some areas are rather sensitive, e.g. in the Barents Sea.
- In general, regions with many conflict of interests and/or low wind power potential receive low WPSS.
- The MCDA method using AHP is a promising tool for optimal offshore wind farm siting, but that the results obtained are tied to the choice of MCDA method and the considered criteria.

5 Future perspectives

This thesis synthesizes studies assessing and evaluating the large-scale Norwegian wind resources in the context of future offshore wind power deployment. In addition, issues related to wind power intermittency and optimal wind farm siting have also been addressed.

In paper I the reduction of wind power intermittency and zero-production events through interconnection of wind farms clearly show the advantage of a more coupled electricity grid. The ability to exploit the large scale variability in weather systems will be increasingly more important as wind power is projected to constitute a larger potion of the electricity mix in the future (*IEA*, 2021c). As the five sites used in paper I mainly were located along a north-south axis, a natural next step would be to investigate the sensitivity of the smoothing effect regarding spatial orientation of the connected sites. As the main source of weather variability over open ocean is tied to the passage of extra-tropical cyclones traveling from west to east, it would be of interest to investigate, and potentially quantify, if there are any differences in the smoothing effect between coupling sites along a east-west axis compared to north-south oriented sites. Future research questions regarding the smoothing effect for connected wind farms at the Norwegian offshore areas:

1. Given that all locations in the North Sea and the Norwegian Sea could be used for wind power production; where are the best sites for interconnection in terms of a) reducing intermittency, and b) maximizing power output.

2. Is the wind power correlation between production sites largest in the east-west or the north-south direction?

3. Should the installed capacity at each production site be unequal in terms of a) reducing intermittency, and b) maximizing power output.

Wake effects are excluded in this thesis. In reality, wake effects are not negligible. Large-scale exploitation of the Norwegian offshore area for wind power application can through wake effects disturb the offshore wind conditions for neighboring wind farms, both in the NEZ and in the exclusive economical zones of neighboring countries. To what extent the "theft of wind resources", especially along international borders, actually occurs is unknown. Looking into this will be necessary to avoid conflicts with neighboring countries. This rise the following future research questions regarding wake effects across domestic and international borders:

1. Since Sørlige Nordsjøen II (SN2) is located on the border of the Danish economic zone (DEZ); on average, how far down-wind into DEZ does the wind-farm wake extend?

2. How sensitive is the spatial extent of the wind-farm wake to the upwind wind characteristics, sea state, and atmospheric stability, etc?

In paper IV we have used the framework of multi-criteria decision analysis (MCDA) and analytical hierarchical process (AHP) approach for the purpose of obtaining wind power suitability scores (WPSS) for the entire Norwegian economic sone (NEZ). However, like all MCDA-based studies, the results obtained are to some extent constrained by the choice of method (i.e., AHP), the data quality, the selected criteria, and their subjective pairwise comparison. Therefore, an advancement would be to challenge the aforementioned limitations to investigate how the method, data, and criteria affect the results. The following research questions related to paper IV could be addressed in the future:

1. Considering excluded criteria, such as icing on turbines, soil conditions, regulatory regimes, and wind-farm interconnection to the continent, etc.: to what degree does an inclusion of these criteria influence the WPSS?

2. By deriving WPSS using a different methods; how sensitive are the WPSS to the choice of method?

6 Papers

Paper I

Mitigation of offshore wind power intermittency by interconnection of production sites

Solbrekke, Ida M., Kvamstø, Nils G., Sorteberg, Asgeir
Wind Energy Science, **5/4** (2020)

Wind Energ. Sci., 5, 1663–1678, 2020
https://doi.org/10.5194/wes-5-1663-2020

eawe european academy of wind energy
Open Access
WIND ENERGY SCIENCE

Mitigation of offshore wind power intermittency by interconnection of production sites

Ida Marie Solbrekke[1,2], **Nils Gunnar Kvamstø**[1,2,3], **and Asgeir Sorteberg**[1,2,3]

[1]Geophysical Institute, University of Bergen, Allegaten 70, 5020 Bergen, Norway
[2]Bergen Offshore Wind Centre (BOW), University of Bergen, Bergen, Norway
[3]Bjerknes Centre for Climate Research (BCCR), University of Bergen, Bergen, Norway

Correspondence: Ida Marie Solbrekke (ida.solbrekke@uib.no)

Received: 3 April 2020 – Discussion started: 13 May 2020
Revised: 3 September 2020 – Accepted: 14 October 2020 – Published: 26 November 2020

Abstract. This study uses a unique set of hourly wind speed data observed over a period of 16 years to quantify the potential of collective offshore wind power production. We address the well-known intermittency problem of wind power for five locations along the Norwegian continental shelf. Mitigation of wind power intermittency is investigated using a hypothetical electricity grid. The degree of mitigation is examined by connecting different configurations of the sites. Along with the wind power smoothing effect, we explore the risk probability of the occurrence and duration of wind power shutdown due to too low or high winds. Typical large-scale atmospheric situations resulting in long term shutdown periods are identified. We find that both the wind power variability and the risk of not producing any wind power decrease significantly with an increasing array of connected sites. The risk of no wind power production for a given hour is reduced from the interval 8.0 %–11.2 % for a single site to under 4 % for two sites. Increasing the array size further reduces the risk, but to a lesser extent. The average atmospheric weather pattern resulting in wind speed that is too low (too high) to produce wind power is associated with a high-pressure (low-pressure) system near the production sites.

1 Introduction

Renewable power generation from various sources is continuously increasing. This is a desired development due to, among others things, emission goals that are linked to mitigation of global warming. Offshore wind power, and especially floating offshore wind power, is only in an initial phase compared to other more mature and developed energy sources. A study by Bosch et al. (2018) has found the global offshore wind energy potential to be 329.6 TWh, with over 50 % of this potential being in deep waters (> 60 m). These numbers underline the need to take advantage of the floating offshore wind energy source with a view to addressing the continuous growth in global energy consumption.

Exploiting the offshore wind energy potential introduces a number of challenges, one of which is the variable nature of the energy source. The wind varies on both spatial and temporal scales, ranging from small features existing for a few seconds to large and slowly evolving climatological patterns. This intermittency results in a considerable variability on different time and spatial scales, leading to highly fluctuating power production and even power discontinuities of various durations.

Fluctuating wind power production is shown to be dampened by connecting dispersed wind power generation sites (Archer and Jacobson, 2007; Dvorak et al., 2012; Grams et al., 2017; Kempton et al., 2010; Reichenberg et al., 2014, 2017; St. Martin et al., 2015). This smoothing effect was demonstrated as early as 1979 by Kahn (1979), who evaluated the reliability of geographically distributed wind generators in a California case study. As weather patterns are heterogeneous, the idea behind connecting wind farms that are situated far apart is that the various sites will experience different weather at a certain time. There is therefore potential to reduce wind power variability as wind farms, unlike single locations, are area-aggregated.

Previous studies examine this smoothing effect almost exclusively over land (Archer and Jacobson, 2007; Grams et al., 2017; Kahn, 1979; Reichenberg et al., 2014, 2017; St. Martin et al., 2015). For example, Reichenberg et al. (2014) presented a method to minimize wind power variability using sequential optimization of site location applied to the Nordic countries and Germany. They found that by using optimal aggregation the coefficient of variability CV ($\mathrm{CV} = \frac{\sigma}{\mu}$) was reduced from 0.91 to 0.54, meaning that wind power variability was substantially reduced when utilizing the fact that the connected production sites were located far apart and in different wind regimes. In addition to intermittency reduction, combining a number of wind power sites situated throughout Europe has also resulted in a reduced number of low-power events. Reichenberg et al. (2017) focused on minimizing the variables related to wind power variability and maximizing the average wind power output and found that periods of low output were almost completely avoided.

A few studies have examined the smoothing effect of production sites distributed over the ocean (Dvorak et al., 2012; Kempton et al., 2010). Kempton et al. (2010) studied the stabilization of the wind power output by placing the production sites in an optimal meteorological configuration and connecting them. They used data from 11 (more or less) meridionally oriented meteorological stations spanning 2500 km along the east coast of the US. They concluded that connecting all 11 sites resulted in a slowly changing wind power output, in addition to a production that rarely reached either full or zero wind power output. Dvorak et al. (2012) also used the east coast of the US as a study area, but at shallow water depths (≤ 50 m), in an attempt to identify an ideal offshore wind energy grid in terms of, among other things, a smoothed wind energy output and a reduced hourly ramp rate and hours of zero power. They found that by connecting all four farms included in the study the power output was smoothed and the hourly zero-power events were reduced from 9 % to 4 %. They also found that wind power production in regions driven by both synoptic-scale storms and mesoscale sea breeze events experienced a substantial reduction in low- or zero-production hours and in the amplitude of the hourly ramp rates when all four farms were connected, compared to production from single farms.

This study is based on 16 years of wind observations from a unique string of sites along the Norwegian coast. We analyze the potential intermittency reduction of wind power output over open ocean by potentially connecting up to five power-producing sites in different combinations. The water depth at these locations ranges from 75 m at Ekofisk to over 350 m at Norne, which means that floating offshore wind is more or less the only option. We approximate the wind power output by transforming hourly observed wind speed observations to wind power output through a conversion function. Along with the smoothing effect, we also investigate statistical wind power characteristics as a function of production site combinations. Additionally, we quantify the potential reduction in the occurrence and duration of shutdown events (no production of wind power).

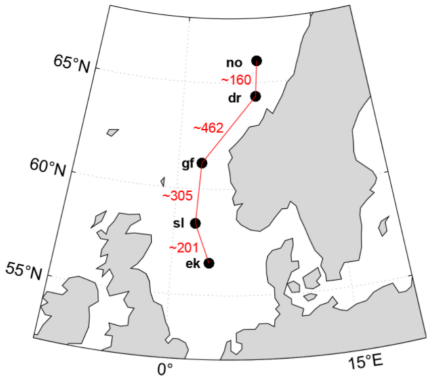

Figure 1. Position of the five sites and the distance (km) between them (red lines). Abbreviations are as follows. ek: Ekofisk; sl: Sleipner; gf: Gullfaks C; dr: Draugen; no: Norne.

Identifying typical atmospheric weather conditions that often result in long-term zero wind power production is crucial. During these shutdown events the power demand has to be covered by other energy sources or through energy storage systems such as hydrogen or batteries. It is therefore important to map and identify these critical weather patterns, particularly if wind is likely to constitute a large share of the global energy and electricity mix. Kempton et al. (2010) examined a few high- and low-power events using reanalysis data to gain insight into the corresponding large-scale atmospheric situation. In contrast to Kempton's work, we have, by examining the composition of the atmospheric situations related to zero events, revealed the typical (composite mean) atmospheric condition related to zero events caused by "too low" and "too high" wind speed.

The paper is structured as follows: Sect. 2 includes the data and the corresponding post-processing, Sect. 3 describes the methods used, and Sect. 4 presents the results of the study and discusses the results. Finally, Sect. 5 summarizes the main results in bullet points.

2 Data and post-processing

In this study we examine the effect of collective wind power at five locations (oil and gas platforms) along the coast of southern Norway. The data sites included in this study are Ekofisk (ek), Sleipner (sl), Gullfaks C (gf), Draugen (dr), and Norne (no) (see Fig. 1 for location and Table 1 for further information on the various sites).

The observed data constitute a unique data set retrieved from the Norwegian Meteorological Institute, and the time series covers the 16-year period between 2000 and 2016. We

Table 1. Name, abbreviation, and location (in latitude and longitude) of each site, as well as the height (m a.s.l.) of the chosen wind sensor (A or B), giving the representative wind speed time series for each site. The chosen sensor at Ekofisk (ek) has two heights since the sensor was moved during the period 2000–2016.

Platform	Abbreviation	Lat	Long	Sensor	Height
Ekofisk	ek	56.55	3.21	A	69/103
Sleipner	sl	58.36	1.91	A	136
Gullfaks C	gf	61.22	2.27	B	141
Draugen	dr	64.35	7.78	A	78
Norne	no	68.01	8.07	A	45

use hourly 10 min average values[1]. The observed data at each site underwent a quality check, both automatic and visual. Some of the values in the data sets were recorded as NaN (not a number). In addition, some observed wind speed values were regarded as nonphysical and replaced with NaN in the time series prior to the analysis. If the data point fell into one of the three categories below, it was flagged and replaced by NaN:

- observations with a wind speed tendency $\frac{\delta u}{\delta t} \geq 15\,\mathrm{m\,s^{-2}}$ over each of 2 consecutive hours – a spike in the wind speed time series;
- observations dropping to zero from $u \geq 5\,\mathrm{m\,s^{-1}}$ in 1 h;
- observations of $\boldsymbol{u} = 0$ surrounded by NaN.

At each platform two anemometers were mounted at different heights, measuring the wind speed and direction. The two anemometers record two separate time series, and one of the data sets was selected to represent the wind conditions at the site in question. When choosing the most representative wind speed time series, the data set had to fulfill certain criteria, namely

- containing the most valid observations after the flagging procedure above and
- having the highest correlation with NORA10 reanalysis data, i.e., nearest grid point with wind speed at 100 m. (Reistad et al., 2011).

As an approximation, we can estimate the wind speed at a height level z_2 by extrapolation of the wind speed from height z_1 by the following relation:

$$u_{z_2} = u_{z_1}\left(\frac{z_2}{z_1}\right)^{\alpha}, \tag{1}$$

where u_{z_1} and u_{z_2} are the wind speed at heights z_2 and z_1, respectively. α is the power-law exponent modifying the shape and steepness of the vertical wind speed profile, depending on both the surface roughness and the atmospheric stability (Emeis, 2018). In our study z_2 is the hub height of 100 m a.s.l. and z_1 is the height of the wind sensors and $\alpha = 0.12$. This way we obtain the extrapolated wind speeds at the hub height for each site. This power law is used and discussed by Barstad et al. (2012), among others.

After replacement of the physically unrealistic observations with NaN, and the aforementioned height extrapolation and correlation check with the NORA10, we selected the wind speed data set assumed to be the most representative for the site in question. In the following sections all estimates involve only wind speed, since we assume that turbine technology allows utilization of wind power to be independent of wind direction. Moreover, we performed calculations for one turbine at each site, since we assumed that the park effect was not relevant for the results obtained.

3 Method

3.1 Estimation of wind power

The maximum part of the kinetic wind energy per time unit passing the area spanned by a wind turbine that can be utilized is defined as the wind power, P (see e.g., Jaffe and Taylor, 2019) and is written as

$$P = \beta\frac{1}{2}\rho A u^3, \tag{2}$$

where β is the Betz limit, ρ is the density of the air, A is the swept area of the rotors, and u is the wind speed.

An analysis of the actual or theoretical wind power potential would involve an analysis of the time series of P. However, a more practical approach is needed as current technology only allows turbines to produce power at certain wind speed intervals. Power production starts when the wind exceeds a "cut-in" value u_{ci}. Subsequently, total wind power production, $P_{\mathrm{w}}^{\mathrm{T}}$, increases according to $P_{\mathrm{w}}^{\mathrm{T}} = \beta\frac{1}{2}\rho A\left(u^3 - u_{\mathrm{ci}}^3\right)$ until u reaches the rated wind speed value u_{r}. The rated wind speed denotes the transition limit where the turbine starts to produce at rated power. For higher wind speeds, $u > u_{\mathrm{r}}$, $P_{\mathrm{w}}^{\mathrm{T}}$ is kept constant until u reaches a "cut-out" value, u_{co}. Thereafter the production is terminated ($P_{\mathrm{w}}^{\mathrm{T}} = 0$) abruptly with increasing wind. This abrupt termination of wind energy due to too high winds is a storm shutdown and is called "storm control". In practice, the described production regime for $u > u_{\mathrm{r}}$ is brought about by instantaneous pitching of turbine blades. This pitching allows a portion of the energy to pass through the blades without utilization and is done to shelter the turbines from the harsh drag force and to minimize the turbines' maintenance. Consequently, the maximum power outtake for a turbine occurs when $u_{\mathrm{r}} \leq u < u_{\mathrm{co}}$ and can be written as $P_{\mathrm{w}}^{\max} = \mathrm{const} = \beta\frac{1}{2}\rho A\left(u_{\mathrm{r}}^3 - u_{\mathrm{ci}}^3\right)$. In practice, $P_{\mathrm{w}}^{\max}$ is the installed capacity. In order for our results to be as general as possible in the rest

[1] The 10 min average is the average of 5 min before and 5 min after every hour.

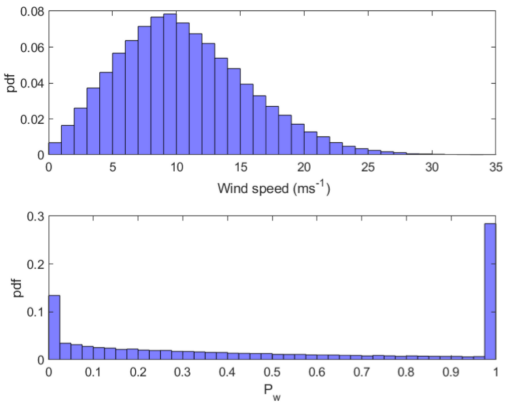

Figure 2. Example distribution for Ekofisk (ek) showing the probability density function (pdf) for both wind speed (m s^{-1}) and normalized wind power (P_w).

of the paper, and since the turbine park at each site is only imaginary and of unknown capacity, we normalize the power calculations $P_w = \frac{P_w^T}{P_w^{max}}$. The technological characteristics of the turbines thus result in a transformation $P \rightarrow P_w$, which can be written as

$$P_w = \begin{cases} 0, & u < u_{ci} \\ \frac{u^3 - u_{ci}^3}{u_r^3 - u_{ci}^3}, & u_{ci} \le u < u_r, \\ 1, & u_r \le u < u_{co} \\ 0, & u \ge u_{co}, \end{cases} \quad (3)$$

where u is the wind speed data, $u_{ci} = 4\,\mathrm{m\,s^{-1}}$ is the cut-in wind speed, $u_r = 13\,\mathrm{m\,s^{-1}}$ is the rated wind speed, and $u_{co} = 25\,\mathrm{m^{-1}}$ is the cut-out wind speed. These numbers are retrieved from the SWT-6.0-154 turbines used in Hywind, Scotland (Siemens AG, 2011). The SWT-6.0-154 turbines were selected as they are the turbines used in the world's first commercially operating floating wind farm off the coast of Scotland.

4 Results and discussion

4.1 Wind speed and wind power characteristics

Some statistical quantities are studied to reveal both wind speed and wind power characteristics: for the wind speed the Weibull mean (μ) and standard deviation (σ), together with the scale and shape parameters (a and b), are calculated (see upper panel of Fig. 2 for an example wind speed distribution).

After conversion of wind speed to wind power via Eq. (3), the data obtain an entirely different distribution (see lower panel of Fig. 2 for an example of wind power distribution). Calculating the arithmetic mean and standard deviation will most likely not result in values representing the typical wind power output and the associated variability. Instead, we use the median (q_2) and interquartile range (IQR) as a measure of the middle value and the spread in the data, respectively. Both q_2 and IQR are independent of the data distribution, which makes them adequate choices to represent the statistical characteristics of the wind power data.

The mean wind speed values (μ) for the five sites demonstrate that the potential for wind power harvest is very good, with the mean ranging from 9.97 to 11.25 m s^{-1}. Zheng et al. (2016) regarded the wind speed at 90 m a.s.l. in the Norwegian Sea and the North Sea as "superb" and ranked it in the highest wind category (category 7) with the potential to produce more than 400 W m^{-2} of wind energy. By comparison, many of the wind parks already operating in the Yellow Sea (east of China) are only ranked in categories 4–6, ranging from "good" to "outstanding", with the potential to produce 200–400 W m^{-2}, respectively.

As mentioned earlier, the wind power intermittency is a huge problem due to the balancing difficulties and high economic costs related to a fluctuating power output. Among the five platforms, Ekofisk (ek) has the lowest variability, with a standard deviation of 5.3 m s^{-1}. Gullfaks C (gf) is the site with the highest variability, where $\sigma = 6.0\,\mathrm{m\,s^{-1}}$. a is the scale parameter giving the height and width of the Weibull distribution. A large (small) scale parameter indicates a wide and low (high and narrow) distribution. For this data set a ranges from 11.2 to 12.7 for Draugen (dr) and Sleipner (sl), respectively. b tells us about the shape of the distribution. A small b ($b < 3$) means that the distribution is positively skewed, with a long tail to the right of the mean. The smaller the number, the more right-skewed the distribution. Here, b ranges from 1.73 to 2.09 for Draugen (dr) and Ekofisk (ek), respectively, meaning that all the distributions are positively skewed, confirming that the wind speed has more of a Weibull distribution than a Gaussian distribution. Since the goal of a functioning wind park is to produce as much wind power as possible, it is desirable that the wind speed data fall between $4\,\mathrm{m\,s^{-1}} \le u < 25\,\mathrm{m\,s^{-1}}$, or even more preferably between $13\,\mathrm{m\,s^{-1}} \le u < 25\,\mathrm{m\,s^{-1}}$ which will give $P_w = 1$. Sleipner (sl) is the site that most frequently operates at rated power: slightly over 30 % of the time. This is a result of the fact that Sleipner (sl) has an optimal combination of the scale (12.3) and shape (1.9) parameter, with the largest portion of the wind speed distribution falling between 4 and 25 m s^{-1}.

For the wind power, the median values (q_{50}) range from 0.33 for Draugen (dr) to 0.52 for Norne (no). Another measure of the performance of a wind park is the capacity factor (CF), which is defined as the annual mean power production divided by the installed capacity. Draugen (dr) has the lowest capacity factor, CF = 0.45, and Norne (no) has the highest, with CF = 0.53. The wind power IQR is high, around 0.9. This means that $q_{50} \pm \frac{IQR}{2}$ contains 50 % of the

Table 2. Statistical measures of the wind speed and wind power. μ and σ are the Weibull mean and standard deviation, respectively, a and b are the scale and shape parameter of a Weibull distribution, respectively, q_{50} is the median (second quartile), IQR is the interquartile range, RCoV is the robust coefficient of variability, and CF is the wind power capacity factor.

		Wind speed				Wind power			
Platforms	Abbreviation	μ	σ	a	b	q_{50}	IQR	RCoV	CF
Ekofisk	ek	10.49	5.28	11.85	2.09	0.43	0.89	0.90	0.5
Sleipner	sl	10.86	5.89	12.25	1.92	0.47	0.90	0.95	0.52
Gullfaks C	gf	10.77	6.04	12.13	1.85	0.46	0.92	0.96	0.51
Draugen	dr	9.97	5.93	11.19	1.73	0.33	0.95	1.00	0.45
Norne	no	11.25	5.75	12.70	2.05	0.52	0.89	0.92	0.53

wind power output. There is therefore potential for reducing wind power intermittency by combining sites.

Reichenberg et al. (2014) concluded that the coefficient of variability for wind power can be substantially reduced by geographic allocation of the production sites. They used the arithmetic mean (μ) and standard deviation (σ), calculating the coefficient of variability ($\mathrm{CV} = \frac{\sigma}{\mu}$). As mentioned above, using the arithmetic mean and standard deviation gives rise to a misleading interpretation of the actual middle value and the accompanying variability of the wind power output. This is due to the very different wind power distribution arising from the nonlinear conversion of the wind speed data to wind power output through the power conversion curve (see Eq. 3). Hence, another more robust and resistant measure of wind power variability is the RCoV (Lee et al., 2018). The $\mathrm{RCoV} = \frac{\mathrm{MAD}}{q_{50}}$ is the median absolute deviation (MAD) divided by the median (q_{50}) and is a normalized measure of the spread in the data set. Here, RCoV ranges from 0.9 for Ekofisk (ek) to 1.00 for Draugen (dr), meaning that a typical deviation from the median value is approximately equal to the median value itself.

4.1.1 Interannual and seasonal wind power variability

How CF varies from one year to another gives a good indication of the long-term fluctuations in wind power production. The annual variation in CF can be quite substantial and is presented in Fig. 3a. For all the sites, the interannual variation can change by up to 0.12 (12 % of installed capacity) from one year to the next (i.e., 2010–2011). On this timescale, the CF values for the five stations follow each other more or less, bearing in mind that on an annual timescale, the production in the whole region will strongly co-vary. The strong interannual variations in CF clearly demonstrate that measuring the wind conditions over too short of a time period (i.e., 1 year) is generally not sufficient to estimate a representative wind power potential for a site at these latitudes.

Figure 3b presents the seasonal variation in CF. The highest CF values are found during the autumn and winter (October–February) and range from 0.58 to 0.68 for the northernmost sites Draugen (dr) and Norne (no), respectively. The lowest CF values occur during the summer and range from 0.32 at Draugen (dr) to 0.38 at Gullfaks C (gf).

4.2 Correlation and intermittency

In terms of reducing wind power variability, the optimal hypothetical case would have been to combine production from two stations with correlation coefficient $r = -1$. The two combined sites would then be completely out of phase, and the sum of the individual productions would be constant in time, given equally installed capacity at each site. Since the synoptic weather systems constitute the main source of spatiotemporal variance in wind over open ocean, the connected production sites situated far apart in our site array will probably experience the most contrasting weather and therefore result in the largest dampening of the wind power intermittency. To quantify this, we investigated the pairwise correlation between the different wind power time series (P_w) as a function of distance and time lag between the hypothetically connected sites. Sinden (2007) analyzed the characteristics of the wind power resource for 66 onshore sites in the United Kingdom. He found a substantial reduction in the correlation between site pairs at separation distances less than 600 km. However, for wind sites located more than 800 km apart, the decrease in correlation is less pronounced, despite a further increase in the distance between them. Our results confirm this distance dependency of the correlation found in Sinden (2007): Fig. 4 illustrates how the correlation between station pairs changes as a function of the separation distance. The correlation drops off quickly as the distance (x) between the sites increases. After $x \approx 800$ km the decrease in correlation with distance is reduced to 0.1 and continues to decrease more slowly with increasing separation distance. It is expected that the correlation between site pairs will approach zero when the separation distance becomes large enough, meaning that the wind at these sites is completely independent. Some site pairs can even have slightly negative correlation. Reaching this slowdown in the relation between the correlation and the separation distance after $x \approx 800$ km indicates that combining sites outside a radius of $x \approx 800$ km for further variability reduction has almost a negligible effect

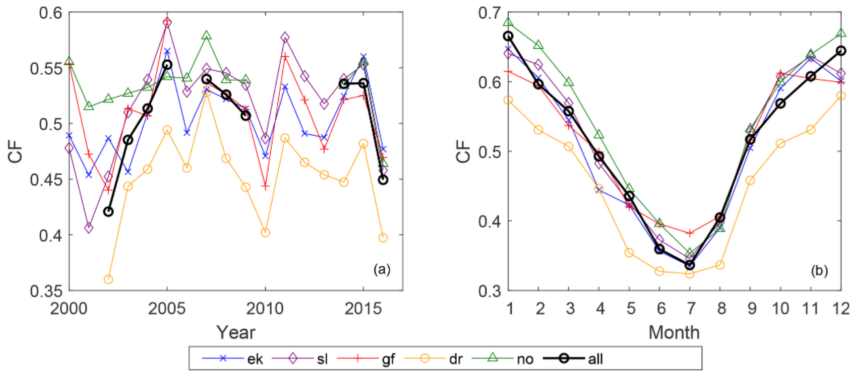

Figure 3. **(a)** Interannual variation in the capacity factor (CF) for the five sites and the total interconnected system ("all"). If more than half of the data in 1 year were missing, the value for that year was excluded in the plot. **(b)** The seasonal variation in CF for the five sites and the interconnected system ("all").

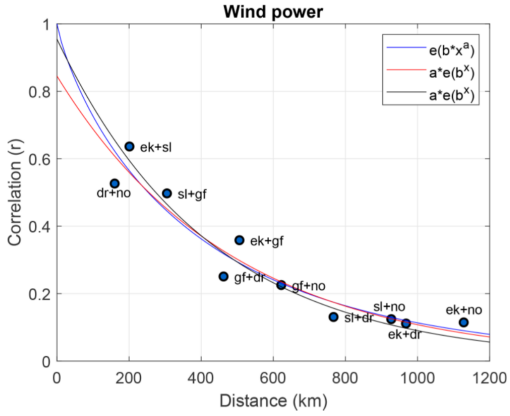

Figure 4. How the correlation between site pairs changes with distance, including three exponential curves giving the best least-squares fit for the 10 correlation points.

for the length and timescales considered here. Nevertheless, the correlation coefficient never drops to zero, or below zero, over the range of the data covered in this study, indicating that none of these station pairs will either be anticorrelated or have completely independent production ($r \leq 0$).

The decorrelation length illustrates at what radius the wind power correlation drops to a fraction of the initial value at $x = 0$. In our study, we use the e-folding distance[2] as a measure of the decorrelation length L. The 10 station pairs are used to identify a best-fitting curve describing the dependency between correlation and separation distance, which will give a general description of the decorrelation length L (in kilometers). Identifying such a best-fitting curve may be challenging, and we therefore use three exponential functions with slightly different properties to indicate the uncertainty in the estimates due to the choice of fitting function. The exponential curves, together with the 10 correlation points are presented in Fig. 4, while the corresponding decorrelation lengths are presented in Table 3. The decorrelation length L is slightly more than 400 km. St. Martin et al. (2015) identify decorrelation lengths in the same order using the e-folding distance ($L = 388$, $L = 685$, and $L = 323$ km for three different regions: southeastern Australia, Canada, and the northwestern US, respectively). Further, they argue that more correct decorrelation lengths can be obtained by using the e-folding distance times the nugget effect (βL) and even better results by using the integral-scale matrix ξ_τ. The integral-scale matrix is a measure of the distance required for the correlation to fall to a small value compared to unity. Both measures mentioned above gave a decorrelation length substantially less than the e-folding distance with $\beta L = 273, 447, 130$ km and $\xi_\tau = 273, 368, 89$ km. St. Martin et al. (2015) also concluded that the decorrelation length is highly sensitive to the variability timescale. This result is also obtained in this study (not shown) and in Czisch and Ernst (2001). On timescales longer than a day, St. Martin et al. (2015) found that the benefit of variability reduction from aggregation of wind power over a region of a given size is independent of timescale. Therefore, if two of our offshore wind-producing sites were to balance each other at short timescales (< 1 h), the separation distance could be further reduced from $L = 400$ km. On the other hand, if they were to balance each other on longer timescales (> 1 h), the separation distance would be larger than $L = 400$ km. This is a significant result because it underlines the importance of con-

[2]The distance where the correlation has dropped to $\frac{1}{e} = 0.37$.

Table 3. Annual and seasonal decorrelation length L (in kilometers) for the three exponential functions in Fig. 4. The third column represents a fit where the point $[x, y] = [0, 1]$ is added to the data points to include that the correlation = 1 when the $x = 0$.

Season	Decorrelation length L		
	e^{bx^a}	ae^{bx}	ae^{bx}
Winter	288.97	293.51	300.69
Spring	364.80	366.74	367.20
Summer	388.11	394.91	394.53
Autumn	385.82	388.99	389.04
Annual	403.01	414.56	413.65

sidering timescales when combining wind-power-producing sites to reduce wind power intermittency.

In general, the seasonal L is shorter than the annual decorrelation length (see Table 3). The winter months (December–February) contain the shortest decorrelation lengths, varying from $L = 289$ to 301 km, depending on the exponential fit. During the winter, the atmosphere is more irregular and chaotic in both space and time, meaning that two stations located a given distance apart will more often enter different wind regimes during the winter than the other seasons. The summer months (June–August) have the longest decorrelation lengths, spanning from $L = 388$ to 395 km. The large-scale atmospheric patterns are larger, smoother, more stationary, and last longer. As demonstrated by St. Martin et al. (2015), among others, the decorrelation length is sensitive to the variability timescale. The decorrelation length increases when the variability timescale increases. When looking at variability on an annual timescale, the seasonal variability also has to be balanced. Hence, the annual decorrelation length is larger than the seasonal decorrelation length.

Figure 5 demonstrates how the time lag of maximum correlation between station pairs changes with distance. In accordance with our expectations, the sites that are closest to each other have the shortest time lag and the highest correlation, implying shorter time for the feature to propagate between them, resulting in a higher correlation. The high-pressure and especially the low-pressure systems that sweep over the North Sea and the Norwegian Sea have a prevailing traveling direction from west to east, due to the strong westerlies at these latitudes. This implies that winds accompanying the system will strike the westernmost site, Sleipner (sl), first, followed by Ekofisk (ek) and Gullfaks (gf) C at short time intervals, and later Draugen (dr) and Norne (no). A large time lag is beneficial for wind energy production. Then, a wind event will not occur simultaneously at both the connected sites. To ensure a time lag approaching 10 h, from one site experiencing a certain wind event to the other connected site experiencing the same wind event, the separation distance needs to exceed ≈ 600 km.

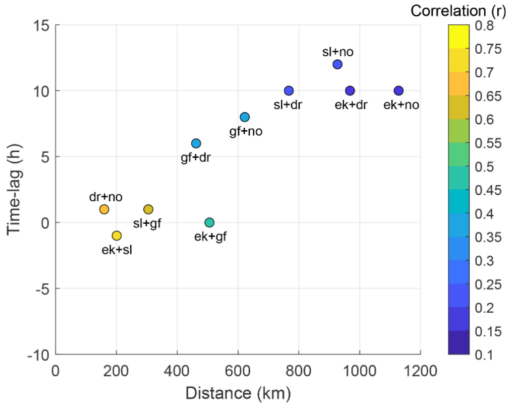

Figure 5. Time lag (h) of maximum correlation between the connected sites as a function of the distance between them.

4.3 Connecting wind power sites

To study the effect of interconnected production sites, we have to make combined wind power time series for all the different site configurations. The collective wind power time series, P_w^c, for different configurations of sites are found by calculating the average power production for each time step. Time steps containing NaN values for any of the sites in the configuration in question are not included. Hence, for a given time step,

$$P_w^c(i) = \frac{1}{j}\sum_{j=1}^{J} P_w^j(i), \tag{4}$$

where $i = 1, 2, \ldots, N$ is the time step, $j = 1, 2, \ldots, J$ is the number of sites combined, and $P_w^j(i)$ is the different wind power time series for an array combination of j sites (one to five sites) at time step i.

For example, a combination of two sites (a and b) at time step i will be

$$P_w^c(i) = \frac{1}{2}\sum_{j=1}^{2} P_w^2(i) = \frac{1}{2}\left(P_w^a(i) + P_w^b(i)\right). \tag{5}$$

This calculation is done for each time step i, as long as $P_i^a \neq$ NaN or $P_i^b \neq$ NaN.

As mentioned in Sect. 4.1 the IQR is a candidate for estimating wind power variability (Kempton et al., 2010). According to Lee et al. (2018) a more robust and resistant variability measure is the robust coefficient of variability (RCoV). Figure 6 presents IQR and RCoV for different configurations of collective wind power production, P_w^c. Common to both the variability measures is that the variability generally decreases quickly with increasing array size of connected sites. This result clearly demonstrates the advantage of having interconnected wind power production in

terms of intermittency reduction: Instead of operating wind turbines at two sites separately, we see that the intermittency of a connected site pair is reduced and is further reduced with increased array size. The site with the highest (lowest) IQR is the station with the lowest (highest) RCoV, since RCoV is normalized by the median value.

A counterintuitive result is that for some site combinations the variability (IQR and RCoV) is less than the variability for a larger array size. For example, the combination of ek + sl + gf has a higher variability than most of the pairwise site combinations. Some pairwise combinations even have a lower IQR and RCoV than a four-site combination. This result appears to be a consequence of the geographic locations of the sites in this study. Since Ekofisk (ek), Sleipner (sl), and Gullfaks C (gf) are roughly aligned in a north–south direction, they will experience the same wind event more or less simultaneously (see Fig. 5) due to the passage of extratropical cyclones and the associated fronts. Therefore, a combination of these sites would be poorer in terms of intermittency reduction than other site combinations, and even combinations of smaller array size.

4.3.1 Wind power generation duration

A typical wind power distribution can be seen in Fig. 2 (lower panel). When connecting sites, the wind power distribution changes shape. As the array size of interconnected sites increases, the distribution converges towards a bell-shaped distribution (Kempton et al., 2010). Unlike the individual distributions, where the most frequent wind power production is $P_w = 1$ followed by $P_w = 0$, the interconnection of production sites results in a production capacity that more regularly falls in the middle of the production range ([0 1]). Nevertheless, it is worth mentioning that when all five sites are combined, the most frequent production mode is still $P_w^c = 1$, indicating that full production is still the most common production state. This result arises since the five sites are located in a superb wind speed climate. This result can be further discussed in conjunction with the generation duration curve (GDC). Here, the GDC is given as a percentage of the total time the wind power output is above or below a given threshold. As can be seen in Fig. 7, the individual sites produce no power at all between 8 % and 12 % of the time. This is in contrast to the interconnected system ("all") that almost never experiences zero wind power production. The less steep curve from the interconnected system indicates a less fluctuating output, with a production that more often falls at values near the median value.

4.4 Critical power events

The long record of observations (16 years) enables us to make estimates of the risk of having critically low wind power production. In this study, we have chosen to examine the time fraction the wind power production is zero ($P_w = 0$ or $P_w^c = 0$).

The risk (R_i) of zero wind power is the sum of the risk of having too low (R_i^{low}) and too high (R_i^{high}) wind speed, $R_i = R_i^{low} + R_i^{high}$. R_i is calculated by taking the sum of all the hours the power is zero divided by the total number of time steps (NaN values are not included) and is calculated in the following way:

$$R_i = \frac{1}{n}\sum_{i=1}^{n} i\delta, \quad \delta = \begin{cases} 1 & \text{if } u < 4 \wedge u \geq 25 \\ 0 & \text{else,} \end{cases} \tag{6}$$

where i is the time step and δ is a modifier and takes on the values 0 or 1, depending on the wind speed u. This formula is valid for both the individual wind power time series and the collective wind power time series (see Sect. 4).

A critical question, given a pairwise connection of sites, is how much wind power one of the site produces when the other site is not producing any at all. Figure 8 presents the median wind power production at one site when the wind speed at the other station is causing zero power production. As the distance between two connected sites increases, the median production at the producing site increases. To ensure a median wind power production of at least 25 % of installed capacity at one site when the connected site is not producing any power at all, the separation distance needs to exceed ≈ 600 km for the investigated region.

Since wind is a fluctuating physical parameter, the risk of having a wind speed less than a given low threshold value is rather high. In addition to the well-known smoothing effect achieved by geographic allocation of wind power, Reichenberg et al. (2017) also investigated the resulting impact on low-power events. They found that wind power production below 15 % of installed capacity was hardly ever observed when sites were combined. In contrast to Reichenberg et al. (2017), we study the effect of interconnecting sites on unwanted zero events. However, the effect is similar to that found by Reichenberg et al. (2017), namely that the occurrence of unwanted events is reduced. The left panel of Fig. 9 illustrates how the risk of zero events changes with distance between the sites and with array size of connected sites. Going from a single production site to two sites, the risk of zero power drops dramatically: from a risk of 8 %–11 % for a single site to a risk of less than 4 % for two connected sites. Note that the site combination of Draugen (dr) and Norne (no) has a small risk of $P_w^c = 0$, despite the short distance between them (160 km). The reason is probably the high wind power production at Norne (no), caused by the topographic effect arising from wind interactions with the topography in Norway. Hence, the high wind power at Norne (no) compensates for the relatively low wind power production at Draugen (dr) (see Table 2 for median P_w and CF values). This is relevant for cost estimates related to interconnection. This result also underlines the need for careful selection when connecting neighboring sites in terms of intermittency reduction. Dvo-

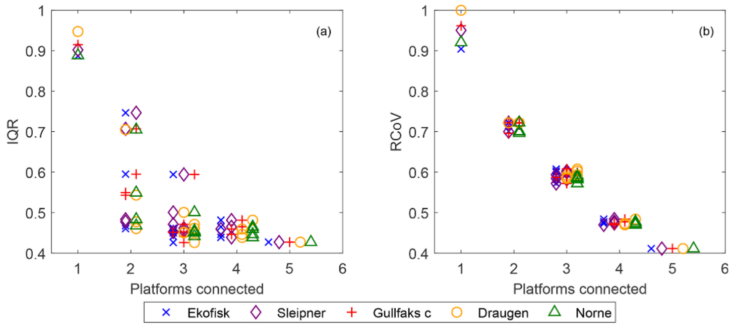

Figure 6. Panels **(a)** and **(b)** demonstrate how IQR (interquartile range) and RCoV (robust coefficient of variability) change as the array size of connected sites increases from one (single sites) to five (all sites connected), respectively.

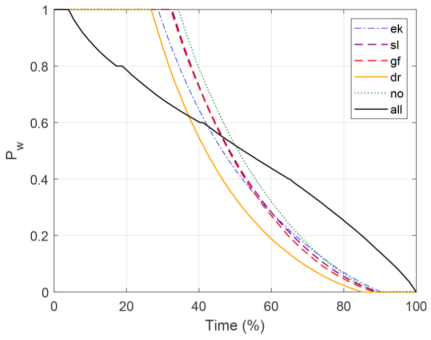

Figure 7. Generation duration curve (GDC) for the five sites and the interconnected system ("all").

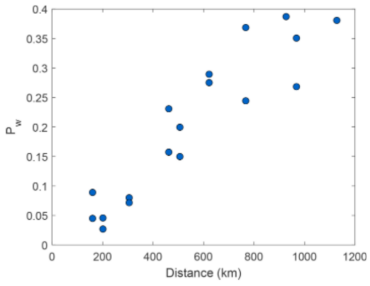

Figure 8. Given a pairwise connection, this figure shows the median P_{w}-production for a site given that the other site are not producing at all ($P_{\mathrm{w}} = 0$) as a function of the distance between the connected site pair.

rak et al. (2012) also found that by connecting four offshore wind farms the occurrence of zero events was reduced from 9 % to 4 %. By contrast, when we connect four of our sites, the risk of having $P_{\mathrm{w}} = 0$ is less than 0.5 %. The significant reduction of the risk in this study is due to the greater separation distance between the sites.

An even more detailed view of the risk of having $P_{\mathrm{w}}^{\mathrm{c}} = 0$ can be seen in the right panel of Fig. 9. This figure tells us which site configuration that has the lowest risk of having $P_{\mathrm{w}}^{\mathrm{c}} = 0$. As can be seen in the upper panel, the largest risk reduction is achieved when shifting from individual site production to a combined two-site production. Increasing the array size further reduces the risk, but the reduction is smaller. The configurations with an array size of three or more have a risk of less than 0.5 % (except the combination of Ekofisk (ek), Sleipner (sl), and Gullfaks C (gf) which has a risk of ≈ 1 %). This indicates that increasing the array size beyond three might not be financially sound. The fact that the intermittency reduction ceases is in accordance with the result obtained by Katzenstein et al. (2010). They found that at a frequency of $1\,\mathrm{h}^{-1}$ the high- to low-frequency variability was reduced by 87 % when combining four sites, compared to a single production site, and that increasing the array size by the remaining 16 sites resulted in a further intermittency reduction of only 8 %.

4.4.1 Extracting wind power during storms

During a strong low-pressure system the wind speed can reach speeds well above the typical cutout limit of a wind turbine of $25\,\mathrm{m\,s}^{-1}$. To extract the associated wind power would greatly enhance the full load hours. In reality, present-day technology operates with a turbine shutdown when the wind speed becomes too strong to prevent damage and destruction. This is referred to as the well-known storm control. However, new technology allows the turbines to operate at wind speed exceeding the usual cutoff limit. Instead of an abrupt shutdown of the power extraction at the old cutout limit, the idea is to introduce a linear reduction of the extraction of wind energy from the old cutoff limit (usually at $25\,\mathrm{m\,s}^{-1}$) to a new

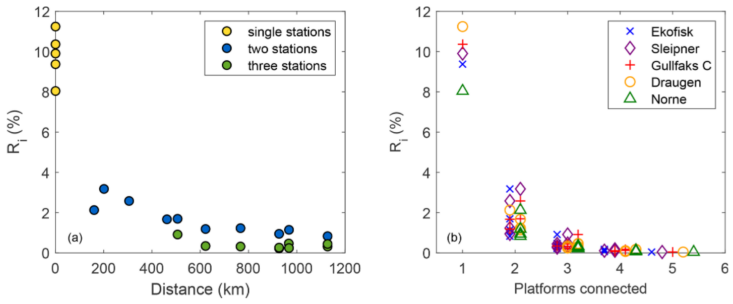

Figure 9. Panel **(a)** demonstrates how the risk (R_i) changes with distance between the connected sites. Panel **(b)** illustrates how the risk (R_i) changes as the array size of connected sites increases from zero (single sites) to five (all sites connected).

Table 4. How much the median wind power and the risk of no production changes when a linear storm control is introduced in the power conversion function (see Eq. 3). The storm control is a linear reduction from the old cutout limit ($25\,m\,s^{-1}$) to a new and higher cutout limit ($30\,m\,s^{-1}$). ST and LST correspond to "storm control" and "linear storm control", respectively. The median "diff" is the change in percentage, while the zero-power "diff" is the difference in percentage points when introducing linear storm control.

	Median			Zero power		
Station	ST	LST	diff (%)	ST	LST	diff
Ekofisk (ek)	0.43	0.45	+2.37	9.35	8.70	−0.65
Sleipner (sl)	0.47	0.49	+4.29	9.9	8.84	−1.06
Gullfaks C (gf)	0.46	0.48	+3.98	10.37	9.27	−1.1
Draugen (dr)	0.33	0.35	+4.84	11.24	10.44	−0.8
Norne (no)	0.52	0.54	+3.69	8.04	7.03	−1.01

and higher cutout limit (i.e., $30\,m\,s^{-1}$), here called "linear storm control". The difference in wind power production using abrupt power shutdown at the old cutout limit and using linear storm control is showed in Table 4.

The table shows that the median wind power production increases with several percent when introducing linear storm control from 2.37 % for Ekofisk (ek) to 4.84 % for Draugen (dr), which is quite substantial. On the other hand, for all the sites the risk of having a zero-power event is reduced when introducing the linear storm control. The difference, in percentage points, ranges from 0.65 to 1.1. This result indicates that by introducing a linear storm control the turbine will produce more wind power and experience fewer events of zero power.

4.4.2 Wind power sensitivity related to the power-law exponent

The vertical structure of the atmosphere is of major importance when dealing with wind power extraction. How the vertical wind profile looks depends on the background wind speed, atmospheric stability, and roughness of the surface. As an approximation, we can estimate the vertical wind speed profile by extrapolation of the wind speed at height z_1 to z_2 (see Eq. 1).

Table 5. Sensitivity in the median wind power production and the risk of zero power production as a function of the power-law exponent α. $\alpha_l = 0.08$, $\alpha_m = 0.12$, and $\alpha_h = 0.16$. α_m is the value used throughout the paper.

	Median			Zero power (%)		
Station	α_l	α_m	α_h	α_l	α_m	α_h
Ekofisk (ek)	0.42	0.43	0.45	9.47	9.35	9.23
Sleipner (sl)	0.48	0.47	0.45	9.76	9.91	10.02
Gullfaks C (gf)	0.48	0.46	0.44	10.29	10.37	10.50
Draugen (dr)	0.32	0.33	0.34	11.36	11.24	11.16
Norne (no)	0.48	0.52	0.56	8.18	8.04	7.97

The atmospheric stability varies from day to day and even throughout the day. The relation between the power-law exponent α and atmospheric stability gives an increase in α with increasing stability. The surface roughness over calm ocean is very low. However, due to the frequent passage of extratropical cyclones at the latitudes in question the ocean surface is often characterized by large swells and smaller wind-driven waves. An increasing surface roughness also increases the value of α.

Determining and using a correct α-value when mapping the wind power potential is very important but also demanding. Therefore, a sensitivity analysis of the wind power dependency on the α-value is conducted. In Table 5 the median wind power and the risk of zero wind power production for varying power-law exponents are listed.

The wind sensor mounted on each platform is located at different heights, some above ("above-hub": sl and gf) and some below ("below-hub": ek, dr, and no) the hub height of the SWT-6.0-154 turbine (100 m a.s.l.). As can be seen from Table 5, choosing a wrong α-value to modify the vertical wind speed profile influences both the median wind power

production and the risk of zero power production. Using a too low α-value in the extrapolation, the wind speed for the above-hub (below-hub) sites will result in a higher (lower) wind power production at 100 m a.s.l. and hence a decreased (increased) risk of having zero wind power production. Vice versa is true if α takes on a too high value. The wind speed for the above-hub (below-hub) sites will result in a lower (higher) wind power production at 100 m a.s.l. and an increased (decreased) risk of having zero wind power production.

By using the same power-law exponent, we assume the same state of the ocean surface and also the same atmospheric stability at all five sites. This can of course lead to erroneous wind speed values and hence wind power output. Further investigation in the choice of the power-law exponent is outside the scope of this paper.

4.4.3 The influence of large structures on the wind field

Oil- and gas platforms are large structures, ranging several tens of meters above the sea surface. The platforms are often located far offshore at areas that are poorly covered in terms of observational data. However, wind sensors mounted on top of these large structures enable us to map the wind conditions at each of these sites to some extent.

The wind field over the open ocean is almost undisturbed. However, when the flow is approaching a platform the wind field will start to alter. Several studies have looked at the impact of these large structures on the background flow (Vasilyev et al., 2015; Berge et al., 2009). A common result is that these large offshore structures impact the wind field. Depending on the wind direction the wind speed is to some extent either accelerated or decelerated by the structure, together with a backing or veering of the wind direction. These structures disturb the background flow, causing downwind turbulence to appear.

Using these observations to map the wind characteristics and the associated wind power might give a wrong picture of the actual wind power potential at the site in question. On the other hand, using climate models to produce wind speed climatology for the same site also introduces uncertainties. So, in this study, looking at the effect of interconnection of wind power production sites, we believe that the alteration of the wind power potential by using observations from oil and gas platforms might be of minor importance.

4.5 Zero events caused by too low or too high wind

Since a zero event ($P_w = 0$) occurs when both $u < 4\,\mathrm{m\,s^{-1}}$ (too low wind) and $u \geq 25\,\mathrm{m\,s^{-1}}$ (too high wind), we choose to split the zero-power events, when investigating associated meteorological processes. Figure 10 presents both the occurrence and duration of zero events for two seasons, namely winter and summer, when the most contrasting results occur.

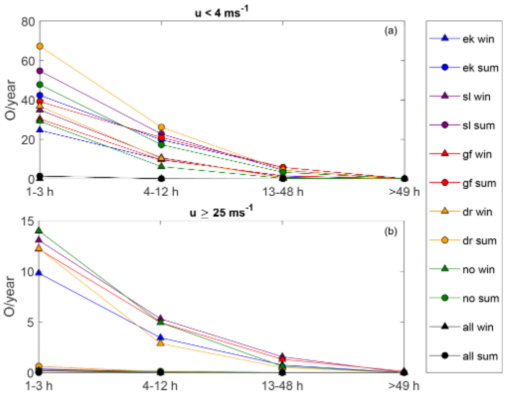

Figure 10. Average number of yearly occurrences (O per year) of zero wind power production for different durations (1–3, 4–12, 13–48, and > 49 h) both for $u < 4\,\mathrm{m\,s^{-1}}$ **(a)** and for $u \leq 25\,\mathrm{m\,s^{-1}}$ **(b)**. The occurrence of zero power is plotted for winter (triangles) and summer (circles), where the largest differences are seen.

The first thing to notice is that the occurrence of zero events decreases as the duration increases. In addition, the occurrence of zero events has almost ceased when all the sites are connected (black curve), and the reduction is most distinct for the shortest duration (1–3 h). More zero events are caused by too low wind (a total of 684.5 yearly zero events for all the sites) than too high wind (102.75). The occurrence of zero events caused by too high wind (too low wind) is highest during winter (summer). In addition, we see that the seasonal difference is largest for the zero events resulting from too high winds, where the occurrence during the winter is of a larger magnitude than during the summer.

To explain the seasonal differences in the occurrence of zero events, it is necessary to examine the main driving force of variability in the weather phenomena over the open ocean. Synoptic high- and low-pressure systems give rise to the changing weather at our specific sites and are the main contributor to weather variability over the open ocean. Winds strong enough to terminate power production ($u \geq 25\,\mathrm{m\,s^{-1}}$) are often associated with the passage of intense low-pressure systems and their accompanying fronts. The occurrence of such strong wind events is more likely to take place during winter than during summer at the latitudes in question (Serreze et al., 1997; Trenberth et al., 1990). Throughout the year, differences in solar insolation give rise to an increased meridional temperature gradient during the northern hemispheric winter. These winter conditions result in a stronger background flow that favors low-pressure activity. On the other hand, the lack of these strong low-pressure systems during summer is probably the main reason why the occurrence of zero events caused by too low wind is highest during summer. In addition, the fact that blocking high-pressure events

are more likely during spring also contributes to the seasonal difference in the too-low-wind events (Rex, 1950).

4.6 Atmospheric conditions causing long-term power shutdown

The previous section demonstrated that the occurrence and duration of zero events are sensitive to the season and the atmospheric state. Klink (2007) has related long-lasting above- or below-average mean monthly values to variability in selected large-scale atmospheric circulation patterns. This section more closely examines surface pressure patterns associated with zero events lasting longer than 12 h using NORA10-reanalysis data (Reistad et al., 2011).

Surface pressure is a key quantity that contains considerable information about the atmospheric structure in the lower atmosphere. Figures 11 and 12 present the average surface pressure conditions (composite mean) and the corresponding standard deviation associated with zero events due to too low wind ($u < 4\,\mathrm{m\,s^{-1}}$) and too strong wind ($u \geq 25\,\mathrm{m\,s^{-1}}$) for the two site combinations ek + sl and dr + no, respectively. The average atmospheric condition (comprised of 360 maps) resulting in too low wind speed for ek + sl is a high-pressure system extending from the North Sea and into the Norwegian Sea. This pattern is similar to the positive phase of the Scandinavia pattern (SCAND) (Barnston and Livezey, 1987). The variability given by the standard deviation (SD) is only a few hectopascals, indicating that the atmospheric patterns causing too-low-wind events are relatively similar to each other and that most of the variability lies in the patterns' extension towards the west. By contrast, the average atmospheric situation (comprised of 15 maps) due to too strong wind is an intense low-pressure system hitting the northwest coast of southern Norway, bringing tight isobars and strong winds over Sleipner (sl) and Ekofisk (ek). This situation is similar to the positive phase of the North Atlantic Oscillation (NAO). The SD is large in the center of the low-pressure system. The small spatial extension of the maximum standard deviation indicates uncertainty regarding the depth of the system. However, the SD is less over Ekofisk (ek) and Sleipner (sl), indicating that these sites seem to be located to the south of the extratropical cyclone where the strongest winds are often found.

Figure 12 contains the same information as in Fig. 11, but for the site combination Draugen + Norne (dr + no). The average atmospheric condition (comprised of 159 maps) caused by too low wind is different from that in Fig. 11a. The typical atmospheric condition here is a high-pressure system covering the entire Norwegian Sea and extending across Norway and into eastern Europe. The SD states that the eastern extension of the high-pressure system is unclear, giving rise to the large uncertainty east of Norway. Again, as in the case of too high wind for ek + sl, the site combination dr + no is located to the south of a strong low-pressure system (panel b). For dr + no, the mean system is now situated off the coast of northern Norway. The corresponding SD is large, indicating that several positions and strengths of the strong low-pressure system can cause situations with too high winds for dr + no.

Even though Kempton et al. (2010) investigated only four specific meteorological situations giving high and low collective wind power, our results are in line with theirs. As for the too-low-wind events in this study, the episodes of too low wind power in Kempton et al. (2010) were associated with a high-pressure system located in the vicinity of the wind power production sites. On the other hand, the episodes resulting in high collective wind power output in Kempton et al. (2010) were characterized by a low-pressure system located in the vicinity of the production sites. This is more or less in line with the results of this paper: our too-high-wind events are caused by intense low-pressure systems. Accordingly, a less intense low-pressure system will result in high-wind-power events.

5 Summary of main results

In this study we quantified the effect of collective offshore wind power production using five sites on the Norwegian continental shelf, which constitutes a unique set of hourly wind speed data observed over a period of 16 years. The sites extend from Ekofisk in the south (56.5° N) to Sleipner, Gullfaks C, Draugen, and Norne in the north (66.0° N). See Fig. 1 and Table 1 for site details. We addressed the well-known intermittency problem of wind power by means of a hypothetical electricity cable connecting different configurations of the sites. The achieved smoothing effect was quantified by investigating the correlation between the sites as a function of the distance (km) and time lag (h) between the different pairs of site combinations. In addition, we studied the potential reduction of critical events (zero wind power-events) for different site combinations. Moreover, we investigated further details of zero events grouped into the two categories of too low and too high wind speed and the corresponding seasonal variations. Finally, the typical atmospheric patterns resulting in zero events caused by too low and too high wind speed for certain site combinations were studied. Our main findings are as follows.

- In the case of all five sites, the wind climate was classified as superb (category 7), which corresponds to a potential of producing more than $400\,\mathrm{W\,m^{-2}}$ of wind energy (Zheng et al., 2016). The mean wind speeds at 100 m a.s.l. range from 9.97 to $11.25\,\mathrm{m\,s^{-1}}$ for Draugen and Norne, respectively.

- Sleipner is the site that most frequently operates at rated power, 31 % of the time. This is due to the fact that Sleipner has an optimal combination of the scale and shape parameter, with the largest portion of the wind speed distribution falling between 13 and $25\,\mathrm{m\,s^{-1}}$.

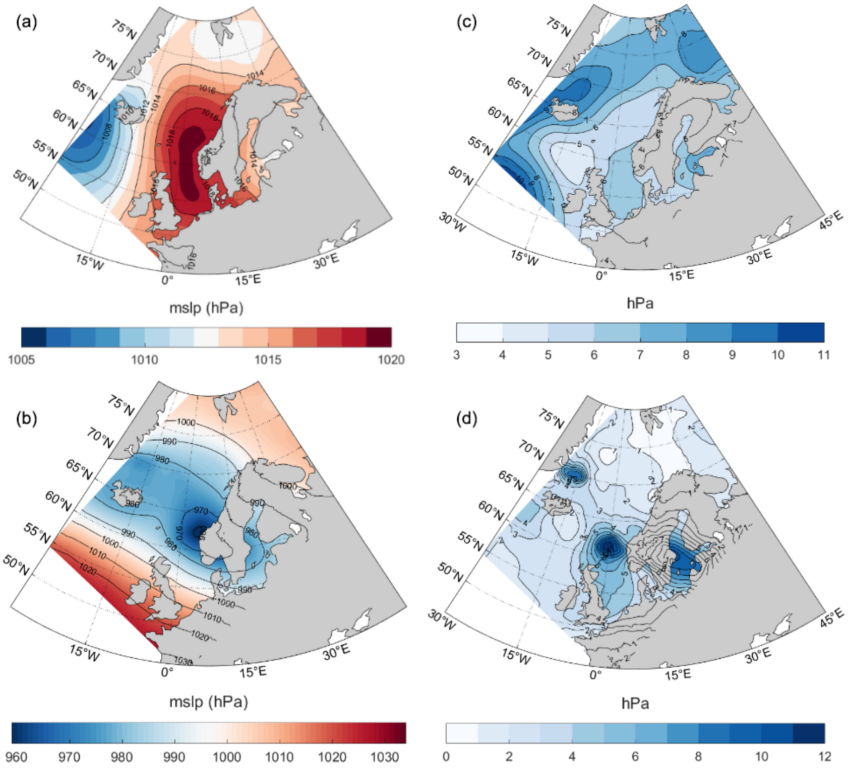

Figure 11. Average (composite mean) large-scale situations **(a, b)** and the corresponding standard deviations **(c, d)** corresponding to $P_{\mathrm{w}}^{\mathrm{c}} = 0$ for the site pair Ekofisk + Sleipner (ek + sl). The upper and lower rows correspond to $P_{\mathrm{w}}^{\mathrm{c}} = 0$ caused by too low wind ($u < 4\,\mathrm{m\,s^{-1}}$) and too high wind ($u \geq 25\,\mathrm{m\,s^{-1}}$), respectively.

- The wind power variability, expressed as IQR and RCoV, ranges from IQR = 0.89 to 0.95 for Norne–Ekofisk and Draugen and RCoV = 0.90 to 1.00 for Draugen and Norne. Both IQR and RCoV decrease quickly with increasing array size of connected sites, indicating that wind power intermittency is reduced when sites are connected.

- The pairwise correlation between sites drops off quickly as the distance between the sites increases. However, after ≈ 800 km the correlation is reduced to 0.1 and continues to decrease more slowly with increasing distance. Reaching this slowdown in the relation between correlation and separation distance after ≈ 800 km indicates that combining sites farther apart for further variability reduction has an almost negligible effect on the length scales possible to explore here.

- The decorrelation length L shows that at a distance $L \approx 400$ km the correlation between site pairs has dropped to $\frac{1}{e}$. This means that combining sites with at least a decorrelation length apart will substantially reduce wind power intermittency.

- The decorrelation length L increases with variability timescale. Hence, if two of the offshore wind-power-producing sites were to balance each other at shorter timescales (< 1 h), the separation distance would decrease ($L < 400$ km).

- To ensure a time lag of 10 h, from one site experiencing a certain wind event to the other connected site experiencing the same wind event, the separation distance needs to exceed ≈ 600 km.

- Given a pairwise site connection, the separation distance exceeds ≈ 600 km to ensure a median wind power production of 25 % of installed capacity at one site when the production at the other site is zero.

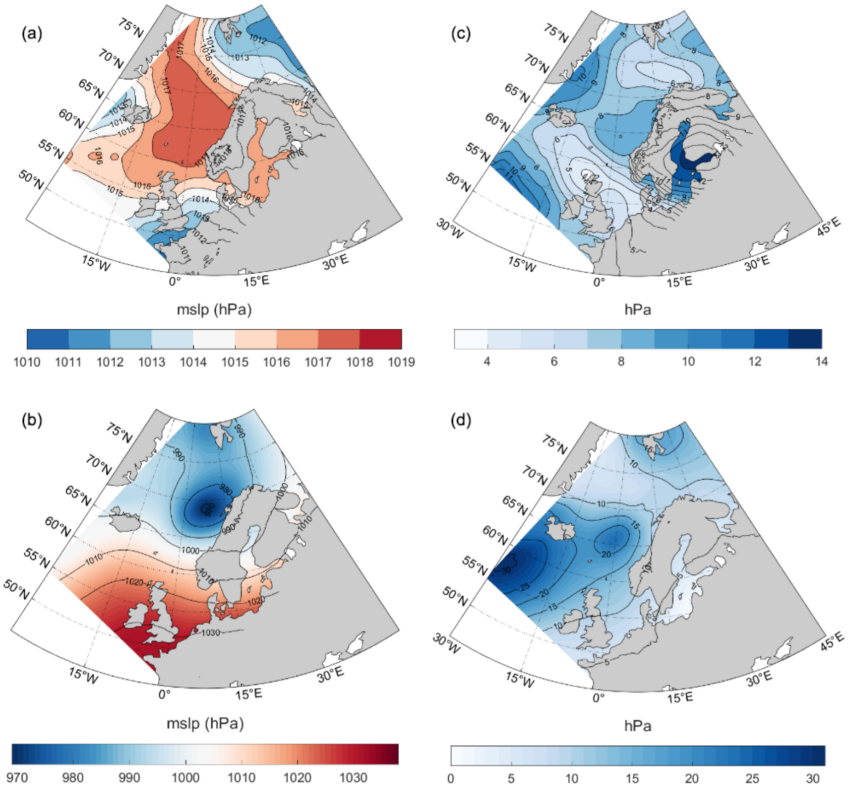

Figure 12. Same as in Fig. 11, but for the site pair Draugen + Norne (dr + no).

– The risk of having zero wind power for a given hour decreases from interval 8.0 %–11.2 % for the individual sites to less than 4 % when two sites are connected. Increasing the array size further reduces the risk, but the reduction is smaller.

– The occurrence of zero events for a given site decreases as the duration increases. Thus, the shorter zero events (1–3 and 4–12 h) are more likely to occur than the zero events lasting longer (more than 13 h).

– For a single site, the total yearly occurrence of zero events caused by too low wind (high wind) is 684.5 h (102.75 h). By comparison, when all the sites are connected, the total yearly occurrence of zero events is 1.5 and 0.2 h for too low and too high wind, respectively.

– The occurrence of zero-power events caused by too high winds (too low winds) is highest during the winter months (summer months). This is due to the increased (decreased) occurrence of strong low-pressure systems at midlatitudes during the winter (summer).

– The average atmospheric pattern resulting in too strong winds is a low-pressure system located to the north of the combined sites in question. This position of the system leaves the connected pair to the south of the core center where the strongest winds are usually found in an extratropical cyclone. By contrast, the atmospheric situation resulting in too low winds is a high-pressure system positioned over the connected sites, resulting in very calm wind conditions.

6 Outlook

This research paper has first of all showed that by connecting wind power production sites the unwanted events like intermittency and zero events are reduced. The results obtained here are of great importance and lead us to some open questions:

- Given that all locations in the North Sea and the Norwegian Sea could be used for wind power production, where are the best sites for interconnection in terms of (a) reducing intermittency and (b) maximizing power output?
- Is the correlation between production sites largest in the east–west or the north–south direction?
- Should the installed capacity at each production site be unequal in terms of (a) reducing intermittency and (b) maximizing power output?

Data availability. The observational data for the sites used in this study can be retrieved at https://seklima.met.no/observations/ (last access: November 2020) (Norsk Klimaservicesenter, 2020) or at https://frost.met.no/index.html (last access: November 2020) (Meteorologisk Institutt, 2020).

Author contributions. IMS and NKG conceptualized the ideas, goals, and overarching research questions. IMS and AS carried out the data curation and formal analysis with the relevant statistics according to the corresponding methodology. NGK was responsible for the funding acquisition. IMS was responsible for the retrieval of the data and programming software, in addition to the validation and visualization of research results, with contributions from AS. IMS provided the original draft with the contribution from NGK, while all the authors contributed to the review and editing process. NGK and AS were responsible for the supervision.

Competing interests. The authors declare that they have no conflict of interest.

Acknowledgements. We thank the Meteorological Institute, and we in particular thank Magnar Reistad, Øyvind Breivik, Ole Johan Aarnes, and Hilde Haakenstad for providing all the data used in this study. We are grateful to David B. Stephenson for discussion of relevant statistics.

Financial support. This work was funded through a PhD grant from Bergen Offshore Wind Center (BOW), University of Bergen.

Review statement. This paper was edited by Joachim Peinke and reviewed by two anonymous referees.

References

Archer, C. L. and Jacobson, M. Z.: Supplying baseload power and reducing transmission requirements by interconnecting wind farms, J. Appl. Meteorol. Clim., 46, 1701–1717, https://doi.org/10.1175/2007JAMC1538.1, 2007.

Barnston, A. G. and Livezey, R. E.: Classification, seasonality and persistence of low-frequency atmospheric circulation patterns, Mon. Weather Rev., 115, 1083–1126, https://doi.org/10.1175/1520-0493(1987)115<1083:CSAPOL>2.0.CO;2, 1987.

Barstad, I., Sorteberg, A., and Mesquita, M. D. S.: Present and future offshore wind power potential in northern Europe based on downscaled global climate runs with adjusted SST and sea ice cover, Renew. Energ., 44, 398–405, https://doi.org/10.1016/j.renene.2012.02.008, 2012.

Berge, E., Byrkjedal, Ø., Ydersbond, Y., and Kindler, D.: Modelling of offshore wind resources. Comparison of a meso-scale model and measurements from FINO 1 and North Sea oil rigs, in: European Wind Energy Conference and Exhibition EWEC, 16–19 March 2009, Marseille, France, 2009.

Bosch, J., Staffell, I., and Hawkes, A. D.: Temporally explicit and spatially resolved global offshore wind energy potentials, Energy, 163, 766–781, https://doi.org/10.1016/j.energy.2018.08.153, 2018.

Czisch, G. and Ernst, B.: High wind power penetration by the systematic use of smoothing effects within huge catchment areas shown in a European example, Windpower, 2001.

Dvorak, M. J., Stoutenburg, E. D., Archer, C. L., Kempton, W., and Jacobson, M. Z.: Where is the ideal location for a US East Coast offshore grid?, Geophys. Res. Lett., 39, 1–6, https://doi.org/10.1029/2011GL050659, 2012.

Emeis, S.: Wind Energy Meteorology, 2nd Edn., Springer, 2018.

Grams, C. M., Beerli, R., Pfenninger, S., Staffell, I., and Wernli, H.: Balancing Europe's wind-power output through spatial deployment informed by weather regimes, Nat. Clim. Change, 7, 557–562, https://doi.org/10.1038/NCLIMATE3338, 2017.

Jaffe, R. L. and Taylor, W.: The Physics of Energy, Cambridge University Press, Cambridge, https://doi.org/10.1017/9781139061292, 2019.

Kahn, E.: The reliability of distributed wind generators, Elect. Power Syst. Res., 2, 1–14, https://doi.org/10.1016/0378-7796(79)90021-X, 1979.

Katzenstein, W., Fertig, E., and Apt, J.: The variability of interconnected wind plants, Energy Policy, 38, 4400–4410, https://doi.org/10.1016/j.enpol.2010.03.069, 2010.

Kempton, W., Pimenta, F. M., Veron, D. E., and Colle, B. A.: Electric power from offshore wind via synoptic-scale interconnection, P. Natl. Acad. Sci. USA, 107, 7240–7245, https://doi.org/10.1073/pnas.0909075107, 2010.

Klink, K.: Atmospheric circulation effects on wind speed variability at turbine height, J. Appl. Meteorol. Clim., 46, 445–456, https://doi.org/10.1175/JAM2466.1, 2007.

Lee, J. C. Y., Fields, M. J., and Lundquist, J. K.: Assessing variability of wind speed: comparison and validation of 27 methodologies, Wind Energ. Sci., 3, 845–868, https://doi.org/10.5194/wes-3-845-2018, 2018.

Meteorologisk Institutt: What is Frost?, available at: https://frost.met.no/index.html, last access: November 2020.

Norsk Klimaservicesenter: Seklima Observasjoner og værstatistikk, available at: https://seklima.met.no/observations/, last access: November 2020.

Reichenberg, L., Johnsson, F., and Odenberger, M.: Dampening variations in wind power generation-The effect of optimizing geographic location of generating sites, Wind Energy, 17, 1631–1643, https://doi.org/10.1002/we.1657, 2014.

Reichenberg, L., Wojciechowski, A., Hedenus, F., and Johnsson, F.: Geographic aggregation of wind power – an optimization methodologyfor avoiding low outputs, Wind Energy, 20, 19–32, https://doi.org/10.1002/we.1987, 2017.

Reistad, M., Breivik, Ø., Haakenstad, H., Aarnes, O. J., Furevik, B. R., and Bidlot, J.-R.: A high-resolution hindcast of wind and waves for the North Sea, the Norwegian Sea, and the Barents Sea, J. Geophys. Res., 116, C05019, https://doi.org/10.1029/2010JC006402, 2011.

Rex, D. F.: Blocking Action in the Middle Troposphere and its Effect upon Regional Climate, Tellus, 2, 275–301, https://doi.org/10.3402/tellusa.v2i4.8603, 1950.

Serreze, M. C., Carse, F., Barry, R. G., and Rogers, J. C.: Icelandic low cyclone activity: Climatological features, linkages with the NAO, and relationships with recent changes in the Northern Hemisphere circulation, J. Climate, 10, 453–464, https://doi.org/10.1175/1520-0442(1997)010<0453:ILCACF>2.0.CO;2, 1997.

Siemens AG: Siemens 6.0 MW Offshore Wind Turbine, Tech. rep., available at: https://www.qualenergia.it/sites/default/files/articolo-doc/6_MW_Brochure_Jan.2012_0.pdf (last access: November 2020), 2011.

Sinden, G.: Characteristics of the UK wind resource: Long-term patterns and relationship to electricity demand, Energy Policy, 35, 112–127, https://doi.org/10.1016/j.enpol.2005.10.003, 2007.

St. Martin, C. M., Lundquist, J. K., and Handschy, M. A.: Variability of interconnected wind plants: Correlation length and its dependence on variability time scale, Environ. Res. Lett., 10, 44004, https://doi.org/10.1088/1748-9326/10/4/044004, 2015.

Trenberth, K. E., Large, W. G., and Olson, J. G.: The Mean Annual Cycle in Global Ocean Wind Stress, J. Phys. Oceanogr., 20, 1742–1760, https://doi.org/10.1175/1520-0485(1990)020<1742:tmacig>2.0.co;2, 1990.

Vasilyev, L., Christakos, K., and Hannafious, B.: Treating wind measurements influenced by offshore structures with CFD methods, Energy Procedia, 80, 223–228, https://doi.org/10.1016/j.egypro.2015.11.425, 2015.

Zheng, C. W., Li, C. Y., Pan, J., Liu, M. Y., and Xia, L. L.: An overview of global ocean wind energy resource evaluations, Renew. Sustain. Energ. Rev., 53, 1240–1251, https://doi.org/10.1016/j.rser.2015.09.063, 2016.

Paper II

The 3 km Norwegian reanalysis (NORA3) - a validation of offshore wind resources in the North Sea and the Norwegian Sea

Solbrekke, Ida M., Sorteberg, Asgeir, Haakenstad, Hilde
Wind Energy Science, **6/6** (2021)

II

Wind Energ. Sci., 6, 1501–1519, 2021
https://doi.org/10.5194/wes-6-1501-2021

eawe european academy of wind energy
Open Access
WIND ENERGY SCIENCE

The 3 km Norwegian reanalysis (NORA3) – a validation of offshore wind resources in the North Sea and the Norwegian Sea

Ida Marie Solbrekke[1], Asgeir Sorteberg[2], and Hilde Haakenstad[3]

[1]Geophysical Institute, Bergen Offshore Wind Centre (BOW), University of Bergen, Allegaten 70, 5020 Bergen, Norway
[2]Geophysical Institute, Bjerknes Centre for Climate Research (BCCR), Bergen Offshore Wind Centre (BOW), University of Bergen, Bergen, Norway
[3]Geophysical Institute, Norwegian Meteorological Institute, University of Bergen, Bergen, Norway

Correspondence: Ida Marie Solbrekke (ida.solbrekke@uib.no)

Received: 12 March 2021 – Discussion started: 1 April 2021
Revised: 27 September 2021 – Accepted: 10 October 2021 – Published: 30 November 2021

Abstract. We validate a new high-resolution (3 km) numerical mesoscale weather simulation for offshore wind power purposes for the time period 2004–2016 for the North Sea and the Norwegian Sea. The 3 km Norwegian reanalysis (NORA3) is a dynamically downscaled data set, forced with state-of-the-art atmospheric reanalysis as boundary conditions. We conduct an in-depth validation of the simulated wind climatology towards the observed wind climatology to determine whether NORA3 can serve as a wind resource data set in the planning phase of future offshore wind power installations. We place special emphasis on evaluating offshore wind-power-related metrics and the impact of simulated wind speed deviations on the estimated wind power and the related variability. We conclude that the NORA3 data are well suited for wind power estimates but give slightly conservative estimates of the offshore wind metrics. In other words, wind speeds in NORA3 are typically 5 % (0.5 m s^{-1}) lower than observed wind speeds, giving an underestimation of offshore wind power of 10 %–20 % (equivalent to an underestimation of 3 percentage points in the capacity factor) for a selected turbine type and hub height. The model is biased towards lower wind power estimates due to overestimation of the wind speed events below typical wind speed limits of rated wind power ($u < 11$–13 m s^{-1}) and underestimation of high-wind-speed events ($u > 11$–13 m s^{-1}). The hourly wind speed and wind power variability are slightly underestimated in NORA3. However, the number of hours with zero power production caused by the wind conditions (around 12 % of the time) is well captured, while the duration of each of these events is slightly overestimated, leading to 25-year return values for zero-power duration being too high for the majority of the sites. The model performs well in capturing spatial co-variability in hourly wind power production, with only small deviations in the spatial correlation coefficients among the sites. We estimate the observation-based decorrelation length to be 425.3 km, whereas the model-based length is 19 % longer.

Published by Copernicus Publications on behalf of the European Academy of Wind Energy e.V.

1 Introduction

Exploiting the Norwegian continental shelf for offshore wind power purposes is advantageous due to the excellent wind climate (Zheng et al., 2016) and the recent increase in political engagement. In June 2020 the Norwegian government decided to open the country's first two offshore areas at the Norwegian continental shelf, "Utsira Nord" and "Sørlige Nordsjøen II", for concessions to build and operate large wind power installations (Regjeringen, 2020). In this context, the ability to map the spatial and temporal wind power potential is crucial for selecting the best areas for wind power production.

Observational sites in the North Sea and the Norwegian Sea are sparse, and their numbers are insufficient to map the regional wind power potential. The lack of observational data makes it challenging for stakeholders and decision makers to choose new sites to open for offshore wind power concessions. Apart from using satellite data on surface winds, the only way to map the total wind power potential for a large offshore area is to use data from high-resolution numerical weather prediction (NWP) models that provide data near a typical hub height.

Several studies have mapped the wind energy potential of the North Sea and/or the Norwegian Sea using simulated data from the mesoscale Weather Research and Forecasting (WRF) Model (Berge et al., 2009; Byrkjedal and Åkervik, 2009; Byrkjedal et al., 2010; Skeie et al., 2012; Hahmann et al., 2015; Hasager et al., 2020). Berge et al. (2009) investigated how well the WRF model captured the offshore wind conditions in the North Sea from 2004–2007. After comparison of the simulated data with observations from oil and gas platforms, the authors conclude that the WRF model is a reliable tool for characterizing the average wind conditions in the region in question. The model was verified using observations from offshore sites in the North Sea but did not undergo a peer-review process. Byrkjedal and Åkervik (2009) simulated the wind resource and wind power potential at the Norwegian economic zone. The WRF model produced the simulated data for 2000–2008 used in their wind power calculations. However, the simulated data set was not validated against observations, and the report was not peer-reviewed. Byrkjedal et al. (2010) used the WRF model to simulate the offshore wind power potential in the North Sea from 2000 to 2009. Based on their 10-year WRF simulation they estimated wind power and identified areas with the greatest wind power potential, in addition to the dependency between separation distance and the correlation between two wind power production sites. The model performance was not compared to observations, and the report was not evaluated in a peer-review process. The more recent data set, the New European Wind Atlas (NEWA), was a joint project between research institutions and the industry. NEWA aims to provide a high-resolution, freely available data set on wind energy resources in Europe (Dörenkämper et al., 2020). NEWA uses meteorological masts on land to validate the onshore model data, while the offshore data are validated at 10 m a.s.l. (meters above sea level) using satellite data. In addition, a validation at 100 m a.s.l. is conducted by extrapolating the equivalent neutral wind speed at 10 m using the log-law relation (Badger et al., 2016). NEWA underwent a peer-review process. A peer-reviewed validation of wind model simulations before using the data for offshore wind power purposes is very important. The degree of data set validation and peer-review process of the results in the preceding studies is either limited or nonexistent.

In this study we perform an in-detail validation of the 3 km Norwegian reanalysis (NORA3), a new and freely available high-resolution data set, to be used for offshore wind resource assessment and wind power estimates. NORA3 is a high-resolution atmospheric dynamic downscaling of the state-of-the-art reanalysis data from ECMWF, called ERA5. The downscaling of ERA5 is performed by the NWP model HARMONIE-AROME (H-A). H-A is a high-resolution NWP model developed and used by many European weather forecast and research institutions (Seity et al., 2011; Bengtsson et al., 2017). The creation of NORA3 will contribute to the growing ensemble of wind resource data sets. Since all currently existing wind resource data sets are generated by the WRF model, the creation of NORA3 by a different NWP model will contribute to a diversity in the available wind resource data sets. When the ensemble of these data sets is considered in wind power planning the overall uncertainty in power production can be better quantified. The usefulness of multi-model ensembles has become increasingly clear over the last few decades in research fields such as weather prediction and climate change. By this extensive validation of the NORA3 data set and documenting the quality of the simulated wind resource and related wind power estimates from a new model, we wish to contribute to the growing literature on offshore wind resources.

The novelty of this study is the in-depth validation of the model data using a new NWP model. Through advanced statistical measures we perform a near-hub-height validation of the NORA3 estimated wind resource and the related wind power production. Besides validation measures like arithmetic mean, standard deviation, relative difference between the data sets, temporal correlations, and seasonality of the variables, we also include comparison and validation of data distributions, hourly ramp rates, spatial correlation, and analysis on the zero-wind-power events including extreme-value analysis. Since this is the first paper to evaluate the wind resource estimates from NORA3, the focus is put on a detailed validation against observations. A comparison of NORA3 against the host data set (ERA5) is also conducted to document the improvement of the downscaling process. To our knowledge this is the first peer-review paper focusing on evaluation of simulated wind resource and wind power estimates against offshore observations in the North Sea and ad-

jacent ocean regions, increasing the relevance of the present study.

We validate the NORA3 data set for wind power purposes using observational wind data from six offshore sites. Details regarding the model and observational data, in addition to the data processing routines, are found in Sect. 2.1 and 2.2. Sections 2.3–2.6 describe the methods used. The result of the downscaling process of ERA5 is quantified through a comparison between output data from NORA3 and ERA5 in Sect. 3. In Sect. 4 we investigate how well NORA3 captures the statistical wind speed measures and the related distributions. We also study the model performance in terms of the wind speed ramp rates (Sect. 4.1), spatial wind speed gradient (Sect. 4.2), and wind direction (Sect. 4.3). In addition, uncertainties related to observations sampled at large structures are discussed in Sect. 4.4. After converting wind speed data to hourly wind power data, we examine the performance of NORA3 related to wind power climatology (Sect. 5), including wind power variables such as median production and capacity factor (CF). Revealing the wind power potential in an area also requires mapping the wind power intermittency and variability at different spatial and temporal scales. The ability of the model to capture wind power variability and intermittency is investigated using hourly wind power ramp rates (Sect. 5.1) and long-term variability in CF (Sect. 5.2). In addition to temporal variability, we also consider the ability of NORA3 to capture the spatial co-variability between production sites (Sect. 5.3). It is crucial for a data set to reveal the length, duration, and total number of hours of zero wind power production, and NORA3's performance against these measures is discussed in Sect. 5.4. Moreover, we calculate and validate the maximum expected length of a zero event occurring during the turbine lifetime (Sect. 5.5). In the last section (Sect. 6) we summarize the validation results.

2 Data and method

2.1 Model data

NORA3 is obtained by high-resolution atmospheric dynamic downscaling of the state-of-the-art ERA5 reanalysis data set from the ECMWF (Hersbach et al., 2020). ERA5 covers the Earth in an approximately 31×31 km horizontal grid, providing hourly information in 137 vertical layers. The model used in the downscaling process is the nonhydrostatic, convection-permitting NWP model HARMONIE-AROME (H-A) (Cycle 40h1.2). Boundary values from ERA5 are provided to the model every 6 h. Hourly[1] NORA3 output data are stored (some outputs are stored every third hour). The model domain in NORA3 encloses almost the entire northern part of the Atlantic Ocean (see Fig. 1), and the model runs with a horizontal resolution of 3×3 km, with the atmosphere divided into 65 vertical layers.

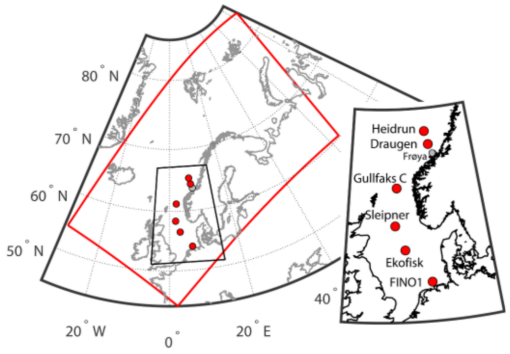

Figure 1. The domain (red rectangle) covered by the HARMONIE-AROME simulation and the locations of the six sites used in verifying the NORA3 data set (red dots), in addition to the meteorological mast located at Frøya. A close-up plot of the positions and the names of the stations is also shown. Details for the sites are given in Table 1.

H-A is a high-resolution NWP model solving the fully compressible Euler equations using forward time integration on a non-staggered horizontal grid. H-A is used in short-range operational forecasting and research by many European weather services and research institutes (Seity et al., 2011; Bengtsson et al., 2017). The NORA3 data set is a hybrid between a hindcast and a reanalysis data set because of the way the observations are treated in the model. The H-A model performs data assimilation of 2 m temperature and 2 m relative humidity.

NORA3 is continuously being generated. When the model integration is finalized (summer 2022) the NORA3 data will cover the time period from 1979 to present and will be regularly updated in the coming years when ERA5 data become available. We will focus on the period 2004–2016 in this study due to the time coverage of the observational data. For further details on the model set-up and the NORA3 generation process see Haakenstad et al. (2021).

2.2 The observational data

The observations used in the verification of NORA3 are hourly wind observations[2] from five oil and gas platforms (Ekofisk, Sleipner, Gullfaks C, Draugen, and Heidrun) retrieved from the Norwegian Meteorological Institute and one meteorological mast (FINO1, mast corrected data) (see Fig. 1 for the location of the sites and Table 1 for further site information). The observational data were quality checked prior to the validation of NORA3. For a detailed description of this quality check process see Solbrekke et al. (2020). In addition to the routine described in Solbrekke et al. (2020), we also

[1] Instantaneous values.

[2] 10 min average values provided at every hour.

Table 1. Relevant information for the sites used in the validation of NORA3. "Abb" lists the site-name abbreviations. "Lat" and "Long" are the latitude and longitude for the site locations, respectively. "WSH" (in meters above sea level) corresponds to the wind sensor height at each site. The sensor type is listed under "Sensor", and the data period for the available observations for each site is listed under "Data period". In addition, the percentage of valid observations is also shown under "Valid obs (%)".

Site information							
Site	Abb	Lat	Long	WSH	Sensor	Data period	Valid obs (%)
FINO1	f1	54.02	06.59	102	A100LK Cup-anemometer	1 Jan 2004–31 Jul 2009	95.8
Ekofisk	ek	56.52	03.22	68/102	Vaisala WMT703	1 Jan 2000–31 Sep 2016	85.3
Sleipner	sl	58.37	01.91	136	Gill Ultrasonic	1 Jan 2000–31 Sep 2016	83.4
Gullfaks C	gf	61.22	02.27	140	Gill Ultrasonic	1 Jan 2000–31 Sep 2016	80.2
Draugen	dr	64.35	07.78	78	Gill Ultrasonic	1 Jan 2002–31 Sep 2016	66.6
Heidrun	he	65.33	07.78	131	Gill Ultrasonic	1 Jan 2000–31 Sep 2016	84.6

exclude all records of zero-wind conditions ($u = 0$) that are likely to be erroneous according to the following:

$$u_{\mathrm{obs}}(i) = 0 \wedge u_{\mathrm{n3}}(i) \geq \frac{5}{m}\frac{1}{n}\sum_{j=1}^{m}\sum_{i=1}^{n}|u_{\mathrm{obs}}(i,j) - u_{\mathrm{n3}}(i,j)| = 5\overline{\mathrm{MAD}}, \quad (1)$$

where $u_{\mathrm{obs}}(i,j)$ and $u_{\mathrm{n3}}(i,j)$ are the observed and modeled wind speeds, respectively, at hour i for site j. n is the total number of hours, m is the total number of sites, and $\overline{\mathrm{MAD}}$ is the mean absolute deviation between the observed and modeled wind speeds averaged over all sites. In other words, whenever the observed wind speed at hour i and site j is zero and the corresponding modeled wind speed exceeds $5\overline{\mathrm{MAD}} = 7.2\,\mathrm{m\,s^{-1}}$, the observed value at hour i is excluded from the time series for site j. This additional quality control leads to the exclusion of up to 5 h of observations per site, except at Heidrun, which excludes 58 h of observations. For Heidrun, the removal of these erroneous records of zero-wind conditions ($u = 0$) corresponds to an exclusion of approximately 0.035 % of the total data.

2.3 Wind interpolation

To avoid introducing additional uncertainties into the observational data set, we verify the wind variables from NORA3 at the wind sensor heights, ranging from 68–140 m a.s.l., for each site (see "WSH" in Table 1 for the sensor heights). By contrast, the wind power verification is performed at a typical hub height, at 100 m a.s.l., to ensure the production estimates are comparable between sites. The interpolation of wind speed data to another height is usually done by either the logarithmic law, the power law, or a combination of the two methods (e.g., the Deaves & Harris model). Gualtieri (2019) reviewed the three aforementioned methods for 96 different locations worldwide. He concluded that the power law was the most reliable and also the most frequently used extrapolation method. In addition, according to Sill (1988) the usage of the logarithmic law (log law) is most suitable near the surface. Despite the aforementioned results from Gualtieri and Sill we have compared the performance of the log law and the power law (with time varying power exponent) for the offshore sites. The results of the comparison show that the model bias using the log law is larger than using the power law method. Therefore, the interpolation of wind speed data to sensor height or hub height is done using the power law relation (Emeis, 2018).

The interpolated wind speed is sensitive to the choice of the power law exponent α. Usually, α is assigned based on assumptions about atmospheric stability and surface roughness, both of which can introduce erroneous results. However, the data from NORA3 allow us to calculate α for each time step (i). Rearranging the power law relation, we get the following expression for the power law exponent α:

$$\alpha(i) = \frac{\ln\frac{u(i)_{z2}}{u(i)_{z1}}}{\ln\frac{z_2}{z_1}}, \quad (2)$$

where the height subscripts $_1$ and $_2$ corresponds to the two layers within which the wind shear is calculated. The heights used to calculate α depend on the wind sensor height (WSH) at the site in question: if WSH < 100 m a.s.l. then α is calculated using NORA3 wind shear between the two model layers $z_1 = 50$ m a.s.l. and $z_2 = 100$ m a.s.l. If WSH > 100 m a.s.l., then α is calculated using the wind shear between $z_1 = 100$ m a.s.l. and $z_2 = 250$ m a.s.l. The mean α for the whole time period for the six stations ranges from 0.05 to 0.08 between 50 and 100 m a.s.l. and from 0.03 to 0.06 between 100 and 250 m a.s.l. For each site, the wind directions at WSH are obtained by interpolating the X and Y component of the wind vector using linear interpolation between the adjacent model layers (50 and 100 m a.s.l. or 100 and 250 m a.s.l.).

2.4 Normalized wind power

To ensure our validation results are as general as possible, and since the wind farm at each site is only imaginary

and of unknown capacity, we use normalized power calculations $P_{\mathrm{w}}(i) = \frac{P_{\mathrm{w}}^{T}(i)}{P_{\mathrm{w}}^{\max}}$ to validate the wind power potential at each site (Solbrekke et al., 2020). $P_{\mathrm{w}}^{T}(i)$ is the produced wind power at each time step (i) for a given site, and $P_{\mathrm{w}}^{\max}$ is the nameplate capacity. Hence, the normalized wind power $P_{\mathrm{w}}(i)$ is defined as follows:

$$P_{\mathrm{w}}(i) = \begin{cases} 0 & u(i) < u_{\mathrm{ci}}, \\ \frac{u(i)^3 - u_{\mathrm{ci}}^3}{u_r^3 - u_{\mathrm{ci}}^3}, & u_{\mathrm{ci}} \le u(i) < u_r, \\ 1, & u_r \le u(i) < u_{\mathrm{co}}, \\ 0, & u_{\mathrm{co}} \le u(i), \end{cases} \tag{3}$$

where $u(i)$ is the wind speed at hour i, $u_{\mathrm{ci}} = 4\,\mathrm{m\,s^{-1}}$ is the cut-in wind speed, $u_r = 13\,\mathrm{m\,s^{-1}}$ is the rated wind speed, and $u_{\mathrm{co}} = 25\,\mathrm{m\,s^{-1}}$ is the cut-out wind speed. These numbers were retrieved from the SWT-6.0-154 turbines used in Hywind Scotland – the first floating wind farm in the world (Siemens Gamesa Renewable Energy, 2011).

2.5 Ramp rates

To validate the ability of NORA3 to capture the wind speed and wind power variability, we calculate the ramp rates (R), defined as how much the wind speed (u) or wind power (P_{w}) changes during a time increment τ (Milan et al., 2014):

$$R_{P_{\mathrm{w}}}(i) = P_{\mathrm{w}}(i) - P_{\mathrm{w}}(i+\tau), \tag{4a}$$

$$R_u(i) = u(i) - u(i+\tau), \tag{4b}$$

and setting $\tau = 1$, we validate the model performance on hourly ramp rates. To gain a general picture of the model performance in terms of how much the wind speed or wind power changes from one hour to the next, we calculate the mean absolute ramp rate (MAR) for each site, for both the observational data and the modeled data. MAR is defined as follows:

$$\mathrm{MAR} = \frac{1}{n}\sum_{i=1}^{n} |R(i)|, \tag{5}$$

where $R(i)$ is the ramp rate at hour i and n is the total number of hours.

2.6 Zero-event duration using extreme-value theory

A wind turbine has an expected lifetime of approximately 20 years. If the right steps are taken, the lifetime can be extended 15 %–25 % depending on whether the structure is bottom-fixed or floating (Wiser et al., 2016). This means that the lifetime is expected to increase to 23–25 years. Therefore, determining the duration of long-lasting shutdowns expected to happen during the lifetime of a turbine is important for estimating the levelized cost of energy (LCOE). The 25-year return value of the duration of a zero event (a period of zero wind power production), the corresponding confidence interval, and the p values are calculated from the observations and the model data using two statistical methods, "block maxima" (BM), in which the data are fitted to a generalized extreme value (GEV) distribution using yearly values of maximum zero-event duration, and "peak over threshold" (POT), in which the data are fitted to a generalized Pareto distribution (for more information see Smith, 2002) using the 99th percentile of the zero-event duration (the highest 1 % of zero event in terms of duration) as the selected threshold. We calculate the Kolmogorov–Smirnov p value (KS_p) to test the null hypothesis. The null hypothesis states that the empirical data are *not* drawn from the chosen data distribution (GEV or Pareto). Testing the null hypothesis is done by the Kolmogorov–Smirnov statistic calculating the distance between the empirical and theoretical cumulative distributions. Hence, the cumulative distribution function from the BM data (POT data) is compared to the cumulative distribution function from the GEV (Pareto) distribution. Thus, given a significance level of $p = 0.025$, if the KS_p value is small ($\mathrm{KS}_p < p$), the distance between the cumulative distributions is too large, and we can conclude that the empirical data (BM or POT) was sampled from a different population than the theoretical GEV or Pareto distribution with a probability of $1 - p$. If the result from the Kolmogorov–Smirnov test tell us that we cannot exclude the possibility that the data are drawn from either of the two data distributions (GEV or Pareto), we fit the observation-based and model-based maximum zero-event durations to GEV and Pareto and find the corresponding 25-year return values for the five sites (FINO1 is excluded from the extreme-value analysis due to the shorter time series: 2004–2009).

3 Comparison of NORA3 and ERA5

The NORA3 wind estimates in 10 m a.s.l. are extensively validated against observations and compared to the ERA5 reanalysis in Haakenstad et al. (2021). Nevertheless, we compare the performance of NORA3 and ERA5 towards the observed wind speed climatology to see the result of the downscaling process in the six wind sensor heights (68–140 m a.s.l.). We compare data every 6 h, which corresponds to the ERA5 data used as boundary information in HARMONIE-AROME in the generation process of NORA3.

The observed seasonal average and standard deviation of the wind speed are shown in Tables 2 and 3, respectively. In addition, the tables also contain the relative difference (in percentage) between the observations and NORA3 (n3 (%)) and between the observations and ERA5 (e5 (%)). Table 2 illustrates that the modeled average seasonal wind speeds from NORA3 are consistently closer to the observed values for all the seasons and for all the sites. The standard deviation (SD) is here a measure of the variability in the wind speed (Ta-

Table 2. Seasonal average of the observed (obs) wind speed ($m\,s^{-1}$) and the model deviation in percentage (%) for both NORA3 (n3) and ERA5 (e5). "DJF" corresponds to December–January–February, "MAM" is March–April–May, "JJA" is June–July–August, and "SON" is September–October–November.

	Seasonal mean wind speed ($m\,s^{-1}$)											
	DJF			MAM			JJA			SON		
Site	obs	n3 (%)	e5 (%)	obs	n3 (%)	e5 (%)	obs	n3 (%)	e5 (%)	obs	n3 (%)	e5 (%)
FINO1	11.14	0.44	−0.9	9.69	−1.5	−3.6	8.31	−1.5	−2.0	10.62	−2.0	−2.2
Ekofisk	12.74	−5.4	−7.5	10.08	−2.8	−5.9	8.60	−5.0	−7.5	11.40	−5.2	−6.9
Sleipner	13.85	−9.2	−11.3	10.75	−8.1	−11.3	8.98	−9.0	−11.6	12.33	−8.9	−10.9
Gullfaks C	13.39	−6.4	−9.9	10.53	−6.7	−10.3	9.09	−7.9	−11.3	11.92	−5.9	−8.8
Draugen	11.81	−4.9	−8.3	9.52	−3.5	−6.7	8.06	−5.6	−9.6	10.76	−4.4	−7.2
Heidrun	12.37	−6.6	−8.7	10.09	−6.5	−8.6	8.28	−7.6	−10.0	11.24	−7.1	−8.7
Average	12.55	−5.3	−7.8	10.11	−4.9	−7.7	8.55	−6.1	−8.7	11.38	−5.6	−7.5

Table 3. Seasonal standard deviation of the observed (obs) wind speed ($m\,s^{-1}$) and the model deviation in percentage (%) for both NORA3 (n3) and ERA5 (e5). "DJF" corresponds to December–January–February, "MAM" is March–April–May, "JJA" is June–July–August, and "SON" is September–October–November.

	DJF			MAM			JJA			SON		
Site	obs	n3 (%)	e5 (%)	obs	n3 (%)	e5 (%)	obs	n3 (%)	e5 (%)	obs	n3 (%)	e5 (%)
FINO1	5.29	−3.3	−6.2	4.35	−2.6	−8.2	3.79	−1.5	−4.5	4.75	−5.0	−8.8
Ekofisk	5.85	−4.4	−6.8	4.47	−1.8	−6.3	4.05	−3.2	−6.7	5.12	−5.5	−8.0
Sleipner	6.41	−7.5	−9.5	4.96	−6.7	−9.7	4.38	−6.4	−10.1	5.49	−6.9	−8.9
Gullfaks C	6.41	−4.2	−4.8	5.18	−4.6	−6.8	4.59	−4.1	−7.8	5.51	−3.8	−5.8
Draugen	5.88	−6.1	−7.3	5.48	−8.2	−11.3	4.50	−9.3	−13.8	5.70	−6.7	−9.7
Heidrun	5.94	−8.4	−11.4	5.33	−7.5	−10.1	4.27	−8.0	−11.2	5.65	−8.3	−11.7
Average	5.96	−5.7	−7.7	4.96	−5.2	−8.7	4.26	−5.4	−9.0	5.37	−6.0	−8.8

ble 3). Compared to ERA5, NORA3 is consistently closer to the observed seasonal SD for all the six sites.

Figure 2 shows a quantile–quantile plot (qq plot) between the observed wind speed and modeled wind speed by NORA3 and ERA5. The qq plot determines if the modeled and observed data sets are drawn from the same sample distribution. If the circles lie on the reference line, the data sets come from the same data distribution. For all the six sites the models perform best for the lowest wind speeds ($u \leq 10\,m\,s^{-1}$). For both models the deviation from the reference line ("ref line") increases with increasing wind speed percentile. Nevertheless, NORA3 is consistently closer to the reference line compared to ERA5, especially for wind speed exceeding a typical cut-off wind speed ($u \geq u_{co}$). A technical feature called "high wind ride through" enables the turbine to exploit more of the very strong wind speeds ($u \geq u_{co}$). In offshore areas, higher winds are occurring more frequently. Therefore, the importance for a NWP model to correctly estimate these strong wind events increases. NORA3 outperforms ERA5 for these high wind speeds ($u \geq u_{co}$).

As illustrated in Fig. 2 the largest difference between the observations, NORA3, and ERA5 is found for wind speeds exceeding a typical cut-out limit of $25\,m\,s^{-1}$ ($u \geq u_{co}$). Since the power production is terminated or at least reduced when $u \geq u_{co}$, we calculate the wind power capacity factors (CF) for the three data sets. This is done to see how the models perform in terms of power production, where the strongest wind speeds are not influencing the result due the power production cut-out limit. Table 4 contains the CF for the observed data, NORA3, and ERA5 for the six sites. NORA3 performs consistently better than ERA5, where NORA3 is on average 1.8 percentage points closer to the average observed CF value compared to ERA5.

The required rate of return when planning offshore wind projects is typically 5 %–10 %. A deficiency of 3 percentage points (approximately 6 % difference in the average power output) in the CF is a sizable error and might be too large in terms of profitability. Nevertheless, this highlights the need for building up archives of different NWP simulations to be able to conduct informed uncertainty calculations for the power production in regions where observational data are limited. However, the comparison of CF between NORA3 and ERA5 shows that the ERA5-based CFs are on average 5 percentage points (approximately 10 % difference in the

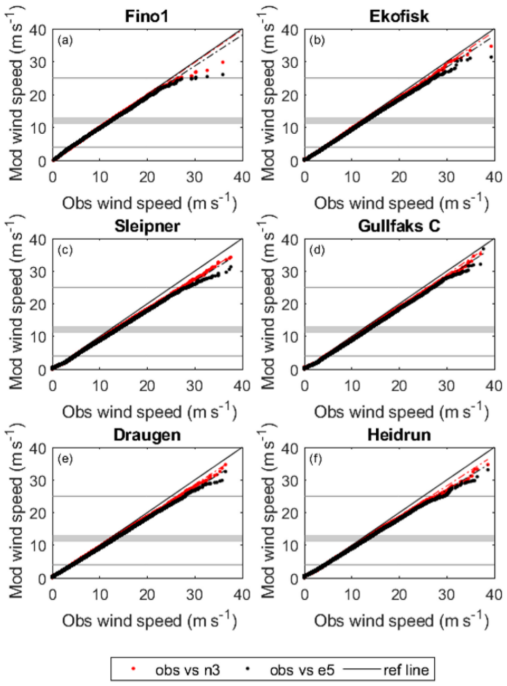

Figure 2. Quantile–quantile plot between the observed wind speed (obs) and the modeled (mod) wind speed, with NORA3 shown in red and ERA5 shown in black, for all the six offshore sites.

power output) lower than the observation-based CFs. Hence, the improvements using NORA3 over ERA5 gives more realistic wind power profitability measures.

The validation of wind climatology in NORA3 and ERA5 shows that the downscaling of ERA5 in the process of creating NORA3 has resulted in an improved wind resource data set. The remainder of this study will focus on the validation of NORA3 towards observed wind climatology.

4 Validation of NORA3 wind speed

Prior to exploiting NORA3 as a wind resource data set in the planning phase of future offshore wind power installations the data set has to be validated and verified against observational data. We start with the validation of mean quantities and wind speed distributions. The most relevant wind speed measures can be seen in Table 5. Arithmetic mean (μ) and standard deviation (σ) are used as measures of the average wind speed and the corresponding variability. Mean wind speeds (μ) for the six sites lie within the interval 10–12 m s^{-1}. For all the sites the observed mean wind speeds are

Table 4. Capacity factor (%) calculated from the observations (obs), NORA3 (n3), and ERA5 (e5) for the six sites. In addition, the differences (diff) between NORA3 and observations and between ERA5 and observations are also listed.

	Capacity factor (%)		
Site	obs	n3 (diff)	e5 (diff)
FINO1	46.8	46.5 (−0.3)	45.6 (−1.2)
Ekofisk	51.2	48.6 (−2.6)	46.8 (−4.4)
Sleipner	54.7	49.6 (−5.1)	47.8 (−6.9)
Gullfaks C	53.4	49.5 (−3.9)	46.9 (−6.5)
Draugen	45.3	43.2 (−2.1)	40.8 (−4.5)
Heidrun	48.5	44.6 (−3.9)	43.1 (−5.4)
Average	50.0	47.0 (−3.0)	45.2 (−4.8)

higher than the wind speeds from NORA3, indicating that the model underestimates the mean wind speed. The largest difference can be seen for Sleipner, where the observed mean wind speed is 8.9 % higher than the simulated wind speed. The wind speed at each site is highly variable, with the SD (σ) for the observations varying from 4.7–5.9 m s^{-1}, with the model wind speed being slightly less variable (3 %–8 %). Hence, the observed wind speed is somewhat more intermittent and variable than the modeled wind speed, indicating that HARMONIE-AROME is missing some of the variability embedded in the wind field.

The Weibull scale parameter ("λ" in Table 5) indicates the height and width of the distribution. A larger scale parameter indicates a wider and lower probability distribution. All the observed scale parameters are slightly higher than the modeled; the modeled scale parameters are on average 3.93 % lower than the observed. In other words, the observations contain more wind speed events at the tails of the Weibull distributions, resulting in a larger scale parameter.

As all observed and modeled Weibull shape parameters ("k" in Table 5) are less than 2.6, the distributions are positively skewed, with a long tail to the right of the mean. The observed shape parameter is equal to or smaller than the modeled one (on average 7.3 % lower), indicating that the observed data are more positively skewed with a longer right tail, again emphasizing that the observed data contain more high-wind-speed events than the NORA3 wind speed data.

According to Table 5 the model underestimates the wind speed at all sites. Since the wind power production is a function of the wind speed cubed, the wind power is highly sensitive to systematic deviations between the observed and simulated wind speeds. However, the sensitivity varies with wind speed and is especially strong within the interval between cut-in and rated wind speeds. Figure 3b–h show the differences in the observed and modeled wind speed probability density functions ($\Delta\text{pdf} = \text{pdf}_{\text{mod}} - \text{pdf}_{\text{obs}}$) for the six sites, in addition to the wind speed distribution for Ekofisk (Fig. 3a). The main finding is that the model underestimates

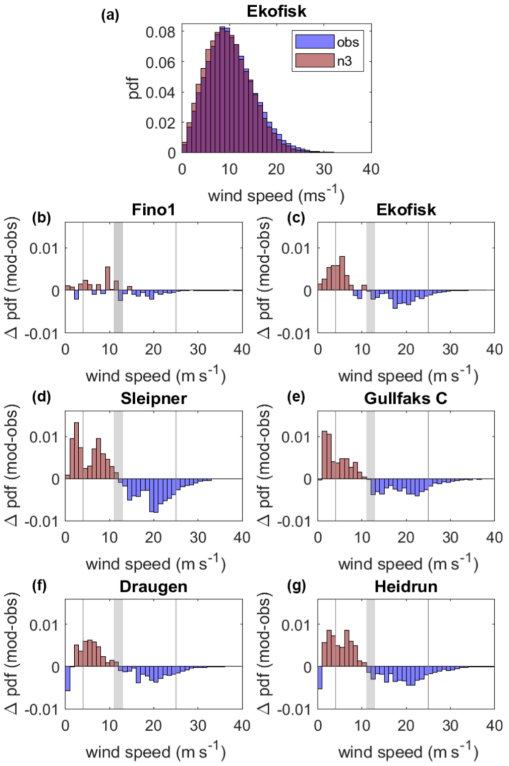

Figure 3. **(a)** Example wind speed probability density function (pdf) (Ekofisk) for NORA3 (n3) in red and observations (obs) in blue. **(b–g)** Differences between NORA3 and observational wind speed probability density functions ($\Delta\text{pdf} = \text{pdf}_{\text{mod}} - \text{pdf}_{\text{obs}}$) for the six sites. When $\Delta\text{pdf} = 0.01$ the probability that the given wind speed will occur is 1 % higher in the model output. The large gray area corresponds to the range within which the rated wind speed usually falls. The gray vertical lines at the left and right mark the cut-in and cut-out wind speed limits used in this study, respectively.

the number of events with high wind speed and overestimates the number of events with low wind speed for all sites. The model is biased towards too few high-wind events and too many low-wind events than observed, and the transition occurs near typical rated wind speeds (11–13 m s^{-1}) for state-of-the-art offshore wind turbines (the widest gray area in Fig. 3b–h). This model bias will have a large impact on the difference between the observed and modeled wind power.

4.1 Wind speed ramp rates

The hourly wind speed ramp rate (m s^{-1}) is a measure of the hourly variability in the data set. In other words, the ramp rate quantifies how much the wind speed changes during 1 h. Figure 4 shows the distributions of observed and modeled hourly wind speed ramp rates for Ekofisk (the other sites have similar distributions). The distribution is wider for the observations than for the modeled data, illustrating that the observed wind speed change from one hour to the next is greater than that in the modeled wind speed data.

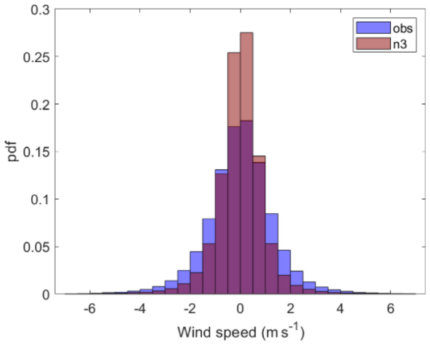

Figure 4. The probability density distribution (pdf) of the modeled (n3) and observed (obs) hourly wind speed ramp rates (m s^{-1}).

The mean absolute ramp rate (MAR) for the observed and modeled wind speed (u) is shown in Table 6. Typically observed MAR is around 1 m s^{-1}, and the difference between modeled and observed ramp rates indicates that the model underestimates the variability in hourly wind speed by 30 %–36 %.

4.2 Far-offshore to coastal wind speed gradient

An important feature of a model wind data set is the ability to properly estimate the horizontal wind speed gradient from far offshore to coastal areas. There are limited possibilities to investigate this using the available observational data. However, we made use of data from an observational meteorological mast situated on the coastal island of Frøya (see Fig. 1) to present some indicative results. Generally, using wind speed data at sensor height for the three sites Heidrun (far offshore), Draugen (near coastal), and Frøya (coastal) shows that there is no clear bias in the model (see Table 7). NORA3 underestimates the local far-offshore to near-coastal wind speed gradient but slightly overestimates the near-coastal to coastal gradient.

4.3 Wind direction

Another important factor for planning a wind farm using simulated data is the quality of the modeled wind direction. State-of-the-art wind turbine technology allows the wind turbines to yaw to face the main wind direction. Mapping the wind direction climatology is important for the wind farm layout. Wind-rose plots (see Sect. A Fig. A1) demonstrate

Table 5. Statistical measures of the wind speed ($m\,s^{-1}$) for the observations (obs) and the model (n3). μ and σ are the arithmetic mean and standard deviation, respectively. λ and k are the Weibull scale and shape parameters, respectively. The wind speed validation is performed at the sensor height to avoid uncertainties related to power law extrapolation (see Table 1 for information on heights).

	Wind speed ($m\,s^{-1}$)									
	μ			σ			λ		k	
Site	obs	n3	%	obs	n3	%	obs	n3	obs	n3
FINO1	9.91	9.77	−1.41	4.66	4.54	−2.57	11.18	11.02	2.24	2.27
Ekofisk	10.35	9.85	−4.83	4.97	4.75	−4.42	11.61	11.12	2.12	2.18
Sleipner	11.70	10.66	−8.89	5.83	5.42	−7.03	12.99	12.02	1.94	2.05
Gullfaks C	11.45	10.70	−6.55	5.90	5.66	−4.07	12.64	12.06	1.82	1.97
Draugen	9.87	9.44	−4.36	5.45	5.07	−6.97	10.95	10.65	1.75	1.94
Heidrun	10.56	9.87	−6.53	5.67	5.22	−7.94	11.50	11.13	1.64	1.97
Average	10.64	10.05	−5.43	5.41	5.11	−5.50	11.81	11.33	1.92	2.06

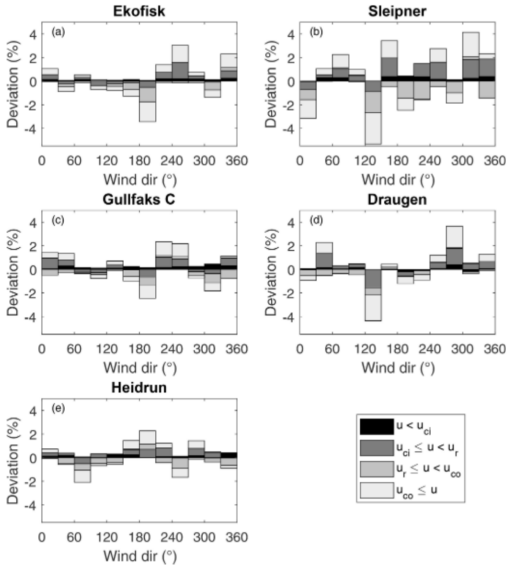

Figure 5. Difference in the occurrence (%) of wind events categorized in different wind direction intervals (30° intervals) between NORA3 and observations (model − obs) for **(a)** Ekofisk; **(b)** Sleipner; **(c)** Gullfaks C; **(d)** Draugen; **(e)** Heidrun. For each wind direction interval the wind events are divided into four different wind speed categories, the first one corresponds to u less than cut-in wind speed ($u < u_{ci}$), the second is the wind speed interval where the wind power is a function of the wind speed cubed ($u_{ci} \le u < u_r$), the third interval contain the wind speeds corresponding to rated wind power production ($u_r \le u < u_{co}$), and the last interval is where the wind speeds are too strong resulting in a terminated wind power production ($u_{co} \le u$).

Table 6. Mean absolute ramp rate (MAR) in meters per second ($m\,s^{-1}$) for the observed and modeled wind speed (u). The difference between the modeled and observed MAR_u divided by the observed MAR_u is given as a percentage (%).

	MAR_u ($m\,s^{-1}$)		
Site	obs	n3	diff (%)
FINO1	0.96	0.67	−29.72
Ekofisk	1.04	0.67	−35.58
Sleipner	1.15	0.75	−34.78
Gullfaks C	1.15	0.81	−29.57
Draugen	1.31	0.85	−35.11
Heidrun	1.22	0.80	−34.43
Average	1.14	0.76	−33.33

Table 7. The average change in wind speed ($m\,s^{-1}$) at sensor height per 100 km for Heidrun–Draugen and Draugen–Frøya.

	Wind speed gradient ($m\,s^{-1}$)		
Site	obs	n3	diff (n3 − obs)
Heidrun–Draugen	0.66	0.43	−0.23
Draugen–Frøya	1.52	1.68	0.16

that the modeled and observed data in general show the same wind direction distributions, with only small differences. FINO1 is excluded from the verification of wind direction because the wind rose for that site shows a clear directional disturbance, as the wind is affected by the observation mast. Figure 5 graphs the differences between the modeled and observed data (%) in the number of wind direction events (30° intervals) for four wind speed categories ($u < u_{ci}$, $u_{ci} \le u < u_r$, $u_r \le u < u_{co}$, and $u_{co} \le u$). There is no systematic bias in wind direction that can be seen across the sites, and the biases in frequency are less than 5 % for

all directional intervals and all sites. The wind speed interval with the greatest difference between the model and the observations features wind events corresponding to $u \geq u_{co}$. The wind speed intervals with the smallest difference between the model and the observation are the too low wind events ($u < u_{ci}$). Hence, the model is better at capturing the wind direction when the wind speed is low.

Sleipner is the site with the greatest difference between model and observations for almost all wind direction intervals (see Fig. 5b). The mismatch between the observed and modeled wind direction events for Sleipner is probably tied to the model performance. However, we cannot exclude the possibility that the platform design at Sleipner affects the flow field more than the design of the other platforms.

4.4 Uncertainties in observed wind speed

Working with observational data and numerical weather prediction models involves dealing with data that contain uncertainties and errors of known or unknown character. The majority of the observational sites used in this study (five of six sites) are oil and gas platforms. The platforms are large structures that may influence the upcoming flow. On the other side, an observational mast may also influence the flow when the upcoming wind is guided to pass through the mast before being recorded by the sensor.

Flow alteration by structures is a complex issue and might lead to both speedup and slowdown effects of the wind speed but also deflection of the wind vector resulting in a change in wind direction. A potential alteration of the wind would be a function of the platform layout, the atmospheric stability, the upcoming wind direction, and the ambient wind speed. To what extent large offshore structures influence the ambient flow field is unclear (Berge et al., 2009; Vasilyev et al., 2015; Furevik and Haakenstad, 2012). To investigate the distortion caused by these large structures, we compared wind speed data from the platforms with data from FINO1 and from the meteorological mast at the Frøya field station. The result (not shown) indicates that flow disturbance by large oil and gas platforms is to some extent visible in the wind speed and wind direction data for some of the platforms. However, indicating the portion of the wind data difference between the observations and NORA3 that is caused by flow distortion or by the model performance is not possible.

Despite the aforementioned uncertainties, using observations from oil and gas platforms enable us to validate NORA3 over ocean areas where observational data are sparse.

5 Comparison of estimated wind power from observed and modeled wind speed

Because the conversion from wind speed to wind power is nonlinear (see Eq. 3), the wind power distribution differs greatly from the wind speed distribution. The statistical measures for the wind power are shown in Table 8. Median (q_{50}) and interquartile range (IQR) are independent of data distribution and are therefore good representations of the average wind power production and the related intermittency, respectively. All wind power estimates are calculated at a hub height of 100 m a.s.l. using the wind interpolation method discussed in Sect. 2.3 and the normalized power curve described in Sect. 2.4.

Both the observation-based and model-based median wind power production estimates reveal very good wind power potential for the six sites (see Table 8). Nevertheless, since the model underestimates the wind speed events exceeding the rated wind speed, this partly counteracts the model's overestimation of the lower wind speed events ($u < u_r$), making the modeled average power production slightly underestimated. Therefore, the observation-based estimates of the median hourly power production q_{50} span from 0.3–0.5 (i.e., the median power production for a given hour would typically be 30 %–50 % of installed capacity), compared to 0.3–0.4 for the model-based estimates. IQR, a measure of the variability, is the range between the first and third quartiles ($q_{75} - q_{25}$). Since the range of the normalized wind power is 0–1, IQR values close to 1 correspond to high variability, since almost the entire data range is present between the first and third quartiles. Hourly IQRs range from 0.86–0.95 for the observation-based estimates and from 0.80–0.94 for the model. There is no systematic difference between the IQRs of the model-based estimates and the observation-based estimates.

The capacity factor (CF) is another statistical measure quantifying the wind power potential. CF is here defined as the average wind power potential divided by the installed capacity. The observation-based estimates of CF vary between 46 % and 55 %, and the CF values from the model-based estimates are slightly smaller. The observation-based CF values exceed the modeled values by an average of 3 percentage points.

5.1 Wind power ramp rates

Figure 6 shows the distribution of observation-based and model-based hourly normalized wind power ramp rates for Ekofisk (the other sites have similar distributions). As for the distribution of hourly wind speed ramp rates, the distributions of hourly wind power ramp rates are wider for the observation-based ramp rates than for the model-based ones, illustrating that the hourly estimated wind power variability based on observations is greater than the estimated variability based on NORA3 data. The difference in MARs indicates

Table 8. Statistical measures of the observation-based (obs) and model-based (n3) normalized wind power production. q_{50} is the hourly median production, IQR is the interquartile range of the hourly production, and CF is the wind power capacity factor. The wind power measures and estimates are performed at a typical hub height of 100 m a.s.l. using the interpolation of observed wind speeds as outlined in Sect. 2.3 and the power curve given in Sect. 2.4 for all the sites.

	Wind power								
	q_{50}			CF (%)			IQR		
Site	obs	n3	%	obs	n3	n3 − obs	obs	n3	%
FINO1	0.38	0.37	2.94	47.00	46.24	−0.76	0.88	0.84	−3.98
Ekofisk	0.45	0.40	−11.1	51.02	48.39	−2.63	0.88	0.91	3.41
Sleipner	0.54	0.42	−22.2	54.82	49.60	−5.22	0.88	0.91	3.41
Gullfaks C	0.51	0.42	−17.7	53.30	49.54	−3.77	0.90	0.92	2.22
Draugen	0.33	0.30	−9.10	45.45	43.34	−2.11	0.95	0.91	−4.21
Heidrun	0.39	0.32	−17.95	48.33	44.67	−3.66	0.93	0.94	1.08
Average	0.43	0.37	−16.74	49.99	46.96	−3.03	0.90	0.91	0.42

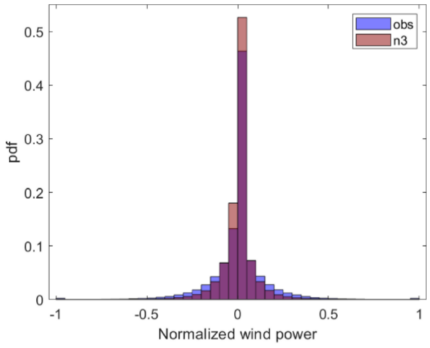

Figure 6. The probability density function (pdf) of the ramp rates for observation-based (obs) and model-based (n3) hourly normalized wind power.

an hour-to-hour variability typically of 7 %–9 % (Table 9) of the installed capacity based on observations. In contrast, the variability for model-based estimates is 5 %–6 % and is underestimated at all sites.

5.2 Inter-annual and seasonal capacity factor

In addition, to encompass short-term variations in wind speed and estimated power production, it is essential for a model data set to contain the correct long-term variations. In this section we evaluate NORA3's ability to capture the longer-term climatic variability of the wind power potential for a given site. The inter-annual and seasonal variations in CF provide a good indication of how NORA3 performs in terms of long-term wind power fluctuations.

Figure 7a and b illustrate the inter-annual and seasonal CF, respectively, from the observation-based estimates. In addition, the CF deviations (ΔCF) between the model-based estimates and the observation-based estimates are illustrated in Fig. 7c and d. The observed year-to-year variation in CF is substantial, varying up to 0.12 (12 % of installed capacity) from one year to the next. Figure 7c shows that the yearly CF values from the model are systematically lower than the observed CF values. This result is most pronounced for Sleipner, where the difference in $\Delta\mathrm{CF} \approx -5$, meaning that the model-based CF is on average 5 percentage points lower than the observation-based CF.

The model's underestimation of CF can also be seen in the seasonal CF values. Fig. 7d shows that $\Delta\mathrm{CF} < 0$ for all the sites. The underestimation of the seasonal CF values is largest during the summer months (May–September), meaning that the relative importance of the summer months in wind power production will be slightly underestimated in the model-based estimates.

Table 9. Mean absolute ramp rate (MAR_{P_w}) for the normalized observation-based and model-based estimates of the wind power output. The difference between the modeled and observed MAR_{P_w} divided by the observed MAR_{P_w} is given in percentage (%).

	MAR_{P_w}		
Site	obs	n3	diff (%)
FINO1	0.073	0.050	−30.73
Ekofisk	0.079	0.049	−37.97
Sleipner	0.077	0.051	−33.77
Gullfaks C	0.079	0.054	−31.65
Draugen	0.092	0.060	−34.78
Heidrun	0.084	0.055	−34.52
Average	0.081	0.053	−34.57

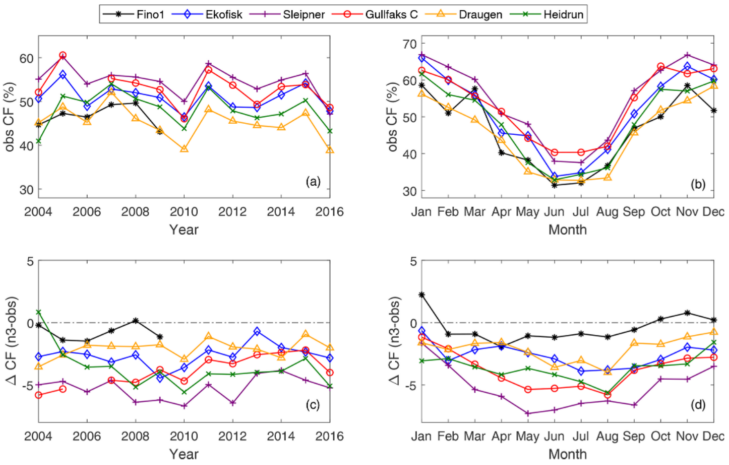

Figure 7. **(a)** The observed inter-annual variation in the capacity factor (obs CF). **(b)** Seasonal variation in CF for the observations. **(c)** The difference in the inter-annual CF (ΔCF) between the model and the observations (n3 − obs). **(d)** The difference in the seasonal CF between the model and the observations (n3 − obs). A specific year was excluded from the plot if more than one-half of the data for that year were missing.

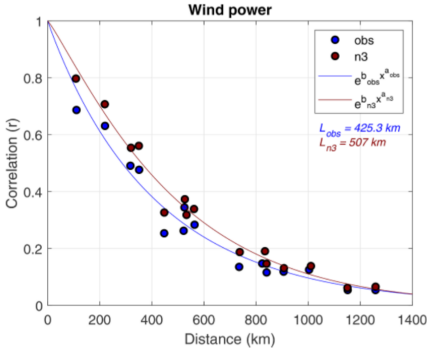

Figure 8. Correlation of wind power time series as a function of the distance between the connected site pairs for the observations (obs, blue) and NORA3 data (n3, red). An exponential fit is also shown (e^{bx^a}) for both data sets with the corresponding decorrelation lengths, L.

5.3 Spatial wind power co-variability

Many studies have shown that interconnection of wind power production sites mitigates wind power intermittency (Kempton et al., 2010; Reichenberg et al., 2014; St. Martin et al., 2015; Reichenberg et al., 2017; Solbrekke et al., 2020). Therefore, simulated data sets for use in decision-making about future wind power installations should be able to represent spatial and temporal co-variability between wind power sites.

Figure 8 illustrates the ability of NORA3 to capture the spatial co-variance in estimated hourly wind power production between the six sites. The figure demonstrates how the correlation between two sites changes as a function of the separation distance, both for the observation-based estimates (blue) and the model-based estimates (red). For almost all separation distances the model overestimates the correlation between two connected sites. The overestimation is generally small but is greatest for small separation distances. This result indicates that NORA3 is better at capturing the large-scale spatial variability than variance on smaller scales.

5.4 Zero-wind-power events

A general description of the dependency between correlation and separation distance can give us information on the decorrelation length for the sites used in this study. Using the station-pair correlations we identify a best-fitting exponential curve and a decorrelation length L (in kilometers). Connecting sites separated by a distance greater than the decorrelation length ensures that the collective wind power intermittency from the two sites is substantially reduced compared to the intermittency from one of the sites. We use the e-folding distance as a measure of the offshore decorrelation length L. The exponential curves and the corresponding decorrelation lengths for both the observations and NORA3 are presented in Fig. 8. The observation-based L is 425 km compared to a 507 km L based on NORA3. The model-based estimates

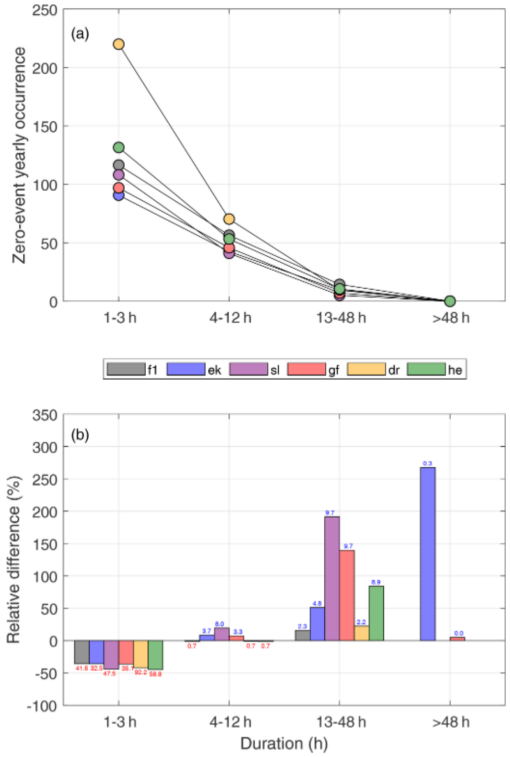

Figure 9. **(a)** Yearly occurrence and corresponding duration of observation-based zero events caused by wind speeds lower than cut-in wind speed ($u < u_{ci}$). **(b)** The differences between model-based (n3) and observation-based (obs) zero-event occurrences divided by the total number of observed occurrences of too low wind speeds. Values over or under each bar correspond to the differences (n3 − obs) in the number of yearly occurrences between the model and observations. Abbreviations: f1: FINO1; ek: Ekofisk; sl: Sleipner; gf: Gullfaks C; dr: Draugen; he: Heidrun.

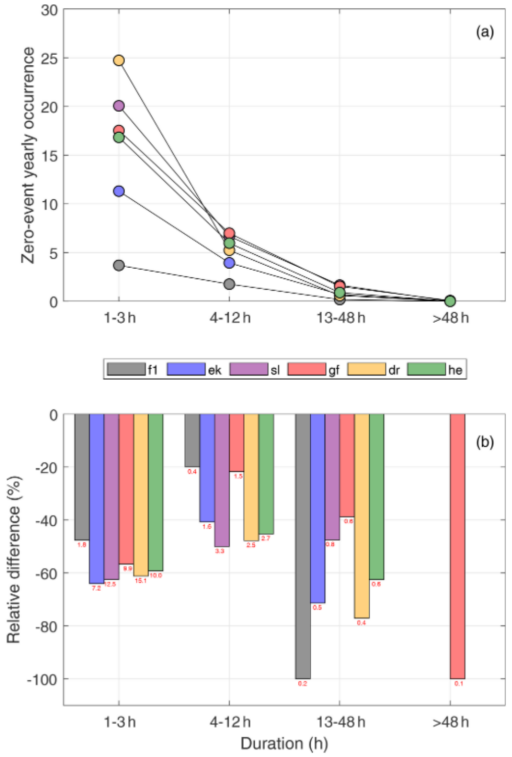

Figure 10. **(a)** Yearly occurrence and corresponding duration of observation-based zero events caused by wind speeds higher than cut-out wind speed ($u \geq u_{co}$). **(b)** The differences between model-based (n3) and observation-based (obs) zero-event occurrences divided by the total number of observed occurrences of too high wind speeds. Values over or under each bar correspond to the differences (n3 − obs) in the number of yearly occurrences between the model and observations. Abbreviations: f1: FINO1; ek: Ekofisk; sl: Sleipner; gf: Gullfaks C; dr: Draugen; he: Heidrun.

indicate that to ensure relatively independent hourly power production, a greater interconnection distance is needed than that indicated by the observation-based estimates.

Knowing about the risk, duration, and frequency of zero events (periods of zero wind power production) is important for decision-making and also in turbine maintenance planning, as these measures influence the levelized cost of energy and hence the decision-making process (Cory and Schwabe, 2009). A zero event is caused by a wind speed that is too low ($u < u_{ci}$) or too high ($u \geq u_{co}$), and these events depend to some extent on the technical specifications of a wind turbine but also, and more significantly, on the ambient wind climate in the area of interest. Table 10 shows the percentages of all hourly wind speed values that fall into each wind power category ($u < u_{ci}$, $u_{ci} \leq u < u_r$, $u_r \leq u < u_{co}$, and $u_{co} \leq u$) for each site. In addition, the table lists the total risk of having zero wind power production ($P_w = 0$). The percentage of hours when the wind is too weak to produce wind energy ($u < u_{ci}$) ranges from 8 % to 14 % in the observation-based estimates and is overestimated by the model by an average of 1.6 percentage points for all sites. On the other hand, the observation-based estimates indicate that the fraction of hours in which the wind speed is too high ($u \geq u_{co}$) is about 0.2 %–2 %, and the model underestimates this by approximately 0.6 percentage points. The model's overestimation of the number of hours with winds that are too weak to produce

[2]The distance where the correlation has dropped to $\frac{1}{e} = 0.37$.

wind power and its underestimation of the number of hours with winds that are too strong results in a well-captured total number of hours of zero wind power production, which differs from the observed value by 1 percentage point.

The atmospheric conditions causing winds that are too weak for wind power production are very different from those causing winds that are too strong. Therefore, we split the zero events accordingly. Figures 9 and 10 illustrate the ability of the NORA3 to capture the observation-based estimates of zero events of different duration. Figure 9a shows the observation-based numbers of zero events of varying duration caused by too weak winds. As expected, the number of zero events decreases as the duration of the events increases, ranging from around 90–130 yearly events lasting less than 3 h for most sites to close to zero such events lasting longer than 2 d. Figure 9b graphs the relative differences (in percentage) between the NORA3 and observation-based estimates of the numbers of zero events by duration. The model-based estimates typically have 40 %–50 % too few zero events of short duration (1–3 h) compared to the observations. For longer zero events the model is biased towards too many events.

The model's underestimation of short zero events caused by too low wind speeds and its overestimation of longer zero events occur as a result of the model having lower variability than the observations, as seen in the ramp-rate analysis (see Sect. 5.1). This lower variability means that when these zero events occur in the model they tends to be of longer duration, but the frequency of such events is too low.

From Fig. 10a it is evident that the yearly average occurrence of zero events caused by too strong winds is a factor of 10 lower than the number of zero events caused by winds that are too weak. Hence, one zero event caused by too strong winds happens for approximately every 10 zero events caused by too weak winds. The model underestimates the number of zero events caused by too strong winds for all sites (Fig. 10b); depending on the zero-event duration, NORA3 typically has 40 %–70 % too few zero events caused by too strong winds.

5.5 Expected maximum zero-event duration over the turbine lifetime

In this section we attempt to validate the model's ability to provide reliable estimates of extremely-long-lasting zero events. This is done by estimating the 25-year return value for the duration of a zero event (the typical length of a zero event that statistically would occur at least once over a 25-year period) using the method outlined in Sect. 2.6. Using the Kolmogorov–Smirnov test, we cannot exclude the possibility that the BM data and POT data are drawn from a GEV distribution and a Pareto distribution, respectively. Thus, it is reasonable to fit the observation-based and model-based extreme zero-event duration estimates to these distributions and find the 25-year maximum expected zero-event duration.

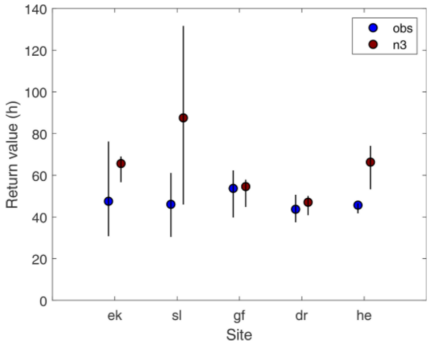

Figure 11. The 25-year return value with the corresponding confidence interval of the maximum duration of a zero event generated by fitting a generalized Pareto distribution to the POT (peak over threshold) data using both observations (obs) and modeled data (n3) for each of the sites. Abbreviations: ek: Ekofisk; sl: Sleipner; gf: Gullfaks C; dr: Draugen; he: Heidrun.

Figure 11 displays the results from fitting the Pareto distribution to the POT data (the results fitting the BM data to the GEV distribution are similar). From the observed data the typical length of the longest zero event expected to occur at least once during the lifetime of a turbine is on the order of 40–60 h, but a zero event of more than 5 d cannot be ruled out. The uncertainty in the estimations makes it difficult to judge which sites have the shortest and longest maximum zero-even duration. Using the model data, the estimates are typically longer than the observation-based estimates (not significant at the 2.5 % significance level for four of five sites) and are in line with the lower variability in the modeled hourly wind speed and wind power as seen in the ramp-rate analysis (see Sects. 4.1 and 5.1). In conclusion, using NORA3 to estimate extreme zero-event duration would lead to a conservative estimate of the return values, and the duration might be overestimated due to the lower variability in the model.

6 Summary

We conduct an in-detail validation of NORA3 offshore wind resource and power production for the time period 2004–2016. NORA3 is a new and freely available high-resolution (3 km) numerical mesoscale weather simulation data set from the Norwegian Meteorological Institute. We perform the validation using observations from six offshore sites along the Norwegian continental shelf. In addition, we quantify the performance of NORA3 against the host reanalysis data set (ERA5). Through advanced statistical measures we validate both the NORA3 wind resource and the related wind power production. Validation measures like arithmetic mean, standard deviation, relative difference between the data sets,

Table 10. The percentages of observed wind speeds (obs) and modeled wind speeds (n3) that fall into the following four categories: (1) the wind speed is less than the cut-in limit ($u < u_{ci}$), (2) the wind speed interval in which the wind power is a function of the cube of the wind speed ($u_{ci} \leq u < u_r$), (3) wind power production is rated ($u_r \leq u < u_{co}$), and (4) wind speed exceeds the cut-out limit ($u_{co} \leq u$). In addition, the total hours of zero wind power production ($P_w = 0$) divided by the total number of observations are shown as a percentage.

	Wind speed in categories (%)									
	$u < u_{ci}$		$u_{ci} \leq u < u_r$		$u_r \leq u < u_{co}$		$u \geq u_{co}$		$P_w = 0$ (total)	
Site	obs	n3	obs	n3	obs	n3	obs	n3	obs	n3
FINO1	9.99	10.13	65.54	66.41	24.24	23.33	0.22	0.14	10.21	10.27
Ekofisk	8.88	10.42	63.45	64.87	27.07	24.42	0.60	0.29	9.48	10.71
Sleipner	7.52	10.62	54.08	57.67	36.48	30.85	1.92	0.86	9.45	11.48
Gullfaks C	8.96	11.52	53.98	55.72	35.07	31.53	2.00	1.23	10.96	12.75
Draugen	13.81	14.12	59.67	62.45	25.59	22.97	0.93	0.46	14.75	14.58
Heidrun	11.05	12.69	58.12	60.85	29.41	25.83	1.42	0.63	12.52	13.32
Average	10.04	11.58	59.14	61.33	29.64	26.49	1.18	0.60	11.23	12.19

temporal correlations, and seasonality of the variables are calculated. In addition, we also include comparison and validation of hourly data distributions, hourly ramp rates, spatial correlation, and analysis on the zero-wind-power events including extreme-value analysis. The general picture is that the NORA3 data are well suited for wind power estimates in the absence of in situ data. Nevertheless, there is a tendency towards the model generating slightly conservative estimates, and the results are summarized below.

The comparison between NORA3 and ERA5 demonstrates that NORA3 outperforms ERA5 in terms of mean and standard deviation of the wind speed climatology for all seasons and for all wind speed intervals, especially for the very strong winds ($u \geq u_{co}$). Since the very strong winds are not contributing to power production, the average power capacity factors (CF) are also compared. Again, NORA3 differs from the observation-based CF by on average 3 percentage points compared to ERA5's deficiency of 5 percentage points. The validation of wind climatology in NORA3 and ERA5 shows that the downscaling process resulted in an improved wind resource data set.

For all the six offshore sites NORA3 data are biased towards lower mean wind speeds ($u_{obs} = 10.64\,m\,s^{-1}$, $u_{n3} = 10.05\,m\,s^{-1}$). The differences in wind speed distribution between the observations and the model output reveal that the model underestimates the number of events with wind speed exceeding the rated wind speed and overestimates the number of events with wind speeds below the rated wind speed (see Fig. 3). The transition between over- and underestimation by the model occurs near typical rated wind speeds (11–13 $m\,s^{-1}$). As the model underestimates the wind episodes above the rated wind speed, this partly counteracts the model's overestimation of low wind speeds, making the total modeled power production slightly underestimated.

NORA3 is also slightly biased towards less variable wind speeds on hourly timescales. Analyses of hourly wind speed ramp rates show that the hour-to-hour variability is typically slightly above 1 $m\,s^{-1}$, while the model-based ramp rates are slightly below 1 $m\,s^{-1}$, resulting in an underestimation of wind speed ramp rates on the order of 30 % (see Table 6).

Generally, estimates of wind power from NORA3 are biased towards too low median values ($P_{w,obs} = 0.43$, $p_{w,n3} = 0.37$) and wind power CFs ($CF_{obs} = 50\,\%$, $CF_{n3} = 47\,\%$). The negative bias is a consistent feature seen in all years and for all months for all the six sites (except at FINO1 for some months).

The wind power ramp-rate analysis shows that the hourly wind power variability of the NORA3-based estimates is too low. The observation-based wind speed variability leads to a corresponding wind power ramp rate that is typically 0.08 (8 % of installed capacity), while the model-based ramp rate estimated is typically 0.05.

By interconnection of site pairs we demonstrate that the spatial co-variability in estimated hourly wind power production between sites is slightly higher for the NORA3 data than for the observational data. Hence, the decorrelation length is estimated to be 19 % longer in the model-based estimates.

The estimation of the occurrence and duration of zero events shows a well-captured total risk of hourly zero events (n3 = 12.19 %, obs = 11.23 % of the time). We split the zero events into episodes of no wind power production caused by either too low ($u < u_{ci}$) or too high ($u \geq u_{co}$) wind speeds. For zero events caused by winds that are too strong, NORA3 underestimates the occurrence of zero events for all durations. For winds that are too weak, NORA3 underestimates the number of short zero events (1–3 h) but is biased towards an excess of zero events with longer duration. As a result, when a zero event occurs in the NORA3 data, it tends to be of longer duration, but the frequency of such events is too low. This deviation from the observation-based zero events is in line with the lower variability in hourly wind speeds seen in the ramp-rate analysis (Sects. 4.1 and 5.1).

In the extreme-value analysis we found that at least once during the lifetime of a turbine (25 years) a zero-power event is expected to last for 1 to 3 d, depending on the site in question (see Fig. 11). However, a zero event lasting longer than 5 d cannot be ruled out for some sites. Overall, the 25-year return values from NORA3 are somewhat conservative, with a tendency towards longer maximum zero-event duration than seen in the observation-based return values.

To a large degree NORA3 resembles the climatological offshore wind resource and wind power characteristics seen in the observations. However, the model slightly underestimates the wind resource and power potential, and the hourly variability in the model output is lower than in the observations. These characteristics should be kept in mind when using the NORA3 data set in the planning phase of a future offshore wind farm.

Appendix A: Wind direction

See Fig. A1 for the observed and modeled wind-rose plot.

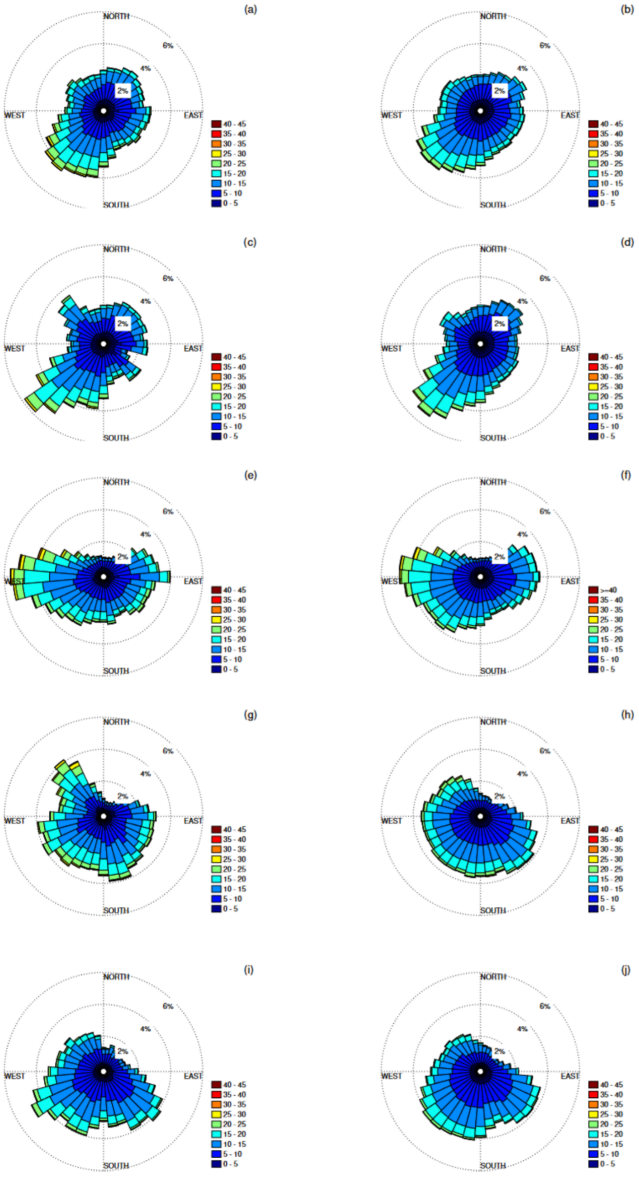

Figure A1. Observed **(a, c, g, e, i)** and modeled **(b, d, f, h, j)** wind roses for the five oil and gas platforms. The colors show the wind speed intervals in meters per second. **(a, b)** Heidrun; **(c, d)** Draugen; **(e, f)** Gullfaks C; **(g, h)** Sleipner; **(i, j)** Ekofisk.

Data availability. The observations from the Norwegian Meteorological Institute can be downloaded at https://seklima.met.no/ (NORSK Klimaservicesenter, 2021). FINO1 data can be downloaded from BSH at http://fino.bsh.de (Bundesamt für Seeschifffahrt und Hydrographie, 2021). NORA3 data can be downloaded at https://thredds.met.no/thredds/projects/nora3.html (Norwegian Meteorological Institute, 2021).

Author contributions. IMS and AS conceptualized the overarching research goals of the study, in addition to conducting formal analysis regarding statistical and mathematical techniques and methods. HH is the creator of NORA3 data set and is responsible for the data resources. IMS was responsible for the data curation and creation of software code, validation, visualization of data, and preparation of the original draft, with contribution from AS. In addition, AS was responsible for the supervision. All the authors contributed to the review and editing process of the paper.

Competing interests. The authors declare that they have no conflict of interest.

Disclaimer. Publisher's note: Copernicus Publications remains neutral with regard to jurisdictional claims in published maps and institutional affiliations.

Acknowledgements. We thank the Norwegian Meteorological Institute and extend a special thank you to Magnar Reistad, Øyvind Breivik, and Ole Johan Aarnes for providing all the observational data used in this study and for interesting discussions. We would also like to thank BSH (the Federal Maritime and Hydrographic Agency of Germany) for providing the data (mast corrected) for FINO1.

Review statement. This paper was edited by Andrea Hahmann and reviewed by Matti Koivisto, Andrea Hahmann, and two anonymous referees.

References

Badger, M., Peña, A., Hahmann, A. N., Mouche, A. A., and Hasager, C. B.: Extrapolating Satellite Winds to Turbine Operating Heights, J. Appl. Meteorol. Clim., 55, 975–991, https://doi.org/10.1175/JAMC-D-15-0197.1, 2016.

Bengtsson, L., Andrae, U., Aspelien, T., Batrak, Y., Calvo, J., d. Rooy, W., Gleeson, E., Hansen-Sass, B., Homleid, M., Hortal, M., Ivarsson, K. I., Lenderink, G., Niemelä, S., Nielsen, K. P., Onvlee, J., Rontu, L., Samuelsson, P., Muñoz, D. S., Subias, A., Tijm, S., Toll, V., Yang, X., and d. Køltzow, M. Ø.: The HARMONIE-AROME model configuration in the ALADIN-HIRLAM NWP system, Mon. Weather Rev., 145, 1919–1935, https://doi.org/10.1175/MWR-D-16-0417.1, 2017.

Berge, E., Byrkjedal, y., Ydersbond, Y., and Kindler, D.: Modelling of offshore wind resources. Comparison of a meso-scale model and measurements from FINO 1 and North Sea oil rigs, in: vol. 4, European Wind Energy Conference and Exhibition 2009, EWEC 2009, 16–19 March 2009, Marseille, France, 2327–2334, 2009.

Bundesamt für Seeschifffahrt und Hydrographie: FINO1 data, available at: http://fino.bsh.de, last access: November 2021.

Byrkjedal, Ø. and Åkervik, E.: Vindkart for Norge, Tech. rep., Kjeller Vindteknikk, available at: https://www.nve.no/media/2470/vindkart_for_norge_oppdragsrapporta10-09.pdf (last access: September 2021), 2009.

Byrkjedal, Ø., Harstveit, K., Kravik, R., Løvholm, A. L., and Berge, E.: Analyser av offshore modellsimuleringer av vind, Tech. rep., Kjeller Vindteknikk, available at: http://publikasjoner.nve.no/oppdragsrapportA/2009/oppdragsrapportA2009_10.pdf (last access: April 2021), 2010.

Cory, K. and Schwabe, P.: Wind Levelized Cost of Energy: A comparison of Technical and Financing Input Variables, Tech. rep., National Renewable Energy Laboratory, Scholar's Choice, 2009.

Dörenkämper, M., Olsen, B., Witha, B., Hahmann, A., Davis, N., Barcons, J., Ezber, Y., García-Bustamante, E., González-Rouco, J. F., Navarro, J., Sastre-Marugán, M., Sīle, T., Trei, W., Žagar, M., Badger, J., Gottschall, J., Sanz Rodrigo, J., and Mann, J.: The Making of the New European Wind Atlas – Part 2: Production and Evaluation, Geosci. Model Dev., 13, 5079–5102, https://doi.org/10.5194/gmd-13-5079-2020, 2020.

Emeis, S.: Wind Energy Meteorology, 2nd Edn., Springer, Wind Energy Meteorology, 2018.

Furevik, B. R. and Haakenstad, H.: Near-surface marine wind profiles from rawinsonde and NORA10 hindcast, J. Geophys. Res.-Atmos., 117, 1–14, https://doi.org/10.1029/2012JD018523, 2012.

Gualtieri, G.: A comprehensive review on wind resource extrapolation models applied in wind energy, Renew. Sustain. Energ. Rev., 102, 215–233, https://doi.org/10.1016/j.rser.2018.12.015, 2019.

Haakenstad, H., Breivik, Ø., Furevik, B. R., Reistad, M., Bohlinger, P., and Aarsnes, O. J.: NORA3: A non-hydrostatic high-resolution hindcast for the North Sea, the Norwegian Sea and the Barents Sea, J. Appl. Meteorol. Clim., 60, 1443–1464, https://doi.org/10.1175/JAMC-D-21-0029.1, 2021.

Hahmann, A. N., Vincent, C. L., Peña, A., Lange, J., and Hasager, C. B.: Wind climate estimation using WRF model output: method and model sensitivities over the sea, Int. J. Climatol., 35, 3422–3439, https://doi.org/10.1002/joc.4217, 2015.

Hasager, C. B., Hahmann, A. N., Ahsbahs, T., Karagali, I., Sile, T., Badger, M., and Mann, J.: Europe's offshore winds assessed with synthetic aperture radar, ASCAT and WRF, Wind Energ. Sci., 5, 375–390, https://doi.org/10.5194/wes-5-375-2020, 2020.

Hersbach, H., Bell, B., Berrisford, P., Hirahara, S., Horányi, A., Muñoz-Sabater, J., Nicolas, J., Peubey, C., Radu, R., Schepers, D., Simmons, A., Soci, C., Abdalla, S., Abellan, X., Balsamo, G., Bechtold, P., Biavati, G., Bidlot, J., Bonavita, M., De Chiara, G., Dahlgren, P., Dee, D., Diamantakis, M., Dragani, R., Flemming, J., Forbes, R., Fuentes, M., Geer, A., Haimberger, L., Healy, S., Hogan, R. J., Hólm, E., Janisková, M., Keeley, S., Laloyaux, P., Lopez, P., Lupu, C., Radnoti, G., de Rosnay, P., Rozum, I., Vamborg, F., Villaume, S., and Thépaut, J. N.: The ERA5 global reanalysis, Q. J. Roy. Meteorol. Soc., 146, 1999–2049, https://doi.org/10.1002/qj.3803, 2020.

Kempton, W., Pimenta, F. M., Veron, D. E., and Colle, B. A.: Electric power from offshore wind via synoptic-scale interconnection, P. Natl. Acad. Sci. USA, 107, 7240–7245, https://doi.org/10.1073/pnas.0909075107, 2010.

Milan, P., Morales, A., Wächter, M., and Peinke, J.: Wind Energy: A Turbulent, Intermittent Resource, Wind Energy – Impact of Turbulence, Springer, 73–78, https://doi.org/10.1007/978-3-642-54696-9_11, 2014.

NORSK Klimaservicesenter: Observations, Norwegian Meteorological Institute, available at: https://seklima.met.no/, last access: November 2021.

Norwegian Meteorological Institute: NORA3 data, available at: https://thredds.met.no/thredds/projects/nora3.html, last access: November 2021.

Regjeringen: Opening sites at the Norwegian continental shelf for wind power production, available at: https://www.regjeringen.no/no/aktuelt/opner-omrader/id2705986/ (last access: April 2021), 2020.

Reichenberg, L., Johnsson, F., and Odenberger, M.: Dampening variations in wind power generation – The effect of optimizing geographic location of generating sites, Wind Energy, 17, 1631–1643, https://doi.org/10.1002/we.1657, 2014.

Reichenberg, L., Wojciechowski, A., Hedenus, F., and Johnsson, F.: Geographic aggregation of wind power – an optimization methodology for avoiding low outputs, Wind Energy, 20, 19–32, https://doi.org/10.1002/we.1987, 2017.

Seity, Y., Malardel, S., Hello, G., Bénard, P., Bouttier, F., Lac, C., and Masson, V.: The AROME-France convective-scale operational model, Mon. Weather Rev., 139, 976–991, https://doi.org/10.1175/2010MWR3425.1, 2011.

Siemens Gamesa Renewable Energy: Siemens 6.0 MW Offshore Wind Turbine, Tech. rep., available at: https://en.wind-turbine-models.com/turbines/657-siemens-swt-6.0-154 (last access: March 2021), 2011.

Sill, B. L.: Turbulent boundary layer profiles over uniform rough surfaces, J. Wind Eng. Indust. Aerodynam., 31, 147–163, 1988.

Skeie, P., Steinskog, D. J., and Näs, J.: Kraftproduksjon og vindforhold, Tech. rep., StormGeo AS, available at: https://publikasjoner.nve.no/rapport/2012/rapport2012_59.pdf (last access: September 2021), 2012.

Smith, E. P.: An Introduction to Statistical Modeling of Extreme Values, Springer Series of Statistics, Springer, https://doi.org/10.1198/tech.2002.s73, 2002.

Solbrekke, I. M., Kvamstø, N. G., and Sorteberg, A.: Mitigation of offshore wind power intermittency by interconnection of production sites, Wind Energ. Sci., 5, 1663–1678, https://doi.org/10.5194/wes-5-1663-2020, 2020.

St. Martin, C. M., Lundquist, J. K., and Handschy, M. A.: Variability of interconnected wind plants: Correlation length and its dependence on variability time scale, Environ. Res. Lett., 10, 44004, https://doi.org/10.1088/1748-9326/10/4/044004, 2015.

Vasilyev, L., Christakos, K., and Hannafious, B.: Treating wind measurements influenced by offshore structures with CFD methods, Energy Procedia, Elsevier, https://doi.org/10.1016/j.egypro.2015.11.425, 2015.

Wiser, R., Jemmi, K., Seel, J., Baker, E., Hand, M., Lantz, E., and Smith, A.: Forecasting Wind Energy Costs and Cost Drivers: the Views of the World' S Leading Experts, Tech. rep., IEA Wind, NREL, Berkeley Lab, available at: https://escholarship.org/uc/item/0s43r9w4 (last access: November 2021), 2016.

Zheng, C. W., Li, C. Y., Pan, J., Liu, M. Y., and Xia, L. L.: An overview of global ocean wind energy resource evaluations, Renew. Sustain. Energ. Rev., 53, 1240–1251, https://doi.org/10.1016/j.rser.2015.09.063, 2016.

Paper III

NORA3-WP: A high-resolution offshore wind power dataset for the Baltic, North, Norwegian, and Barents Seas

Solbrekke, Ida M., Sorteberg, Asgeir
Accepted for publication in *Scientific data - Nature*, -/- (2022)

III

NORA3-WP: A high-resolution offshore wind power dataset for the Baltic, North, Norwegian, and Barents Seas

Ida Marie Solbrekke[1,*] **and Asgeir Sorteberg**[2]

[1]Geophysical Institute, Bergen Offshore Wind Centre (BOW), University of Bergen, Allègaten 70, 5020 Bergen, Norway
[2]Geophysical Institute, Bjerknes Centre for Climate Research (BCCR), Bergen Offshore Wind Centre (BOW), University of Bergen, Norway
[*]corresponding author(s): Ida Marie Solbrekke (ida.solbrekke@uib.no)

ABSTRACT

We present a new high resolution wind resource and wind power dataset named NORA3-WP. The dataset covers the North Sea, the Baltic Sea and parts of the Norwegian and Barents Seas. The 3-km Norwegian reanalysis (NORA3) forms the basis for the new dataset. NORA3-WP is an open access dataset intended for use in research, governmental management and for stakeholders to attain relevant wind resource and wind power information in the planning phase of a new wind farm project. The variables are available as monthly data, and provides a climatological overview of 25 wind resource and wind power related variables for three selected turbines for the ocean areas surrounding Norway. In addition, the underlying hourly wind speed data and hourly wind power generation for three selected turbines are also available for higher frequency analysis and case-studies.

1 Background & Summary

Offshore wind power continues to take larger portions of the global energy mix. Using good quality data to identify new potential areas for offshore wind power exploitation is important. Offshore wind observations are very sparse and wind power estimations have to rely on stimulated wind speeds. Here we present a high resolution, freely available wind resource and wind power dataset for the offshore areas enclosing Norway called NORA3-WP.

NORA3 forms the basis for the new wind power data set NORA3-WP. NORA3[1] is most recent high resolution reanalysis from the Norwegian Meteorological institute. NORA3 is generated by a dynamically downscaling of the state-of-the-art reanalysis from the European Center for Medium-Range Weather Forecast (ECMWF) - ERA5[2]. The downscaling is conducted using the high resolution non-hydrostatic numerical weather prediction (NWP) model HARMONIE-AROME[3,4]. NORA3 differs from other existing wind resource datasets in terms of the choice of NWP model used in the downscaling process of ERA5. In contrast to other existing wind energy resource datasets which are created by the Reasearch and Forecasting Model (WRF), NORA3 is created by the NWP model HARMONIE-AROME (Cy 40h1.2). HARMONIE-AROME is a mesoscale-permitting NWP model developed as a European cooperation, and used by many European weather forecast and research institutions[3,4]. The downscaling of ERA5 is performed by solving the fully compressible Euler equations, on a non-staggered horizontal grid in a non-hydrostatic atmospheric mode. NORA3 is extensively evaluated against observations and the host dataset (ERA5)[1,5]. The validation of the wind climatology in NORA3 show that the downscaling of ERA5 resulted in an improved wind resource dataset.

NORA3-WP is generated using hourly wind speeds in several model layers near the surface, together with air temperature and pressure, to estimate relevant wind resource and wind power variables. NORA3-WP consist of statistical measures for 7 wind resource and 18 wind power related variables. The power estimates are generated using three different turbines having different rated powers, turbine diameters, and hub heights (6 MW at 101 m.a.s.l., 10 MW at 119 m.a.s.l., and 15 MW at 150 m.a.s.l.). All variables are stored on a 3 x 3 km horizontal grid covering the North Sea, Norwegian Sea, Baltic Sea and parts of the Barents Sea (See Fig. 1). NORA3-WP spans the period 1996 - 2019 (will be updated to go back to 1979) and contains monthly values for all variables. In addition, NORA3-WP contains the underlying hourly wind speed and hourly generated wind power data. The hourly variables provides high-frequency data available for more detailed analysis.

NORA3-WP is a state-of-the-art fully open wind resource and wind power dataset facilitated for researchers, decision makers, stakeholders, and investors. The goal of NORA3-WP is to create a dataset for research and for usage in the planning phase of new wind farms. NORA3-WP will give useful information on the climatological features of the wind resource and wind power variables, and provides the underlying hourly wind data for users to perform their own detailed analyses.

NORA3-WP is an open access wind power dataset under the Norwegian Licence for Open Government Data (NLOD). The dataset contributes to the continuously growing ensemble of wind resource datasets (e.g. NEWA[6], GWA[7]). The growing ensemble of wind resource datasets makes it possible to quantify wind resource uncertainty and we recommend future users to use the NORA3-WP together with other sources of wind resource information.

A detailed description of NORA3 and NORA3-WP can be found under section 2.1 and section 2.2, respectively. Wind turbine specifications and assumptions made in the generation of NORA3-WP are described in Section 2.3. In addition, we explain how all the wind resource variables (section 3.1) and wind power related variables (Section 3.2) are calculated. For a detailed evaluation of the dataset quality we refer to the extensive offshore validation done in[5]. The added value of the downscaling compared to the boundary forcing of ERA5 is given in[1]. We provide a short summary of the evaluation result in section 3.2.10. A brief instruction and assistance to future users of NORA3-WP are given in section 3.2.10. In addition, examples of usage of the NORA3-WP dataset are provided in sections 3.2.10 (Climatology) and 3.2.10 (Case-study).

2 Data and methods

2.1 NORA3: The 3-km Norwegian reanalysis

NORA3 dataset is created by the Norwegian Meteorological Institute by running the non-hydrostatic NWP model HARMONIE-AROME (Cy 40h1.2), solving the fully compressible Euler equations[3,4]. The state-of-the-art reanalysis ERA5 from ECMWF is used as initial and boundary forcing[2]. ERA5 is a global reanalysis product, providing hourly information for 137 vertical layers, and covers the Earth with 0.28125° resolution, corresponding to a horizontal grid of approximately 31 x 31 km. The improved resolution of ERA5 over ECMWF's former reanalysis ERA-Interim (≈ 79 km) provides a detailed initial and boundary information in the downscaling process. NORA3 covers large parts of the North Atlantic and the Nordic countries in a 3 x 3 km non-staggered horizontal grid (see Fig. 1 in[5] for the complete NORA3 domain), dividing the atmosphere into 65 vertical layers. The NORA3 near surface output data are available every hour, and is so far covering the period 1996-2019. When the model integration is finalized (Summer 2022) the NORA3 data will cover the time period from 1979 to present, and will be regularly updated in the coming years. For more details on the generation of the dataset see[1].

2.2 NORA3-WP: A high-resolution offshore wind power dataset

NORA3-WP is created by estimating wind resource and wind power related variables using NORA3 hourly wind speeds, as well as air temperature and pressure, in several near-surface model levels. The geographical domain covered by NORA3-WP is smaller than the original NORA3-domain. The domain in NORA3-WP covers the eastern parts of the Norwegian sea, the North Sea, the Baltic Sea and part of the Barents Sea (see Fig. 1 for the NORA3-WP domain). The horizontal grid resolution is 3 x 3 km. The dataset have 652 grid points in the x-direction (longitude) and 1149 grid points in y-direction (latitude). Wind power variables are calculated for three different turbines having different turbine specifications (see section 2.3) and the wind resource variables are available at the same heights: 101 *m.a.s.l.*, 119 *m.a.s.l.* and 150 *m.a.s.l.*. The NORA3-WP data covers the period from 1996 to 2019, and the variables are stored as monthly data. To facilitate more detailed analysis with increased temporal resolution, hourly wind speed and hourly generated wind power for the different turbines are also available.

2.3 Wind turbine specifications

Specifications about the three turbines used to create the wind power related variables of NORA3-WP are listed in Table 1. SWT-6.0-154 from Siemens is the floating three bladed electricity generator used in Hywind Scotland, the first floating wind farm in the world[8]. SWT-6.0-154 has a rated power of 6 MW with a rotor diameter and hub-height of 154 m and 101 m.a.s.l., respectively. DTU-10.0-RWT is the widely used reference wind turbine from the Technical University of Denmark (DTU)[9]. The rated power of DTU-10.0-RWT is 10 MW and the rotor diameter and hub-height corresponds to 178.3 m and 119 m.a.s.l., respectively. We have also used a new offshore reference turbine from the National Renewable Energy Laboratory, IEA-15-240-RWT[10]. This large turbine with a rotor diameter of 240 m produces 15 MW at rated power at the hub-height of 150 m.a.s.l.. See Fig. 2 for the three normalized power curves considered in this study. The advantage of the reference turbines is the open access to all design parameters. The easy access to key design parameters makes it easier to explore the technical specifications and enables and facilitates collaboration between the industry and the research community.

When calculating the wind power related variables we assume a stand-alone wind turbine experiencing no wind farm effects or other disturbances that can reduce the power production.

2.4 Statistics

This section contains the statistics used in the generation of NORA3-WP, here expressed by x (x can be e.g. wind speed, power density, wind power etc,.):

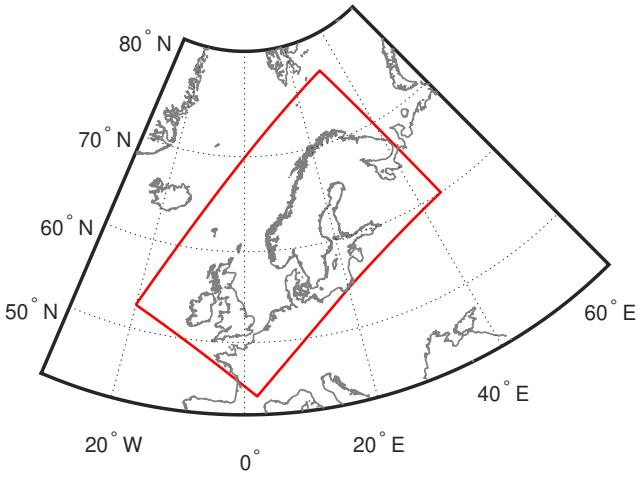

Figure 1. The geographical domain covered by NORA3-WP (red rectangle).

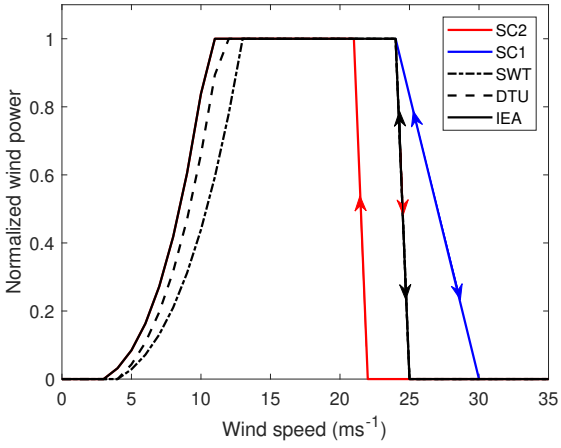

Figure 2. Power curves for the three turbines (SWT-6.0-154, DTU-10.0-RWT, IEA-15-240-RWT). In addition, the figure illustrates how the high wind speed end of the power curve changes when storm control 1 (SC1) and storm control 2 (SC2) are included. The arrows indicate how the different power curves shut down (arrow down) and restart (arrow up) at high wind speeds.

Table 1. Turbine specifications for the three turbines used to generate the wind power related variables in NORA3-WP.

	SWT-6.0-154	**DTU-10.0-RWT**	**IEA-15-240-RWT**
Rated power, C_r (W)	6 000 000	10 000 000	15 000 000
Hub height (m)	101	119	150
Rotor diameter (m)	154	178.3	240
Specific rated power C_r/A (Wm^{-2})	161.1	200.3	165.8
cut-in (ms^{-1})	4.0	4.0	3.0
rated (ms^{-1})	13.0	11.4	10.59
cut-out (ms^{-1})	25.0	25.0	25.0

2.4.1 Arithmetic mean ($\overline{x}$) of x:

$$\overline{x} = \frac{1}{n}\sum_{t=1}^{n} x(t) \tag{1}$$

2.4.2 Maximum value (x_{max}) of x:

$$x_{max} = max(x) \tag{2}$$

2.4.3 Percentiles (x_{yy}) of x:

After sorting x in ascending order, yy-percentile of x (x_{yy}) gives us the value of x where yy percent of the data falls at and below x_{yy}, and (1-yy) percent of the data falls above x_{yy}.

2.4.4 Weibull distribution, scale (a), and shape (b) parameters of x:

The probability density function $f(x;a,b)$ for a Weibull variable x, with scale and shape parameters a and b, respectively, is:

$$f(x;a,b) = \begin{cases} \frac{b}{a}\left(\frac{x}{a}^{(b-1)}\, e^{(x/a)^b}\right), & x \geq 0 \\ 0, & x < 0 \end{cases} \tag{3}$$

By fitting a Weibull probability distribution function to the data in x we are able to get the maximum likelihood estimates of the Weibull scale ($\hat{a}$) and shape ($\hat{b}$) parameters:

$$\hat{a} = \left[\frac{1}{n}\sum_{t=1}^{n} x(t)^{\hat{b}}\right]^{\frac{1}{\hat{b}}}, \tag{4}$$

$$\hat{b} = \frac{n}{\frac{1}{\hat{a}}\sum_{t=1}^{n} x(t)^{\hat{b}} log(x(t)) - \sum_{t=1}^{n} log(x(t))}, \tag{5}$$

n is the number of samples (here: hours). The scale parameter (a) gives the height of the distribution. A relative large a corresponds to a high and narrow Weibull distribution. The shape parameter (b) gives the shape of the distribution. If $b < 3$ the data distribution is right-skewed, with a long tail to the right of the mean.

2.4.5 Weibull standard deviation (σ_x) of x:

$$\sigma_x = a\sqrt{\Gamma\left(\frac{2}{b}+1\right) - \Gamma\left(\frac{1}{b}+1\right)^2} \tag{6}$$

where $\Gamma(n) = \int_0^\infty e^{-x}x^{n-1}dx$ is the Gamma function evaluated at $\left(\frac{2}{b}+1\right)$ and $\left(\frac{1}{b}+1\right)$.

3 Data records

This section contains explanations and calculations for each data record associated with NORA3-WP[11]. Each subsection describes a variable in the dataset. The heading of the subsection corresponds to the variable names in Table 2 and Table 3.

3.1 Wind speed variables

The wind speed related variables included in the NORA3-WP dataset are listed in Table 2 and described below.

Table 2. The wind speed related variables available in NORA3-WP. All the listed variables are available as monthly means of hourly data for each months in the study period, except "Hourly wind speed" which is available as hourly output for each month. h_{month} is the number of hours in the current month, n_{month} is the total number of months in the study period (288 months), hh1, hh2, and hh3 corresponds to the hub height of the three turbines, 101 m.a.s.l., 119 m.a.s.l., and 150 m.a.s.l., respectively (see Table 1).

Variable	Stat	unit	X grid x Y grid x time	height (m)
Hourly wind speed	-	ms^{-1}	652 x 1149 x h_{month}	hh 1, hh 2, hh 3
Wind speed	Mean, 25-, 50-, 75-, 95-percentile, std, max	ms^{-1}	652 x 1149 x n_{month}	hh 1, hh 2, hh 3
Exponential power law coefficient (α)	Mean	-	652 x 1149 x n_{month}	10-100, 50-100, 100-250
Weibull wind speed parameters	Scale, shape	ms^{-1},-	652 x 1149 x n_{month}	hh 1, hh 2, hh 3
Prevailing wind direction sector	Mean	degrees	652 x 1149 x n_{month}	100
Vertical wind shear	Mean, max	ms^{-1}	652 x 1149 x n_{month}	50-100, 100-250
Wind speed absolute ramp-rate (ARR)	Mean, max	ms^{-1}	652 x 1149 x n_{month}	hh 1, hh 2, hh 3

3.1.1 Wind speed

Both hourly, monthly mean, monthly maximum and monthly percentiles (25-, 50-, 75-, and 95-percentile) of the wind speed are available. For the wind speed to be valid at the relevant turbine hub heights the NORA3 wind speed data at height z_1 ($z_1 = 50 m.a.s.l.$, $z_1 = 100 m.a.s.l.$ and $z_1 = 250 m.a.s.l.$) are interpolated to the turbine hub height (z_2) using the exponential relation with hourly varying power law coefficient $\alpha(t)$:

$$u_{z_2}(t) = u_{z_1}(t)\left(\frac{z_2}{z_1}\right)^{\alpha(t)}, \tag{7}$$

Eq. 1 and Eq. 2 are applied to Eq. 7 to obtain monthly mean and maximum wind speed values, respectively.

3.1.2 Exponential power law coefficient, α

The exponential power law exponent (α) modifies the wind speed profile and is a function of the undisturbed wind speed, atmospheric stability, and surface roughness. The hourly power law exponent is obtained by solving Eq. 7 for α;

$$\alpha(t) = \frac{ln\left(\frac{u_{z_2}(t)}{u_{z_1}(t)}\right)}{ln\left(\frac{z_2}{z_1}\right)} \tag{8}$$

where Z_1 and Z_2 correspond to the two layers within the wind shear is calculated. α is calculated between 10 and 100 $m.a.s.l$, 50 and 100 $m.a.s.l$, and 100 and 250 $m.a.s.l$ depending on the hub height of the wind turbine. Eq. 1 is applied to Eq. 8 to obtain the monthly mean values of the power law exponent.

3.1.3 Weibull wind speed parameters

The wind speed distribution can be approximated through the Weibull **scale factor** (a) and **shape factor** (b) parameters[12,13]. Using these factors an approximated wind distribution for a each month can be generated without having to download the hourly data. The combination of a and b brings information about the fraction of the data that falls between cut-in and cut-out wind speed. Together, a and b are indicative of the wind power production without using a specific wind turbine. Nevertheless, we want to stress that using the hourly wind speed data for wind power production estimates will give a more realistic power output compared to a Weibull distribution fit. Monthly scale and shape factors are calculated for each grid cell by using Eq. 4 and Eq. 5. Typical values for the average scale and shape parameters at the Norwegian offshore area are $9 \text{ms}^{-1} \leq a \leq 12 \text{ms}^{-1}$ and $1.7 \leq b \leq 2.7$.

3.1.4 Vertical wind shear

The vertical distribution of the wind speed with height is relevant in wind energy application. Wind turbine height and rotor diameter are parameters that have been continuously increasing. As a consequence, the wind turbine rotor sweeps a large portion of the atmospheric boundary layer where the wind changes rapidly with height. In NORA3-WP the atmospheric vertical wind shear ($u_{z_2} - u_{z_1}$) are calculated between the three most relevant model layers for wind energy; between 50

and 100 m; and between 100 m and 250 m. The vertical wind shear (δu) is how much the wind speed changes over a given height interval:

$$\delta u = u_{z2} - u_{z1}, \tag{9}$$

where z_1 and z_2 correspond to the two layers within which the wind shear is calculated. Eq. 1 and Eq. 2 are applied to the wind shear ($u_{z_2} - u_{z_1}$) to obtain the monthly mean and maximum values, respectively.

3.1.5 Prevailing wind-direction sector

Mapping the wind direction climatology is important for wind farm layout. Wind turbine technology allow the wind turbines to yaw to face the main wind direction. However, the wind farm layout are optimized according to the wind direction climatology. The wind direction is calculated from the original NORA3 data taken into account that the NORA3 data is using a rotated grid configuration. NORA3-WP contains the monthly mean wind direction for the prevailing wind-direction sector. This is done by first finding which of the eight 45-degree wind sectors (the sector splitting starts at 0 degrees) is the most frequent in terms of hourly directions. Monthly averaging (Eq. 1) is then applied to all the winds direction events contained in the prevailing sector. Directions are given as where the wind blows from.

3.1.6 Wind speed absolute ramp-rate (ARR)

Wind speed variability is one of the major challenges related to wind power generation. The wind speed variability combined with the power curve generates an even more intermittent wind power production. This fluctuating wind power output requires a highly flexible power system[14]. How much the wind speed changes from one hour to the next is a good measure of the variability in the wind speed, and is here given by the hourly absolute ramp rate (ARR(t)).

$$ARR_u(t) = |u(t) - u(t+1)| \tag{10}$$

Taking the mean ($M_{ean}ARR$) and maximum ($M_{ax}ARR$) values of the ARR by using Eqs. 1 and Eqs. 2, respectively, will quantify the hourly absolute temporal wind speed variability at hub height for each month.

3.2 Wind power variables

The wind power related variables in NORA3-WP are listed in Table 3, and described below.

3.2.1 Power density

The total power in the atmosphere for a wind turbine to extract is the power density at hour t ($P_d(t)$), and is expressed by the following relation:

$$P_d(t) = \frac{1}{2}\rho(t)u(t)^3, \tag{11}$$

which gives us the amount of kinetic energy contained in the air per square meter (Wm^{-2}) , and is a function of the air density (ρ) and wind velocity (u) at hub height. The hourly air density at the three hub heights is calculated using the hourly temperature and pressure by assuming hydrostatic balance in the following way:

$$\rho(t)_{hub} = \rho_s e^{\left(\frac{-gz}{R_d T_{avg}}\right)}, \tag{12}$$

where $\rho_s = \frac{p_s}{R_d T_{2m}}$ is the density at the surface, R_d is the gas constant for dry air, T_{2m} is the temperature at 2m, p_s is the surface pressure, $T_{avg} = \frac{1}{2}(T_{2m} + T_z)$ is the bulk-average between the temperature at 2m and the temperature at the hub height. $T_z = T_{2m}\frac{dT}{dz}(z-2)$ is the temperature at height z. $\frac{dT}{dz} = -6.5$K/km.

3.2.2 Power capture

Equation 11 gives the total kinetic energy in the air per square meter. Since the extracted wind energy is a function of the turbine diameter, and hence the rotor disk area (A), we multiply Eq. 11 by the sweep area A to get the theoretical power (W) captured by the rotor disk at hour t:

$$P_c(t) = \frac{1}{2}\rho(t)u(t)^3 A. \tag{13}$$

The monthly mean of P_c is calculated using P_c in Eq. 1.

Table 3. Wind power variables available for download in NORA3-WP. All the listed variables are monthly data, except "Hourly generated power" which is hourly data. "std" is the standard deviation, "SC1" is the storm control 1, "SC2" is the storm control 2 scenario with high wind hysteresis. h_{month} is the number of hours in the current month, n_{month} is the total number of months in the study period (288 months), "hh1", "hh2", and "hh3" correspond to the hub height of the three turbines, 101 m.a.s.l., 119 m.a.s.l., and 150 m.a.s.l., respectively (see Table 1).

Variable	Stat	unit	X grid x Y grid x time	height (m)
Power density, P_d	Mean	Wm^{-2}	652 x 1149 x n_{month}	hh 1, hh 2, hh 3
Power capture, P_c	Mean	$Warea^{-1}$	652 x 1149 x n_{month}	hh 1, hh 2, hh 3
Hourly generated power, P_w	-	W	652 x 1149 x h_{month}	hh 1, hh 2, hh 3
Power generated, P_w	Mean, 25- , 50-, 75-percentile	W	652 x 1149 x n_{month}	hh 1, hh 2, hh 3
Power generated, density correction	Mean	W	652 x 1149 x n_{month}	hh 1, hh 2, hh 3
Power generated, SC1 $P_{w,SC1}$	Mean	W	652 x 1149 x n_{month}	hh 1, hh 2, hh 3
Power generated, SC2 $P_{w,SC2}$	Mean	W	652 x 1149 x n_{month}	hh 1, hh 2, hh 3
Power capture coefficient, P_{cc}	Mean	%	652 x 1149 x n_{month}	hh 1, hh 2, hh 3
Generated power absolute ramp-rate (ARR)	Mean, max	W	652 x 1149 x n_{month}	hh 1, hh 2, hh 3
Time fraction cubed power ($u_{ci} \leq u < u_r$)	-	%	652 x 1149 x n_{month}	hh 1, hh 2, hh 3
Time fraction rated power ($u_r \leq u < u_{co}$)	-	%	652 x 1149 x n_{month}	hh 1, hh 2, hh 3
Time fraction zero power ($u < u_{ci}, u \geq u_{co}$)	-	%	652 x 1149 x n_{month}	hh 1, hh 2, hh 3
Time fraction zero power, SC1 ($u < u_{ci}, u \geq u_{co}$)	-	%	652 x 1149 x n_{month}	hh 1, hh 2, hh 3
Time fraction zero power, SC2 ($u < u_{ci}, u \geq u_{co}$)	-	%	652 x 1149 x n_{month}	hh 1, hh 2, hh 3
Capacity factor	-	%	652 x 1149 x n_{month}	hh 1, hh 2, hh 3
Full load hours	-	h	652 x 1149 x n_{month}	hh 1, hh 2, hh 3
Full load hours, SC1	-	h	652 x 1149 x n_{month}	hh 1, hh 2, hh 3
Full load hours, SC2	-	h	652 x 1149 x n_{month}	hh 1, hh 2, hh 3

3.2.3 Power generated

Turbine specifications pose limitations to the theoretical power potential. The generated power at hour t ($P_w(t)$) is the wind power that can be produced for a specific turbine, and is given by the installed (rated) capacity (C_r) multiplied by the normalized non-linear power conversion function ($P_{w,n}(t)$);

$$P_w(t) = C_r P_{w,n}(t), \qquad P_{w,n}(t) = \begin{cases} 0, & u(t) < u_{ci} \\ \frac{u(t)^3 - u_{ci}^3}{u_r^3 - u_{ci}^3}, & u_{ci} \leq u(t) < u_r, \\ 1, & u_r \leq u(t) < u_{co} \\ 0, & u_{co} \leq u(t). \end{cases} \tag{14}$$

where $u(t)$ is the wind speed at hour t, u_{ci} is the cut-in wind speed, u_r is the rated wind speed, and u_{co} is the cut-out wind speed. The specification of these numbers varies for the different turbines and can be seen in Table 1. See also Fig. 2 for the different power generation functions.

Eq. 1 is applied to Eq. 14 to derive the monthly mean wind power production. In addition, the 25-, 50-, and 75-percentile are calculated to obtain the typical monthly wind power output, and monthly range of wind power production in each grid cell (see Section 2.4.3). In addition to the power estimation described above, the dataset contain three different ways of estimating the generated power. We supply NORA3-WP with these additional power generation methods to consider density corrections and storm control options. They are described in the sections below.

3.2.4 Power generated, density correction

The atmospheric wind power is directly proportional to the air density (see Eq. 11). For inter comparison of power production curves from different wind turbines and for expressing the power production as a function of the wind speed only, the power curves are calculated using reference air density (ρ_{ref}). At $T = 15°C$ and $P_0 = 1013.25$ hPa the reference atmospheric density is $\rho = 1.225 \frac{kg}{m^3}$. However, the atmospheric density is not constant. Whenever the air density deviates from the reference air density will result in erroneous power production estimates, on average 1-2%. To include density

variations (both temporal, spatial and changes with height) while retaining the single-variable dependency of the power curve, we correct the wind speed at hub height (u_{corr}). The corrected wind speed is here expressed as a function of the reference air density (ρ_{ref}) and the site-specific air density at hub height (ρ_{z_2}). The density corrections follow the work by Svenning (2010)[15]:

$$u_{corr}(t) = \begin{cases} u_{z_2}(t)\left(\frac{\rho_{ref}}{\rho_{z_2}(t)}\right)^{\frac{1}{3}} & u_{z_2}(t) \leq 8ms^{-1}, \\ u_{z_2}(t)\left(\frac{\rho_{ref}}{\rho_{z_2}(t)}\right)^{\frac{1}{3}(1+\frac{u_{z_2}(t)-8}{5})} & 8ms^{-1} < u_{z_2}(t) < 13ms^{-1}, \\ u_{z_2}(t)\left(\frac{\rho_{ref}}{\rho_{z_2}(t)}\right)^{\frac{2}{3}} & u_{z_2}(t) \geq 13ms^{-1}, \end{cases} \tag{15}$$

where u_{corr} and u_{z_2} are the density-corrected wind speed and site-specific wind speed at hub-height (z_2), respectively. However, this density correction of the power curve will result in a disturbed relationship between the power production and the wind speed. If $\rho_{z2} < \rho_{ref}$ the power production as a function of u_{corr} will be underestimated, and vice versa if $\rho_{z2} > \rho_{ref}$. Therefore, for the density corrected wind power to be valid at the original and unaffected wind speed, the wind power is linearly interpolated back to the original wind speeds (see[15] for details).

3.2.5 Storm control of generated wind power

A storm control is typically implemented in the control software of a wind turbine to increase the stability of the power output for wind events close to the cut-out limit. The mean wind speed at the Norwegian offshore areas range between 9-11 ms^{-1}. A high mean wind speed increases the risk of wind events where the wind speed exceeds the cut-out limit. However, for each grid point in NORA3-WP the number of zero-events caused by too high wind will vary. More than 22% of the offshore grid points experience these unwanted zero-events 1-2% of the time.

The ability to produce power during wind speed events exceeding the cut-out limit is important for the production credit and will increase the profitability of the wind farm. In addition, the wind power variability due to start-up and shut-down of the wind power production at high wind speeds requires a highly flexible power system[14]. Here, we introduce two methods to cope with the aforementioned challenges related to power production at high wind speeds.

Power generated using smooth shut-down and restart at high wind speeds, SC1

Storm control 1 (SC1) is a turbine control strategy which increases the generated wind power at high wind speed and reduces power intermittency. Instead of an abrupt shut-down of the power production when the wind speed exceeds the cut-out limit a smooth shut-down and start-up procedure is practiced. The power production implementing the SC1 method follows the power conversion equation Eq. 14 until $u(t) \geq u_{co}$, then the power production follows a linear decrease until a new and higher cut-out limit ($u_{co,new}$, here: 30 ms^{-1}) is reached (see blue line in Fig. 2). In this study, when $u_{co} \leq u(t) < u_{co,new}$, SC1 is calculated as follows:

$$P_{w,s}(t) = \frac{u_{co,new} - u(t)}{u_{co,new} - u_{co}}, \qquad u_{co} \leq u(t) < u_{co,new} \tag{16}$$

where $u(t)$ is the wind speed at hour t, u_{co} is the cut-out limit for the turbine in question, and $u_{co,new}$ is the new and higher cut-out limit.

Power generated using high wind hysteresis, SC2

Power generation using high wind hysteresis is here called Storm control 2 (SC2). SC2 is a solution used to avoid frequent wind power shut-downs and start-ups when the wind speed fluctuates around the cut-out limit. When the wind speed exceeds the cut-out limit, the SC2 involves a termination of wind power generation until the wind speed is below a given wind speed threshold ($u_{P,start}$), lower than the cut-out limit:

$$u_{p,start} = u_{co} - u_{incr} \tag{17}$$

u_{incr} is a wind speed increment in the order of $\frac{u_{co}}{10}$ (here: 3 ms^{-1}). For $u(i) < u_{co}$ the wind power generation follows Eq. 14. See Fig. 2 for the power generation curve using SC2.

3.2.6 Power capture coefficient

How much of the available power embedded in the air per area that actually generates wind power is here called the power-capture coefficient P_{cc}. This coefficient describes how efficient a specific turbine is at extracting the available power in the air. P_{cc} is a non-dimensional number that gives the fraction of produced power (P_w) per available power (P_c):

$$P_{cc} = \frac{P_w}{P_c} \tag{18}$$

The monthly mean of P_{cc} is calculating using Eq. 1. In addition, the monthly maximum P_{cc} is calculating using Eq. 2.

3.2.7 Generated power absolute ramp-rate (ARR)

The hourly wind power ramp-rate measures how much the wind power generation changes from one hour to the next ($ARR_{P_w}(t)$). It is calculated in the same way as the wind speed ramp rate using the generated power (section 3.2.3) instead of the wind speed.

3.2.8 Capacity factor

The capacity factor (C_f) is a common performance measure of a wind turbine or a wind farm. C_f is defined as the average power production divided by the rated power production (C_t):

$$C_f = \frac{\frac{1}{n}\sum_{t=1}^{n} P_w(t)}{C_t} \tag{19}$$

where C_f is the monthly capacity factor, and n is the number of hours in a month.

3.2.9 Full load hours

Full load hours (FLH) is another performance measure. FLH is calculated by taking the monthly sum of the power production divided by the rated power production (C_r). The resulting quantity provides the number of hours the turbine has to operate at rated capacity to produce the monthly power production delivered by the specific wind turbine:

$$FLH = \frac{\sum_{t=1}^{n} P_w(t)}{C_r} \tag{20}$$

where FLH is the monthly full load hours, hence n is the numbers of hours in a month. Full load hours using the two storm control methods are also calculated (**Full load hours, SC1** and **Full load hours, SC2**).

3.2.10 Power production categorization

It is of major importance for the wind power profitability to quantify the time fraction the power production falls into the following four categories:

- **Time fraction zero power low wind** - time fraction when the wind power is zero due to wind speeds below the cut-in wind speed limit: $u < u_{ci}$
- **Time fraction cubed power** - fractional time when the power production is proportional to the wind speed cubed: $u_{ci} \leq u < u_r$
- **Time fraction rated power** - time fraction of constant wind power production: $u_r \leq u < u_{co}$)
- **Time fraction zero power high wind** - time fraction of terminated wind power due to wind speeds exceeding the cut-out limit: $u_{co} \leq u$

The categorical quantification is done by counting hours of the power production falling into each of the four categories (h_{cat}) and normalizing the sum of hours by the total numbers of hours in a month (h_{tot}) according to the equation below:

$$f_{P_w,cat} = \frac{h_{P_w,cat}}{h_{P_w,tot}} 100\% \tag{21}$$

In addition to the fractional time the production falls into the four categories above, the total amount of zero power production for the scenario of a smooth shutdown (**Time fraction zero generated power, SC1**) and high-wind hysteresis (**Time fraction zero generated power, SC2**) are also quantified according to Eq. 21:

Technical Validation

The NORA3 near surface wind estimates are extensively validated against observations and compared against the ERA5 reanalysis by Haakenstad et al. (2021)[1]. For offshore observations the NORA3 wind estimates were shown to be better than the wind estimates from ERA5 for all months and for all investigated percentiles of wind speed. Monthly wind speed biases were typically reduced from 6-8 % to 3-5 %. The improvement was particularly pronounced for strong winds, where the bias was reduced from 10-20 % to 2-4 %, while the bias reduction for median winds typically was reduced from 7-8 % to 3-4 %. In addition, improvements in coastal winds influenced by topography were shown to be significantly larger than for the offshore stations. Thus, the downscaling of ERA5 resulted in an improved wind resource dataset.

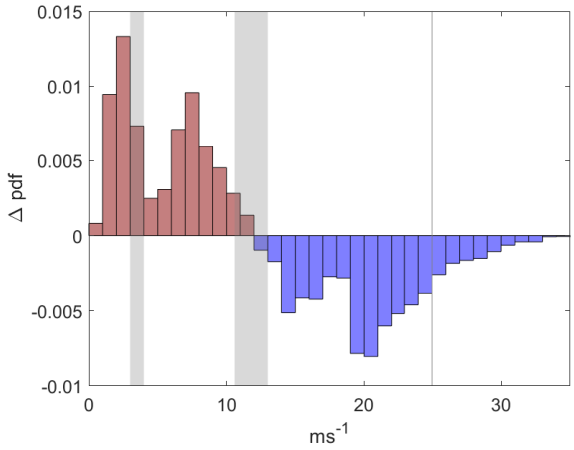

Figure 3. Differences between NORA3 and observational wind speed probability density functions ($\Delta pdf = pdf_{mod} - pdf_{obs}$) for Sleipner (an offshore oil- and gas platform in the North Sea. Lat: 58.36; lon: 01.91). When $\Delta pdf = 0.01$ the probability that the given wind speed will occur is 1 % higher in the model output. Red (blue) colored bars corresponds to $\Delta pdf = pdf_{mod} - pdf_{obs} >$ (<)0. The gray area in the middle corresponds to the range for the rated wind speed for the three turbines used in this study (SWT-6.0-154, DTU-10.0-RWT, IEA-15-240-RWT). The gray area to the left (right) is the range of the cut-in (cut-out) wind speed limits for the three turbines.

The NORA3 dataset was not created specifically for wind power purposes. An in depth validation of the usefulness of the NORA3 wind dataset in estimating wind power related variables was conducted in detail in Solbrekke et al. (2021)[?]. One of the main findings in[?] is that NORA3 wind speeds are typically 5 % ($0.5 ms^{-1}$) lower than observed wind speeds. The simulated winds are somewhat biased towards an excess of low wind speed events ($u < 11 - 13\ ms^{-1}$) and biased towards too few high wind speed events ($u > 11 - 13\ ms^{-1}$) (see Fig. 3). Wind speeds in the order of $11 - 13\ ms^{-1}$ is the wind speed interval where offshore wind turbines generally starts the rated power production. The overestimation of the low wind speed events and the underestimation of the high wind speed events lead to a underestimation of offshore wind power of 10–20 % (equivalent to an underestimation of 3 percentage points in the capacity factor).

The validation in[?] also reveal a slightly lower hourly variability in the NORA3 winds compared to the observational data. Also, there are too few occurrences of unwanted zero-events (zero wind power production due to either too low or too high wind speeds) in the model, and the corresponding event-duration are too long. Hence, the total risk of having an unwanted zero-event is slightly overestimated by NORA3. Solbrekke et. al., (2021) concluded that the NORA3 data was well suited for wind power estimates but gives slightly conservative estimates of the offshore wind resources compared to observational based estimates. The model limitations and weaknesses should be kept in mind when using the dataset as an offshore wind power planning tool.

Usage Notes

The original NORA3 dataset can be downloaded here: https://thredds.met.no/thredds/projects/nora3.html The NORA3-WP[11] dataset can be accessed here: https://archive.sigma2.no/pages/public/searchResult.jsf
The NORA3-WP dataset are available as netCDF4-files (.nc-files). The wind resource parameters available for download are listed in Table 2. The wind power related variables can be found in Table 3.

NORA3-WP is structured and stored following the naming convention of Table 2 and 3. Each file contains monthly data for all the available years (1996-2019). The hourly data are stored as yearly files due to the file size.

The user should note that onshore data are also available in the files. However, validation of NORA3 over land towards wind power usage is not conducted yet and the choice of turbines used in the wind power estimations is not relevant for land-based sites. To exclude the land grid points from the dataset the land-area-fraction matrix can be used (excl_land_NORA3WP.nc).

Example of usage

This section provides two examples of usage for the NORA3-WP dataset. The NORA3-WP dataset can be used for different purposes by wind power stakeholders, decision makers, politicians, researchers, journalists etc. Data for a specific variable can be viewed in spatial maps for a smaller region or the whole NORA3-WP domain. Plotting the data in maps gives a spatial overview of the variable considered. The maps provide information on areas suitable for wind energy exploitation. As an alternative to spatial maps, the data can be used to provide temporal information for one or several variables for a specific site, which might be useful to follow the time evolution of the variable in question.

Climatology

An important usage of NORA3-WP is climatological insight into potential wind power production. Figure 4 illustrates the climatology of the wind speed at 150 m.a.s.l. for the years 1996-2019 (a) and the corresponding wind power capacity factor (CF) for the IEA-15-240-RWT turbine (b). Panel a) demonstrates that the mean wind speeds in the area are very high; between $10-12 \mathrm{ms}^{-1}$ in the southern and western regions and slightly lower in the northern and eastern parts1 ($8-10 \mathrm{ms}^{-1}$). The climatological CF (panel b) shows similar spatial patterns with highest values in the southern and western areas, with typically 10-15 percentage point lower CF in the northern and eastern regions. Note that the areas with highest wind speeds not necessarily coincide with the areas of the highest capacity factor.

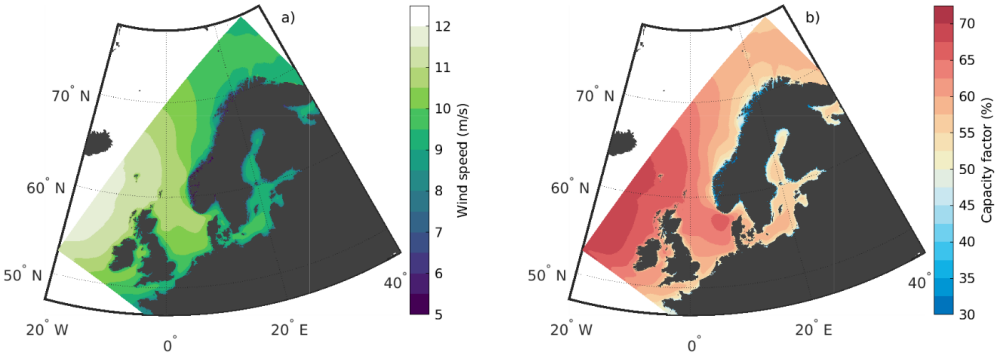

Figure 4. Climatology for the years 1996-2019 of wind speed at 150 m.a.s.l. (a) and the corresponding capacity factor for the IEA-15-240-RWT reference turbine (b).

Case studies

Another application for the NORA3-WP dataset are case-studies with limited spatial and temporal duration. One specific incident is the storm surge that struck the North Sea on the 5th of December 2013. Figure 5 shows the time evolution of the wind speed and the corresponding wind power production during the 25th of December 2013. In panel a) at 5th of December at 00UTC the wind power production is rated as the low pressure system is located to the northwest of Scotland. The system moves towards east and deepens, resulting in an acceleration of the winds. At 06UTC (b) the strongest winds, exceeding 25 ms^{-1}, struck the North Sea and the power production terminates (blue areas in the lower row in Fig. 5). As the center of the strong extratropical cyclone approaches Norway the mean wind speed increases further and reaches 35-40 ms^{-1}.

The time series of the wind speed (a) and wind power (b) at a specific point in the offshore area "Sørlige Nordsjøen 2" (SN2) for the 25th of December from 00UTC to 18UTC are illustrated in Fig. 6. After 06UTC the wind is too strong for the power production to continue and the power production is terminated. This incident illustrates the wind power vulnerability towards strong winds. The figure also demonstrate the advantage of implementing storm control 1 (SC1, dashed line in Fig. 6) to exploit a larger fraction of the high wind speeds for power production.

Code availability

NORA3-WP is created using MatLab (version 2018a). A short description of the functions used to create the variables in NORA3-WP can be found in Table 4.
The matlab scripts are permanently archived at zenodo: https://doi.org/10.5281/zenodo.6138696

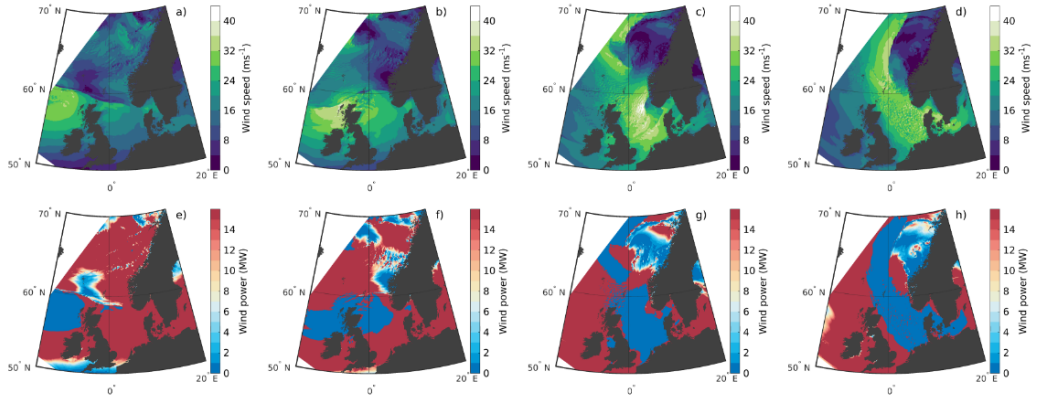

Figure 5. Time evolution of the wind speed (a-d) and generated wind power (e-h) for the 25th of December 2013 when a strong low-pressure system struck the North Sea. a) and e) correspond to the 25th of December 2013 at 00UTC; b) and f) the 25th at 06UTC; c) and g) the 25th at 12UTC; and d) and h) the 25th at 18UTC. The position of Sørlige Nordsjøen 2 (SN2) is also shown

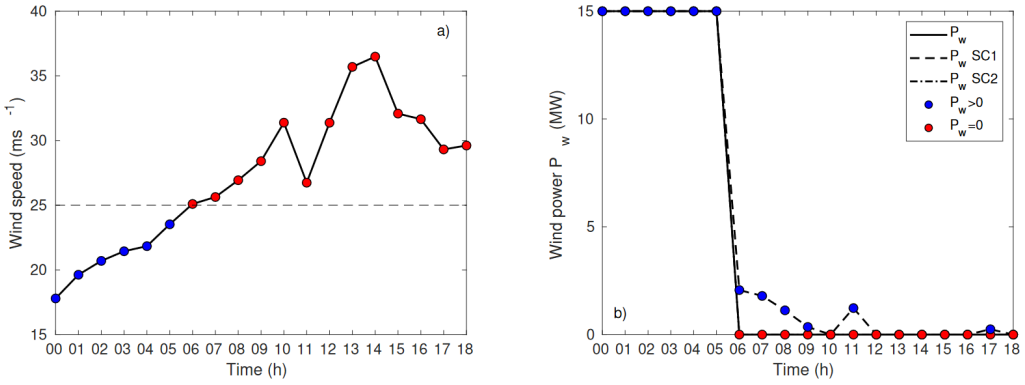

Figure 6. Time series of the wind speed (a) and wind power (P_w) (b) for Sørlige Nordsjøen 2, between the 25th of December 2013 at 00UTC and 18UTC. Blue color indicate wind power production, while red color means terminated power production caused by too strong winds ($u \geq 25 ms^{-1}$). P_w SC1 and P_w SC2 corresponds to power production using storm control 1 and 2, respectively.

References

1. Haakenstad, H. *et al.* NORA3: A non-hydrostatic high-resolution hindcast for the North Sea, the Norwegian Sea and the Barents Sea. *J. Appl. Meteorol. Climatol.* **60**, 1443–1464, I:https://doi.org/10.1175/JAMC-D-21-0029.1 (2021).
2. Hersbach, H. *et al.* The ERA5 global reanalysis. *Q. J. Royal Meteorol. Soc.* **146**, 1999–2049, 10.1002/qj.3803 (2020).
3. Seity, Y. *et al.* The AROME-France convective-scale operational model. *Mon. Weather. Rev.* **139**, 976–991, 10.1175/2010MWR3425.1 (2011).
4. Bengtsson, L. *et al.* The HARMONIE-AROME model configuration in the ALADIN-HIRLAM NWP system. *Mon. Weather. Rev.* **145**, 1919–1935, 10.1175/MWR-D-16-0417.1 (2017).
5. Solbrekke, I. M., Sorteberg, A. & Haakenstad, H. The 3 km Norwegian reanalysis (NORA3) – a validation of offshore wind resources in the North Sea and the Norwegian Sea. *Wind. Energy Sci.* **6**, 1501–1519, 10.5194/wes-6-1501-2021 (2021).
6. Dörenkämper, M. *et al.* The Making of the New European Wind Atlas – Part 2: Production and Evaluation. *Geosci. Model. Dev.* **13**, 5079–5102, 10.5194/gmd-13-5079-2020 (2020).
7. Badger, J. & Jørgensen, H. E. A high resolution global wind atlas - improving estimation of world wind resources. In *Energy Systems and Technologies for the coming Century : Proceedings*, 215–225 (Danmarks Tekniske Universitet, Risø Nationallaboratoriet for Bæredygtig Energi, Roskilde, 2011).
8. AG, S. Siemens 6.0 MW Offshore Wind Turbine. Tech. Rep. (2011). https://en.wind-turbine-models.com/turbines/657-siemens-swt-6.0-154.
9. Wang, S., Nejad, A. R. & Moan, T. On design, modelling, and analysis of a 10-MW medium-speed drivetrain for offshore wind turbines. *Wind. Energy* **23**, 1099–1117, 10.1002/we.2476 (2020).
10. Gaertner, E. *et al.* Definition of the IEA Wind 15-Megawatt Offshore Reference Wind Turbine. Tech. Rep. (2020). https://www.nrel.gov/docs/fy20osti/75698.pdf.
11. Solbrekke, I. M. & Sorteberg, A. NORA3-WP: A high-resolution offshore wind power dataset for the Baltic, North, Norwegian, and Barents Seas. *NIRD research data archive* https://doi.org/10.11582/2021.00068 (2021).
12. Celik, A. N. Energy output estimation for small-scale wind power generators using Weibull-representative wind data. *J. Wind. Eng. Ind. Aerodyn.* **91**, 693–707, 10.1016/S0167-6105(02)00471-3 (2003).
13. Genc, A. *et al.* Estimation of Wind Power Potential Using Weibull Distribution. *Energy Sources* **27**, 809–822, 10.1080/00908310490450647 (2005).
14. Huber, M., Dimkova, D. & Hamacher, T. Integration of wind and solar power in Europe: Assessment of flexibility requirements. *Energy* **69**, 236–246, 10.1016/j.energy.2014.02.109 (2014).
15. Svenning, L. Power curve air density corrections and other power curve options in WindPRO. Tech. Rep. (2010). http://www.emd.dk/files/windpro/WindPRO{_}Power{_}Curve{_}Options.pdf.

Acknowledgements

Thanks to the Meteorological institute, and a special thanks to Hilde Haakenstad and Øyvind Breivik for creating and providing the NORA3 dataset.

Author contributions statement

I.M.S. and A.S. conceptualized the overarching research goals of the study, in addition to conducting formal analysis regarding statistical and mathematical techniques and methods. I.M.S. was responsible for the data curation and creation of software code, validation, visualization of data, and preparation of the original draft, with contribution from AS. In addition, AS was responsible for the supervision. Both the authors contributed to the review and editing process of the paper.

Competing interests

No competing interests to declare.

Table 4. Short description of the MatLab functions used to calculate the variables in NORA3-WP.

Name	Type	Short description
WIND_WndDirSector.m	function	Calculates the mean of the prevailing wind-direction sector
WIND_calc_WndShear.m	function	Calculates the vertical wind shear
WIND_calc_WeibullParams.m	function	Calculates the Weibull shape, scale and standard deviation
WIND_calc_AbsRampRate.m	function	Calculates the absolute wind speed and wind power ramp-rates
WIND_calc_WndPowerDensity.m	function	Calculates the energy density in the air
WIND_calc_PowerDeliver.m	function	Calculates the wind power delivered by the air stream to the turbine rotor
WIND_calc_PowerCaptureCoeff.m	function	The efficiency of a turbine to extract the energy content in the air stream
WIND_calc_TurbinePowerProd.m	function	Calculate wind power production for a selected turbine and method
WIND_calc_FullLoadHours.m	function	Calculates the full load hours for a selected turbine
WIND_calc_CapacityFactor.m	function	Calculates the wind power capacity factor for a selected turbine
WIND_calc_PercCubedProd.m	function	Calculates the time fraction the power production is a function of the wind speed cubed
WIND_calc_PercRatedProd.m	function	Calculates the time fraction the power production is rated
WIND_calc_PercZeroProd.m	function	Calculates the time fraction the power production is zero

Bibliography

Apostolou, D., and P. Enevoldsen (2019), The past, present and potential of hydrogen as a multifunctional storage application for wind power, *Renewable and Sustainable Energy Reviews*, *112*, 917–929, doi:10.1016/j.rser.2019.06.049. 10

Archer, C. L., and M. Z. Jacobson (2007), Supplying baseload power and reducing transmission requirements by interconnecting wind farms, *Journal of Applied Meteorology and Climatology*, *46*(11), 1701–1717, doi:10.1175/2007JAMC1538.1. 4

Badger, J., and H. E. Jørgensen (2011), A high resolution global wind atlas - improving estimation of world wind resources, in *Energy Systems and Technologies for the coming Century : Proceedings*, pp. 215–225, Danmarks Tekniske Universitet, Risø Nationallaboratoriet for Bæredygtig Energi, Roskilde. 3

Barstad, I., and S. Grønås (2005), Southwesterly flows over southern Norwaymesoscale sensitivity to large-scale wind direction and speed, *Tellus A: Dynamic Meteorology and Oceanography*, *57*(2), 136–152, doi:10.3402/tellusa.v57i2.14627. 8, 12

Bengtsson, L., U. Andrae, T. Aspelien, Y. Batrak, J. Calvo, W. d. Rooy, E. Gleeson, B. Hansen-Sass, M. Homleid, M. Hortal, K. I. Ivarsson, G. Lenderink, S. Niemelä, K. P. Nielsen, J. Onvlee, L. Rontu, P. Samuelsson, D. S. Muñoz, A. Subias, S. Tijm, V. Toll, X. Yang, and M. Køltzow (2017), The HARMONIE-AROME model configuration in the ALADIN-HIRLAM NWP system, *Monthly Weather Review*, *145*(5), 1919–1935, doi:10.1175/MWR-D-16-0417.1. 3, 22

Benitez, L. E., P. C. Benitez, and G. C. van Kooten (2008), The economics of wind power with energy storage, *Energy Economics*, *30*(4), 1973–1989, doi:10.1016/j.eneco.2007.01.017. 10

Bhandari, R., B. Kumar, and F. Mayer (2020), Life cycle greenhouse gas emission from wind farms in reference to turbine sizes and capacity factors, *Journal of Cleaner Production*, *277*, 123,385, doi:10.1016/j.jclepro.2020.123385. 13

Boccard, N. (2009), Capacity Factor of Wind Power: Realized Values vs. Estimates, *SSR Energy Policy*, *37*, 2679–2688, doi:10.2139/ssrn.1285435. 13

Bosch, J., I. Staffell, and A. D. Hawkes (2018), Temporally explicit and spatially resolved global offshore wind energy potentials, *Energy*, *163*, 766–781, doi:10.1016/j.energy.2018.08.153. 2, 13

British Petroleum (BP) (2020), Statistical Review of World Energy 2020 69th edition, *Tech. rep.*, https://www.bp.com/content/dam/bp/business-sites/en/global/corporate/pdfs/energy-economics/statistical-review/bp-stats-review-2020-full-report.pdf. 1

Dörenkämper, M., B. Olsen, B. Witha, A. Hahmann, N. Davis, J. Barcons, Y. Ezber, E. García-Bustamante, J. F. González-Rouco, J. Navarro, M. Sastre-Marugán, T. Sīle, W. Trei, M. Žagar, J. Badger, J. Gottschall, J. Sanz Rodrigo, and J. Mann (2020), The Making of the New European Wind Atlas Part 2: Production and Evaluation, *Geoscientific Model Development*, *13*, 5079–5102, doi:10.5194/gmd-13-5079-2020. 3

Dvorak, M. J., E. D. Stoutenburg, C. L. Archer, W. Kempton, and M. Z. Jacobson (2012), Where is the ideal location for a US East Coast offshore grid?, *Geophysical Research Letters*, *39*(6), 1–6, doi:10.1029/2011GL050659. 4

Energy facts Norway (2022), Energy use by sector, doi:https://energifaktanorge.no/en/norsk-energibruk/energibruken-i-ulike-sektorer/. 14, 17

Energy Information Administration (EIA) (2021), International Energy Outlook 2021, *Tech. rep.*, https://www.eia.gov/outlooks/ieo/. 1

Energy Numbers (2021), UK offshore wind capacity factors, doi:https://energynumbers.info/uk-offshore-wind-capacity-factors. 13

Equinor (2021), Hywind Scotland fortsatt best blant havvindparker på britisk sokkel, doi:https://www.equinor.com/no/news/20210323-hywind-scotland-uk-best-performing-offshore-wind-farm.html. 13

Furevik, B. R., and H. Haakenstad (2012), Near-surface marine wind profiles from rawinsonde and NORA10 hindcast, *Journal of Geophysical Research Atmospheres*, *117*(23), 1–14, doi:10.1029/2012JD018523. 23

Gaertner, E., J. Rinker, L. Sethuraman, F. Zahle, B. Anderson, G. Barter, N. Abbas, F. Meng, P. Bortolli, W. Skrzypinski, G. Scott, R. Feil, H. Bredmose, K. Dykes, M. Shields, C. Allen, and A. Viselli (2020), Definition of the IEA Wind 15-Megawatt Offshore Reference Wind Turbine, *Tech. rep.* 9, 13, 14, 15, 24

Grams, C. M., R. Beerli, S. Pfenninger, I. Staffell, and H. Wernli (2017), Balancing Europe's wind-power output through spatial deployment informed by weather regimes, *Nature Climate Change*, *7*(8), 557–562, doi:10.1038/NCLIMATE3338. 4

Haakenstad, H., Ø. Breivik, B. R. Furevik, M. Reistad, P. Bohlinger, and O. J. Aarsnes (2021), NORA3: A non-hydrostatic high-resolution hindcast for the North Sea, the Norwegian Sea and the Barents Sea, *Accepted for publication in Journal of Applied Meteorology and Climatology*, doi:10.1175/JAMC-D-21-0029.1. 3, 4, 21, 22, 23

Hersbach, H., B. Bell, P. Berrisford, S. Hirahara, A. Horányi, J. Muñoz-Sabater, J. Nicolas, C. Peubey, R. Radu, D. Schepers, A. Simmons, C. Soci, S. Abdalla, X. Abellan, G. Balsamo, P. Bechtold, G. Biavati, J. Bidlot, M. Bonavita, G. De Chiara, P. Dahlgren, D. Dee, M. Diamantakis, R. Dragani, J. Flemming, R. Forbes, M. Fuentes, A. Geer, L. Haimberger, S. Healy, R. J. Hogan,

E. Hólm, M. Janisková, S. Keeley, P. Laloyaux, P. Lopez, C. Lupu, G. Radnoti, P. de Rosnay, I. Rozum, F. Vamborg, S. Villaume, and J. N. Thépaut (2020), The ERA5 global reanalysis, *Quarterly Journal of the Royal Meteorological Society*, *146*(730), 1999–2049, doi:10.1002/qj.3803. 3, 22

Hoskins, B. J., and K. I. Hodges (2019), The Annual Cycle of Northern Hemisphere Storm Tracks. Part II: Regional Detail, *Journal of Climate*, *32*(6), 1761–1775, doi:10.1175/JCLI-D-17-0871.1. 7

IEA, I. E. A. (2019), Offshore Wind Outlook, *Tech. rep.*, https://www.iea.org/reports/offshore-wind-outlook-2019. 2

IEA, I. E. A. (2021a), Greenhouse Gas Emissions from Energy: Overview, *Tech. rep.*, https://www.iea.org/reports/greenhouse-gas-emissions-from-energy-overview. 1

IEA, I. E. A. (2021b), Electricity Marked Report - Juli 2021, *Tech. rep.*, https://www.iea.org/news/global-electricity-demand-is-growing-faster-than-renewables-driving-strong-increase-in-generation-from-fossil-fuels. 1

IEA, I. E. A. (2021c), Renewables 2021, *Tech. rep.*, doi:https://www.iea.org/news/renewable-electricity-growth-is-accelerating-faster-than-ever-worldwide-supporting-the-emergence-of-the-new-global-energy-economy. 1, 2, 29

Kahn, E. (1979), The reliability of distributed wind generators, *Electric Power Systems Research*, *2*(1), 1–14, doi:10.1016/0378-7796(79)90021-X. 10

Kempton, W., F. M. Pimenta, D. E. Veron, and B. A. Colle (2010), Electric power from offshore wind via synoptic-scale interconnection, *Proceedings of the National Academy of Sciences of the United States of America*, *107*(16), 7240–7245, doi:10.1073/pnas.0909075107. 4

Laprise, R. (1992), The Euler Equations of Motion with Hydrostatic Pressure as an Independent Variable, *Monthly Weather Review*, *120*(1), 197–207, doi:10.1175/1520-0493(1992)120<0197:TEEOMW>2.0.CO;2. 22

Masson, V., P. Le Moigne, E. Martin, S. Faroux, A. Alias, R. Alkama, S. Belamari, A. Barbu, A. Boone, F. Bouyssel, P. Brousseau, E. Brun, J.-C. Calvet, D. Carrer, B. Decharme, C. Delire, S. Donier, K. Essaouini, A.-L. Gibelin, H. Giordani, F. Habets, M. Jidane, G. Kerdraon, E. Kourzeneva, M. Lafaysse, S. Lafont, C. Lebeaupin Brossier, A. Lemonsu, J.-F. Mahfouf, P. Marguinaud, M. Mokhtari, S. Morin, G. Pigeon, R. Salgado, Y. Seity, F. Taillefer, G. Tanguy, P. Tulet, B. Vincendon, V. Vionnet, and A. Voldoire (2013), The SURFEXv7.2 land and ocean surface platform for coupled or offline simulation of earth surface variables and fluxes, *Geoscientific Model Development*, *6*(4), 929–960, doi:10.5194/gmd-6-929-2013. 22

Norsk Petroleum (2022a), The governmental revenue, doi:https://www.norskpetroleum.no/en/economy/governments-revenues/. 18

Norsk Petroleum (2022b), Activity per sea area, doi:https://www.norskpetroleum.no/en/developments-and-operations/activity-per-sea-area/. 18

Reichenberg, L., F. Johnsson, and M. Odenberger (2014), Dampening variations in wind power generation-The effect of optimizing geographic location of generating sites, *Wind Energy*, *17*(11), 1631–1643, doi:10.1002/we.1657. 4

Reichenberg, L., A. Wojciechowski, F. Hedenus, and F. Johnsson (2017), Geographic aggregation of wind poweran optimization methodology for avoiding low outputs, *Wind Energy*, *20*, 19–32, doi:10.1002/we.1987. 4

Seity, Y., S. Malardel, G. Hello, P. Bénard, F. Bouttier, C. Lac, and V. Masson (2011), The AROME-France convective-scale operational model, *Monthly Weather Review*, *139*(3), 976–991, doi:10.1175/2010MWR3425.1. 3, 22

Simmons, A. J., and D. M. Burridge (1981), An Energy and Angular-Momentum Conserving Vertical Finite-Difference Scheme and Hybrid Vertical Coordinates, *Monthly Weather Review*, *109*(4), 758–766, doi:10.1175/1520-0493(1981)109<0758:AEAAMC>2.0.CO;2. 22

SINTEF (2018), Nasjonal betydning av sjømatnæringen, *Tech. rep.*, https://www.sintef.no/contentassets/d727158330ac4d00a00c77783b89acf2/nasjonal-verdiskapning_2018_endelig_100818.pdf. 18

Soares, P. M. M., D. C. A. Lima, and M. Nogueira (2020), Global offshore wind energy resources using the new ERA-5 reanalysis, *Environmental Research Letters*, *15*(10), 1040a2, doi:10.1088/1748-9326/abb10d. 2

Solbrekke, I. M., and A. Sorteberg (2022), NORA3-WP: A high-resolution offshore wind power dataset for the Baltic, North, Norwegian, and Barents Seas, *Accepted for publication in Scentific data - Nature*. 7, 11, 13, 14

St. Martin, C. M., J. K. Lundquist, and M. A. Handschy (2015), Variability of interconnected wind plants: Correlation length and its dependence on variability time scale, *Environmental Research Letters*, *10*(4), 44,004, doi:10.1088/1748-9326/10/4/044004. 4

Statistics Norway (2018), Vi bruker mindre strøm hjemme, doi:https://www.ssb.no/energi-og-industri/artikler-og-publikasjoner/vi-bruker-mindre-strom-hjemme. 16

Statistics Norway (2022), Boliger, doi:https://www.ssb.no/bygg-bolig-og-eiendom/bolig-og-boforhold/statistikk/boliger. 17

Statnett (2019), Et elektrisk Norge fra fossilt til strøm, *Tech. rep.*, https://www.statnett.no/globalassets/for-aktorer-i-kraftsystemet/planer-og-analyser/et-elektrisk-norge–fra-fossilt-til-strom.pdf. 12

The Norwegian government (2020), Opner områder for havvind i Noreg, doi:https://www.regjeringen.no/no/aktuelt/opner-omrader/id2705986/. 3, 18

The Norwegian government (2022), Storstilt satsing på havvind, doi:https://www.regjeringen.no/no/aktuelt/storstilt-satsing-pa-havvind/id2900436/. 3, 19

The Norwegian society for the Conservation of Nature (2021), The Norwegian area 2021, *Tech. rep.*, https://naturvernforbundet.no/getfile.php/13175941-1642433694/Bilder/Natur/Arealrapport 2021.pdf. 16

The Norwegian Water Resource and Energy Directorate (2012), Havvind - strategisk konsekvensutredning, *Tech. rep.*, http://publikasjoner.nve.no/rapport/2012/rapport2012_47.pdf, doi:http://publikasjoner.nve.no/rapport/2012/rapport2012{_}47.pdf. 18

The Norwegian Water Resource and Energy Directorate (2020), Hva er egentlig potensialet for opprusting og utvidelse av norske vannkraftverk?, doi:https://publikasjoner.nve.no/faktaark/2020/faktaark2020{_}06.pdf. 12

The Norwegian Water Resource and Energy Directorate (2022), Power production, doi:https://www.nve.no/energi/energisystem/kraftproduksjon/. 12

Veers, P., K. Dykes, E. Lantz, S. Barth, C. L. Bottasso, O. Carlson, A. Clifton, J. Green, P. Green, H. Holttinen, D. Laird, V. Lehtomäki, J. K. Lundquist, J. Manwell, M. Marquis, C. Meneveau, P. Moriarty, X. Munduate, M. Muskulus, J. Naughton, L. Pao, J. Paquette, J. Peinke, A. Robertson, J. Sanz Rodrigo, A. M. Sempreviva, J. C. Smith, A. Tuohy, and R. Wiser (2019), Grand challenges in the science of wind energy, *Science*, *366*(6464), doi:10.1126/science.aau2027. 3, 4

Wang, S., A. R. Nejad, and T. Moan (2020), On design, modelling, and analysis of a 10MW mediumspeed drivetrain for offshore wind turbines, *Wind Energy*, *23*(4), 1099–1117, doi:10.1002/we.2476. 11

Wood, D. (2020), Grand Challenges in Wind Energy Research, *Frontiers in Energy Research*, *8*, doi:10.3389/fenrg.2020.624646. 3, 4

Zheng, C. W., C. Y. Li, J. Pan, M. Y. Liu, and L. L. Xia (2016), An overview of global ocean wind energy resource evaluations, *Renewable and Sustainable Energy Reviews*, *53*(667), 1240–1251, doi:10.1016/j.rser.2015.09.063. 2, 13

Graphic design: Communication Division, UiB / Print: Skipnes Kommunikasjon AS

uib.no

ISBN: 9788230856697 (print)
9788230866870 (PDF)